Development of an Improved Low Frequency Transformer Model for Use in GIC Studies

by

Waruna Chandrasena

A Dissertation Submitted to The Faculty of Graduate Studies

In Partial Fulfillment of the Requirements for the

Degree of

Doctor of Philosophy

The Department of Electrical and Computer Engineering

The University of Manitoba

Winnipeg, Manitoba, Canada

THE UNIVERSITY OF MANITOBA

FACULTY OF GRADUATE STUDIES

*****

COPYRIGHT PERMISSION

DEVELOPMENT OF AN IMPROVED LOW FREQUENCY TRANSFORMER MODEL FOR USE IN GIC STUDIES

BY

WARUNA CHANDRASENA

A Thesis/Practicum submitted to the Faculty of Graduate Studies of The University of Manitoba in partial fulfillment of the requirement of the degree

of

DOCTOR OF PHILOSOPHY

To my parents and teachers.

Abstract

Geomagnetically Induced Currents (GIC) are the ground effect of a complicated space weather chain that originates in the sun. During a GIC event, the quasi dc current that enters the transformers through the grounded neutral can cause severe half cycle saturation in the iron core. This results in increased reactive power consumption and generation of significant levels of harmonic currents. A severe GIC event in 1989 caused a complete blackout in the Hydro-Quebec system, and it shows how vulnerable a power system can be.

There have been many simulation studies carried out to model the effects of GIC in power systems using electromagnetic transient simulation programmes. Many of these attempts have used curve fitting techniques to model the hysteresis characteristics of power transformers. However, the correct representation of the hysteresis, including the long term remanence and recoil loops is important, since the source of the harmonic generation is the transformer itself. Therefore, the main objective of this work is to develop a simulation model of a power transformer that represents hysteresis characteristics including long term remanence and recoil loops. Further, the new model is used in simulation studies to analyse the effects of GIC in a power system.

The new model is based on the Jiles Atherton (JA) theory of ferromagnetic hysteresis. The eddy current effects are also incorporated into the same model, so that the simulated B-H loop is frequency dependent. The new model is implemented using the transient simulation software PSCAD/EMTDC, and it is validated by comparing

simulation results with recorded waveforms. A good agreement is achieved between the simulated and recorded waveforms.

Effects of GIC on a power system are analyzed using a simulation model of a power system. Simulation studies show that a transient simulation carried out to model a GIC event requires not only the magnitude of the quasi dc current, but also its history with respect to any particular point of interest. Further, simulation studies demonstrate that it is important to accurately model the remanence effects of the iron core of power transformers.

Acknowledgements

I wish to express my sincere gratitude to Professor Peter McLaren for the guidance, advice, and support extended during the course of this work. I consider myself privileged to have had the opportunity to pursue my doctoral studies under his guidance.

I wish to express my deep appreciation to Professor Udaya Annakkage for his valuable advice, guidance, and support extended during the course of this work. I wish to thank him for sharing his knowledge and expertise on hysteresis modelling, which was the basis of this work.

I am grateful to Professor Rohan Lucas at University of Moratuwa for encouraging me to pursue my doctoral studies at the University of Manitoba, and arranging the opportunity to do so. I wish to thank Dr. Aniruddha Gole for his guidance on power system modelling. Dr. Rohitha Jayasinghe of the Manitoba HVDC Research Centre deserves a special note of thanks for his valuable guidance, and for taking time to answer my questions with EMTDC on many occasions.

I wish to acknowledge the financial support from Manitoba Hydro, the University of Manitoba and the NSERC of Canada, and technological support provided by the System Planning Department of the Manitoba Hydro.

I am thankful to all the staff members of the power systems research group, and the department of Electrical and Computer Engineering for providing research facilities. I would also like to thank my friends for their support in numerous ways, especially Dr. Dharshana Muthumuni.

Finally, this work would not have been a reality without the love and support of my dear family. I extend my heart felt gratitude to my parents. I thank them, my sisters, and my wife for their continuous support, understanding, and encouragement given over the years.

Table of Contents

List of Figures

List of Tables

List of Symbols and Acronyms

$[A]$	branch node connection matrix
A_w	cross sectional area of the winding limb
A_y	cross sectional area of the yoke
a_1, a_2, a_3	three constants in the anhysteretic function
α	mean field constant
B	flux density (magnetic induction)
B_R	remanent flux density
$B_{\max}$	peak flux density
β	a constant
c	coefficient of reversible wall motion
CT	Current Transformer
$\chi'_{\max}$	maximum differential susceptibility
χ'_{Hc}	differential susceptibility at the coercive point
$\frac{dM}{dH}$	differential susceptibility
D	thickness of laminations
δ	directional parameter in the hysteresis equation
Δt	time step of the simulation
$\Delta\phi_i$	incremental flux in the present time step
ΔH_i	incremental H in the present time step
$\Delta H_{i\ \max}$	maximum value of the incremental H in the present time step
ΔM_i	incremental M in the present time step
ΔQ	increase in reactive power demand

ESP	Earth Surface Potential
EMTP	Electromagnetic Transients Program
EMTDC^{TM}	Electromagnetic Transients including DC; a registered trademark of Manitoba Hydro
f	frequency of magnetization
ϕ	vector of branch flux
ϕ_i	flux in the ith branch
GIC	Geomagnetically Induced Currents
G	a constant
H	magnetic field strength
H_c	coercivity
H_e	effective field
H_{tot}	total magnetic field intensity
H_{hyst}	magnetic field determined by the hysteresis
H_{cls}	magnetic field determined by the classical eddy current losses
H_{exc}	magnetic field determined by the excess losses
H_{old}	H value during the previous time step
H_o	parameter representing the internal potential experienced by domain wall
i_i	current in the ith winding
i_s	vector of saturation current sources
i_{si}	magnitude of the saturation current source of the ith winding
I_{rms}	rms value of the magnetizing current

k	pinning coefficient in the hysteresis equation
k_o, k_1, k_2	three constants
$\mathbf{L}$	transformer inductance matrix
l_w	length of the winding limb
l_y	length of the yoke
MMF	magnetomotive force
M	magnetization
M_{sat}	saturation magnetization
M_{an}	anhysteretic magnetization
M_{irr}	irreversible magnetization
M_{rev}	reversible magnetization
M_{old}	M value during the previous time step
μ	permeability
μ_0	permeability of free space
μ_{dif_i}	differential permeability of the ith branch
N_i	number of turns in the ith winding
$[N]$	diagonal matrix containing the number of turns of each winding
n	number of windings
NA	product of the number of windings and the cross sectional area
$\frac{N}{l}$	ratio of the winding turns number and the length

PSCAD^{TM}	Power Systems CAD (Computer Aided Design)
	a registered trademark of the Manitoba HVDC Research Centre Inc.
pu	per-unit
P_i	permeance of the ith branch
[P]	branch permeance matrix
P	power loss per unit volume
P_{total}	total power loss
P_{exc}	excess or anomalous loss
P_{hys}	hysteresis loss
P_{cls}	classical eddy current loss
$\boldsymbol{\theta}$	vector of branch MMFs
θ_i	MMF across the ith branch
θ_{node}	vector of nodal MMF
$[R]$	diagonal matrix containing the reluctance of each branch
r_A	ratio of yoke/winding-limb area
r_L	ratio of yoke/winding-limb length
ρ	resistivity
S	cross sectional area of laminations
v_i	voltage of the ith winding
W_{cls}	energy lost per cycle per unit volume due to classical eddy currents
W_{exc}	energy lost per cycle per unit volume due to excess loss
$\mathbf{Y}_{ss}$	transformer admittance matrix
ω	rated angular frequency

Chapter 1

Introduction

Geomagnetically induced currents (GIC) are the ground effect of a complicated space weather chain that originates in the sun. The effects of GIC on a technological system were first observed by W. H. Barlow in the wires of an electric telegraph system in 1847 [1]. Since then, the effects on long conductors such as electrical power transmission lines, telephone cables, and buried pipe lines have attracted much attention because of various problems caused by GIC [2][3]. In 1940, W. F. Davidson presented an account of the influence of a magnetic storm on power systems [4]. This was the first reported case of power system disturbances linked to a geomagnetic storm in North America. This provides a summary of data on the influence on power systems of the magnetic storm of March 24, 1940. The basic information has been obtained from 22 utilities in Canada and the United States of America.

The flow of GIC through power transformers has been the root cause of operational and equipment problems in power systems during a geomagnetic disturbance or a geomagnetic storm. There have been many reported cases of transformer failures, relay maloperations, increased reactive power consumption, and many adverse effects on generators, static var compensators (SVC), and communication systems [5][6]. The

impact of GIC on the power industry had a greater level of concern when virtually all of the Hydro-Quebec power system plunged into darkness in 1989 [7].

This Chapter briefly describes how this complicated space weather chain is originated in the sun, and how it could affect the earth and power systems. Fig.1.1 summarizes the sequence of events associated with this phenomenon [8]. This discussion also considers the vulnerability of a power system to GIC and how this may lead to a catastrophic system collapse. Further, the mathematical modelling of a GIC event is discussed with an emphasis on electromagnetic transient simulation studies carried out on a power system.

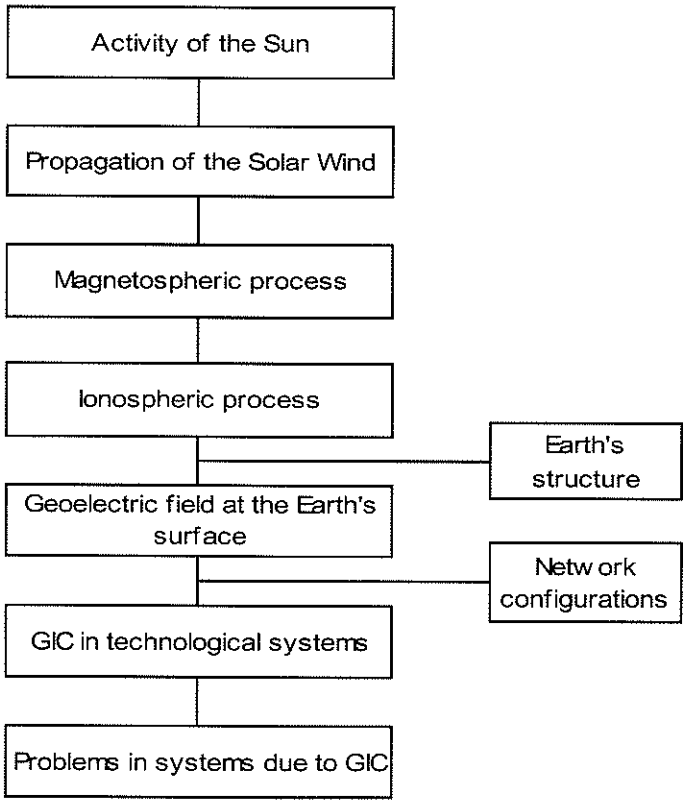

Figure 1.1: Space weather chain

1.1 Solar Phenomena

1.1.1 Background

The sun's corona, the outermost layer of the solar atmosphere, is continuously emitting charged particles consisting of protons and electrons into interplanetary space. The outward flux of solar particles and magnetic fields blown away from the sun is called the solar wind. Typically solar wind velocities are 300 to 1000 km/s and bring the particles to the earth several days after they are ejected from the sun. The solar wind is affected by three categories of solar phenomena; namely, solar flares[1], corona holes[2], and disappearing filaments[3]. It has been observed that the velocity and the charge density of the solar wind increases during periods of solar activity. The sun goes through cycles of high and low activity that repeat approximately every 11 years. The number of dark spots on the sun, called sunspots, marks this variation [9]- [11].

Common scales used to indicate the levels of geomagnetic activity are the A and K indices. The K index is a 3-hourly quasi-logarithmic local index of geomagnetic activity relative to an assumed quiet-day curve for the recording site. The values range from 0 to 9. The storm of March 13, 1989 that caused the Hydro Quebec outage, was a K-9 storm. The A index is a daily index of geomagnetic activity derived as the average of the eight 3-hourly indices. In addition, the Ap and Kp indices are obtained by averaging the A and K indices from a group of observatories distributed around the world. Fig.1.2 shows the variation of the sunspot number, which is a daily

[1] *Solar flares*: A sudden eruption of energy on the visible surface of the sun lasting minutes to hours, from which radiation and particles are emitted.

[2] *Corona holes:* An extended region of the corona, exceptionally low in density and associated with unipolar photospheric regions. Photosphere is the lowest layer of the solar atmosphere; corresponds to the solar surface viewed in white light.

[3] *Disappearing filaments:* A rapid disappearance of a solar filament (timescale of minutes to hours). A filament is a mass of gas suspended over the photosphere by magnetic fields and seen as dark lines threaded over the solar disk.

index of sunspot activity observed from 1930 to 1990. In addition, the cycle of the number of geomagnetic storm disturbed days per year provides vital information on the potential of GIC effects on power systems. This cycle usually lags the peak of the sunspot cycle by three to five years (Fig.1.2). Fig.1.3 shows the progression of the current solar cycle (#23) updated by the Space Environment Center (SEC), in Boulder Colorado, USA.

1.1.2 Interaction with the earth

Interaction of solar wind with the earth has been observed in the form of aurorae for many centuries. However the complex mechanism was not well understood until the arrival of the space age, when satellites with scientific instruments began to aid the study of the interplanetary space surrounding the earth.

In 1930, Chapman and Ferraro described a new theory of magnetic storms by assuming a 'neutral ionized stream of particles' from the sun (i.e. solar wind) [12]. However, the solar wind is magnetized, therefore this magnetization complicates the interaction with the earth. In 1961, a mechanism by which the magnetized solar wind interacts with the magnetosphere[4] was first proposed by Dungey [13]. This model has laid the foundation for most of the research work in this field. The following description briefly summarizes a snapshot of this complex phenomena, that is usually affected by the dynamic nature of the solar wind and its interaction with the magnetosphere.

[4] *Magnetosphere*: The pressure of the solar wind compresses the earth's magnetic field on the sunlit side (day side) of earth and drags the the night side of the earth to form a comet-shaped cavity called the magnetosphere.

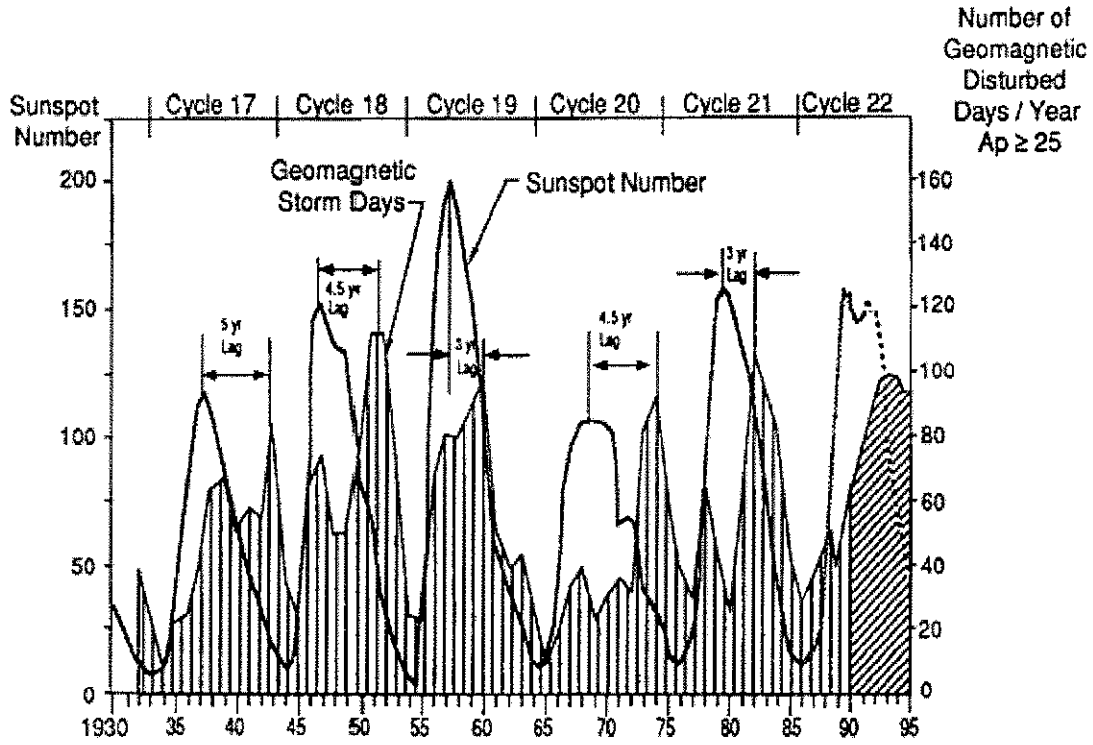

Figure 1.2: Variation of the solar cycle and number of geomagnetic disturbed days per year (Source: Kappenman et al., "Cycle 22: Geomagnetic Storm Threats to Power Systems", Power Engineering Review, pp. 3-5, © 1991 IEEE)

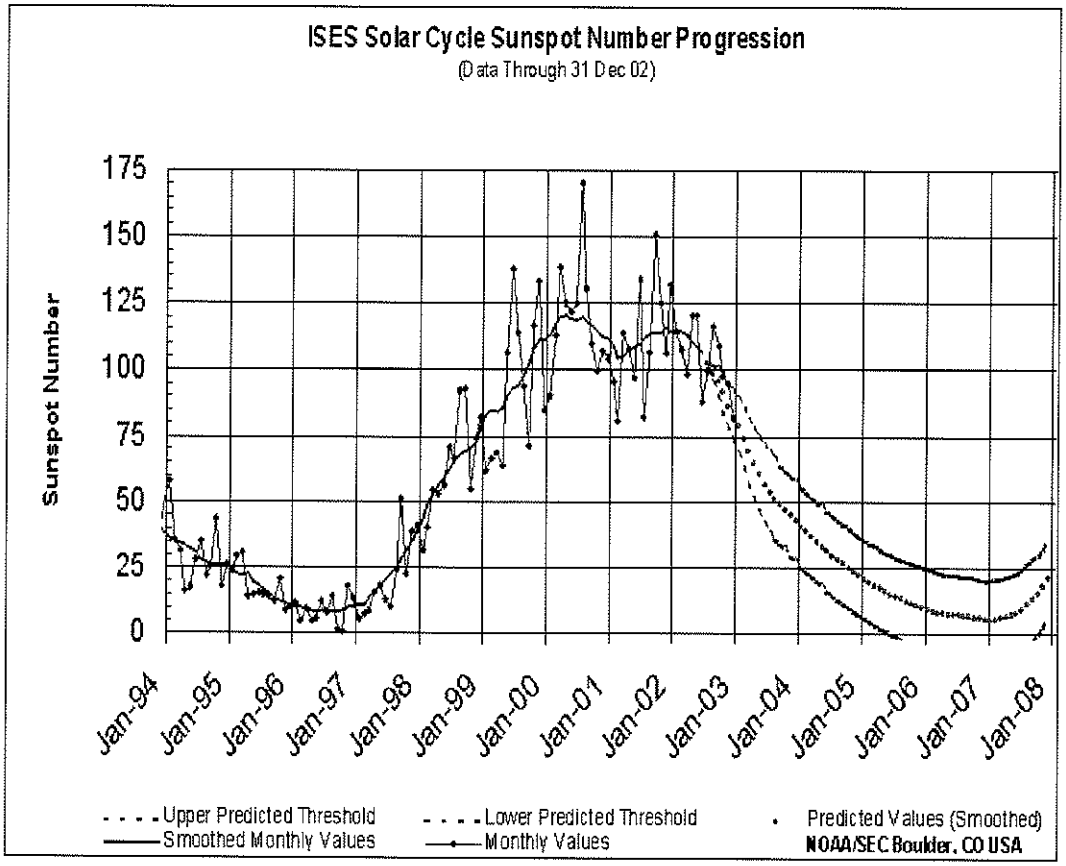

Figure 1.3: Solar cycle 23: Measured and predicted values. (Source: Space Environment Center, Boulder, CO; National Oceanic and Atmospheric Administration; US Dept. of Commerce)

The earth is protected from energetic particles and radiation in the solar wind by the terrestrial magnetic shield. Most of these energetic particles are deflected around the earth by the magnetosphere, except for two small regions on the sunlit side. When the magnetic field of the sun passes the earth, the solar magnetic field and the earth's magnetic field are connected along the boundary of the magnetosphere (magnetopause) in a process known as reconnection [13]. The factors that control the rate of reconnection of the two fields are not understood completely, however a southward component of the interplanetary field is critical to enable reconnection with the magnetosphere. This merging occurs at its best when the solar magnetic field is directed towards the south [14].

The magnetic reconnection across the boundary of the magnetosphere provides a pathway for the solar wind particles to enter into the magnetosphere. During this process, interaction of the reconnected magnetic field and the solar wind plasma causes separation of charges, which is similar to a magnetohydrodynamic generator. The resulting electric field and earth's magnetic field affect the motion of the electrons and protons, and establishes a complex connection between the magnetopause and the ionosphere[5]. Meanwhile, the motion of protons is impeded by the higher density of particles in the lower ionosphere (about 100 km above the ground), and hence due to mobility of electrons over protons, a flow of electrons along the auroral oval[6] called the electrojet can be observed [11].

The aurora borealis is the visual evidence of an electrojet in the northern hemisphere. The auroral lights occur when the incoming electron beams collide energetically with the ionosphere, exciting or ionizing atoms. These excited and ionized

[5] *Ionosphere:* The region of the earth's upper atmosphere containing a small percentage of free electrons and ions produced by photoionization.

[6] *Auroral oval:* An oval band around each geomagnetic pole which is the locus of an aurora.

atoms emit radiation over a wide spectral range, as excited ions jump into lower energy states as they combine with free electrons[7] [10][11].

1.1.3 Geomagnetic Induction

During intense solar activity, an extremely large electrojet current in the lower ionosphere could affect the magnetic field measured at the surface of the earth. The transient magnetic variations caused by the increase or decrease, or a rapid movement of the electrojet, are known as geomagnetic storms or geomagnetic disturbances. During geomagnetic storms, a portion of the earth could experience a time varying magnetic field, and electric fields are induced in the earth by these magnetic field variations. These can have values up to 6 V/km depending on the severity of the geomagnetic storm and the conductivity of the earth[8] [11][15]. The resulting potential difference between two points is called the 'earth surface potential' (ESP).

1.2 Effects on Power Systems

During a geomagnetic storm the ESP acts as a voltage source applied between the grounded neutrals of wye connected transformers or auto transformers that may be located at opposite ends of a long transmission line. The resulting flow of current between the neutrals is called geomagnetically induced current (GIC) (Fig.1.4). The variation of the waveform of ESP is usually in the order of minutes and hence GIC has a frequency of a few millihertz and appears as quasi-dc in comparison to the normal power system frequencies. The storms containing these transients can last for hours,

[7] *Auroral emissions:* The commonest is a whitish-green light with a wavelenth of 557.7 nanometers, which is emitted by oxygen. A pink emission comes from nitrogen.

[8] When the earth's resistivity is greater, the current returns deeper in the earth, and the loop size and the induction is greater

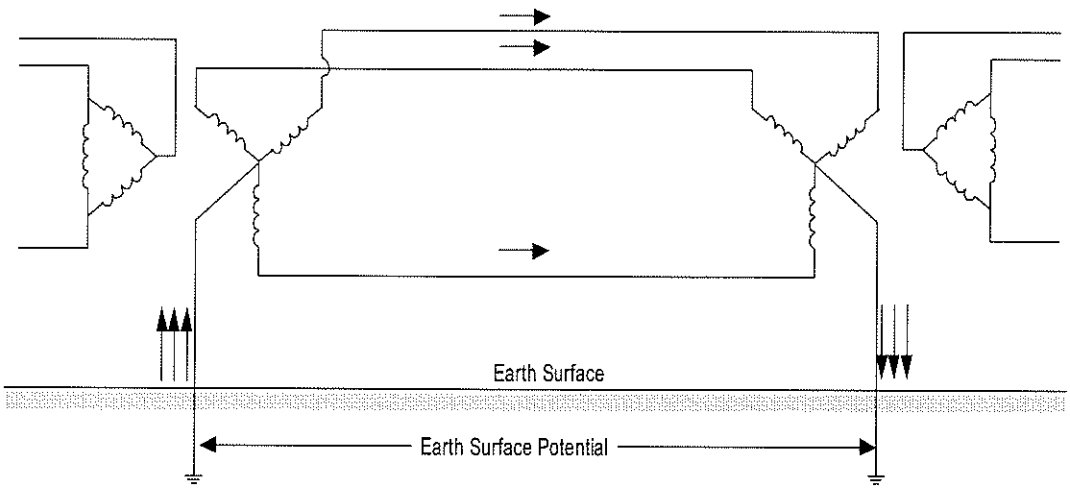

Figure 1.4: ESP between grounded Y connected transformers and the resultant GIC in the transmission lines.

thus relatively small magnitudes could create problems in a power system.

Geomagnetically Induced Current enters the transformer through the grounded neutral and if the zero sequence reluctance of the transformer is low, then the flow of this current in the transformer winding biases the operating point of the magnetization characteristics to one side. Since the peak ac flux in the power transformer is designed to be close to the knee of the magnetization characteristic, this bias causes the transformer to enter the saturation region in the half cycle in which the ac causes a flux in the same direction as the bias. This effect is known as the half cycle saturation of a transformer, and it is the source of nearly all of the operating and equipment problems experienced during a GIC event.

Because of the half-cycle saturation, the transformer draws a large asymmetrical exciting current which results in increased reactive power consumption as well as the generation of significant levels of harmonic currents [5][16]-[18]. Fig.1.5 shows waveforms of magnetizing current when a transformer is excited under rated conditions;

(a) without GIC, and (b) with GIC, in which the presence of GIC has caused half cycle saturation. The severity of half cycle saturation determines the nature of the waveform of an asymmetrical magnetizing current.

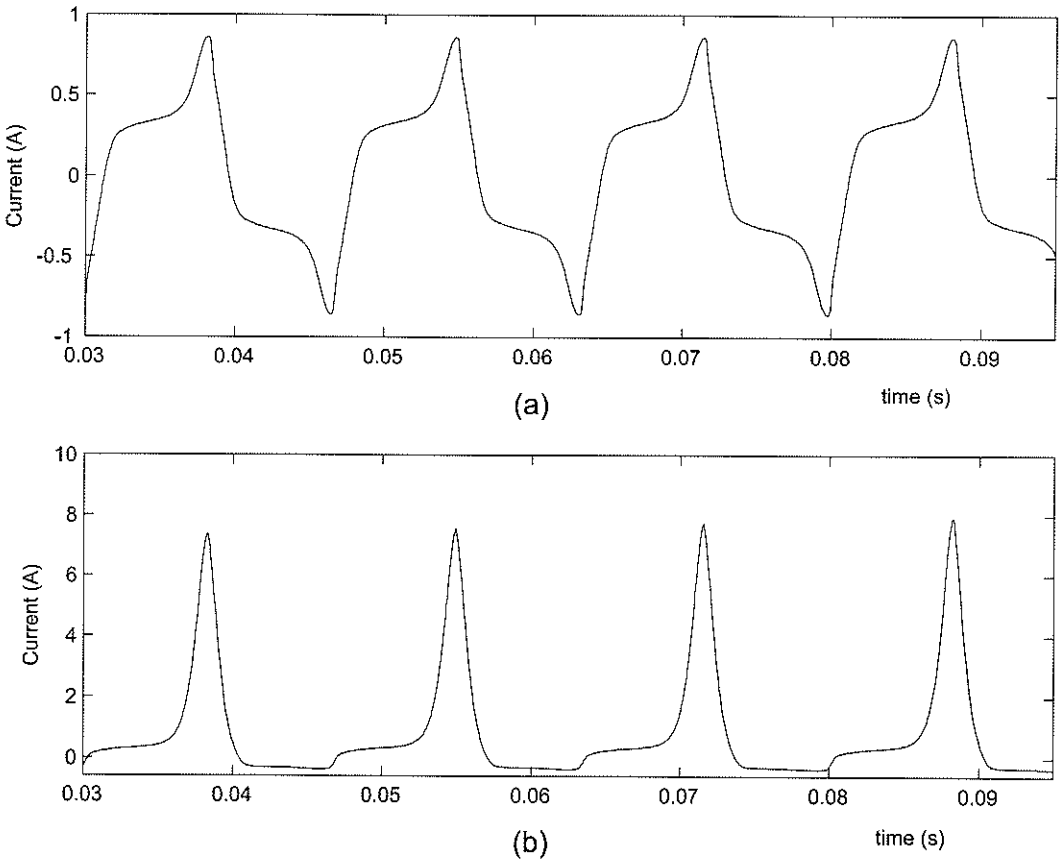

Figure 1.5: Transformer magnetizing current; (a) without GIC; (b) with GIC, undergoing half cycle saturation

There have been many reported cases of undesirable effects on power systems during GIC events. Some of the most significant effects are described below.

- Maloperation of relays due to distorted waveshapes. This undesired operation can be of three types; i.e. detection of a non-existent fault, failure to detect a fault, or failure to detect a fault in an adequate time. Reference [6] has provided

a detailed review of protection relay maloperations that have been related to geomagnetic disturbances during the 1989 - 1992 period.

- Overloading of capacitor banks and static var compensators (SVC) due to significant harmonic currents and possible tripping of protection due to over loading. The system collapse of Hydro-Quebec was triggered by the loss of static var compensators [7].

- Large reactive power consumptions causing intolerable voltage depressions; this was first reported in 1940 [4].

- Severely stressed operation of power transformers. A large number of power transformer failures have been attributed to GIC events [6].

- Overloading of filters on the ac side of HVDC converter terminals and the interaction of ac/dc harmonics in the presence of GIC [19].

- Excessive localized heating and mechanical vibrations due to positive and negative sequence harmonic currents in the generators [20].

In addition to the disruption of the power transmission network, solar phenomena can interfere with utility communication systems as well.

1.3 Vulnerability of Power Systems

GIC are a problem in high geomagnetic latitude areas in Canada, parts of USA, and some Nordic countries. Typically these are the areas in which magnetic storms are the largest and the most frequent. Factors increasing the vulnerability of the power system that are in the regions affected by geomagnetic disturbances include;

- transmission lines of interconnected systems spanning longer distances,
- transmission of higher levels of power over longer distances that require voltage support using capacitor banks or static var compensators, and
- use of single phase units in three phase extra high voltage (EHV) power transformer banks, that are more susceptible to GIC than the three phase units [5][21].

Presently, the North American power transmission networks consist of long transmission lines that span thousands of kilometers. In addition, bulk power transfer within large power pools have become a daily routine in the electricity market. Therefore, an earth surface potential of a few volts per kilometer could cause a large flow of GIC and poses a threat to the security and the stability of the electrical power system.

In addition, vulnerability of a power system to geomagnetic disturbances is increased when the system is more heavily loaded. Increasing power demand and industry deregulation have both led to power systems being operated closer to their limits making them more vulnerable to outside disturbances. A distinctive feature of GIC effects on power systems is that the problems occur simultaneously on many parts of the system. This is contrary to other types of power system problems, i.e. lighting strikes or equipment failures, which are more localized.

1.3.1 Vulnerability of Power Transformers

Extra High Voltage (EHV) systems with grounded wye transformer banks provide conducting paths for GIC. However, different core and winding configurations respond differently to saturation caused by GIC. Therefore, the susceptibility of single phase

banks and three phase transformers have been categorized in the order of decreasing sensitivity as follows [6][21];

1. Single phase, shell or core form design

2a. Three phase shell form design

2b. Three phase core form, five leg core design

3. Three phase core form, three leg core design

1.3.2 A system collapse: Hydro-Quebec

The complete blackout of Hydro-Quebec system during the GIC event of March 13, 1989 gives an example of how vulnerable a power system can be. Hydro-Quebec's 735 kV transmission lines span about 1000 km between the load centres and major generation centres. This system with long transmission lines depends on static var compensators and synchronous condensers for stability.

Just before the event, the system load was 21,500 MW, with exports totalling 1950 MW. The bulk of the power transfer was through the 735 kV transmission network. At the inception of the effects of this storm, a high content of harmonic voltages and currents had been observed in part of the network (La Grande network). This was followed by a high voltage asymmetry that reached about 15%. Within less than a minute, seven static var compensators on line in the La Grande network had tripped one after the other. With loss of the static var compensators, a sudden voltage drop was recorded (0.2 pu) and, as a result, 5 transmission lines carrying 9450 MW to Montreal tripped out. This resulted in a rapid drop in frequency at load centre substations. At this stage, automatic under frequency load-shedding controls functioned, but these controls were not designed for a recovery from a loss of

generation equivalent to about half of the system load. Therefore the rest of the grid collapsed in less than a minute [7]. During this event, extensive damage to several transformers, thyristor and capacitor banks was also reported from Hydro-Quebec and many other utilities across Canada and USA. The aftermath of this event triggered many studies to model the GIC phenomenon and its effects on power systems.

Another area of rapid development was in the area of storm forecasting using advanced satellites. Facilities for real time monitoring for alerts and warnings have become available. With the present technology, a space explorer[9] could alert the onset of a severe geomagnetic storm about one hour in advance [22][23].

1.4 Modelling a GIC Event

Historical records of GIC events have shown the potential for disastrous effects on power systems. However, every solar event does not produce a geomagnetic disturbance on the earth, and therefore it makes forecasting of the impact of GIC events very difficult. Thus various studies have been carried out to analyze this phenomenon, and hence to predict the worst case scenario during an event. In general, modelling of a GIC event can be classified into two categories.

1. Computation of the earth-surface potential (ESP), that involves the consideration of the complex interaction between the solar phenomena and the earth's magnetic field. This can be described as a geophysical problem.

2. Computation of GIC in a power system and its effects due to the earth surface potential. This can be described as an electrical engineering problem.

[9]If the distance is just right, about 4 times the distance to the moon or 1/100 the distance to the sun, a spacecraft will need just one year to go around the sun, and hence it will keep its position between the sun and the earth. That position is known as the Lagrangian Point L_1, named after the French mathematician who pointed it out, Joseph Louis Lagrange.

In the first category, the calculation of the earth surface potential has been carried out using mathematical models with varying degree of complexities [15][24][25]. All of these models have made several assumptions, such as the interaction with the magnetosphere, the form of the auroral electrojet, conductivity of the earth, and form of the electric field etc.

The second category involves the analysis of a power system during a GIC event. It describes the vulnerability of a system for a given GIC, and the possible effects that may be experienced. Even with the present technology, these studies are extremely important as the advanced alerts and warnings leave about an hour for any precautionary measures to be taken.

The effect of GIC on a power system can be analyzed using electromagnetic transient simulation programmes and power system stability analysis programmes. These studies will reveal the vulnerability of a power system to GIC, such as the effect of increased reactive power demand, voltage stability, sensitivity of the protective relays and other equipment etc. The results of these studies are being used as the basis of determining the steps to be taken to mitigate the effects of GIC and recommend guidelines to be followed during an event by the system operators. Utilities and power pools have developed both general system guidelines and specific operating procedures that may be unique to their particular situations. These operating guidelines may be designed to protect a specific equipment from damage, or to protect the security of the power system as a whole.

These guidelines are usually based on simulation studies carried out to predict the worst case scenario during a GIC event, that may be based on historical data or the maximum predicted values. Thus electromagnetic transient simulation studies of GIC events are very useful in this endeavor.

1.4.1 Electromagnetic Transient Simulation of a GIC Event

In order to model the GIC phenomenon in an electromagnetic transient simulation programme, the modelling of iron core non-linearities of the power transformer is important since the source of harmonic generation is the transformer itself. Therefore, a transient simulation study to analyze the effects of GIC on power systems requires accurate representation of the magnetizing characteristics of transformers. The presence of GIC causes half cycle saturation of the iron core, and hence modelling of the waveform of magnetizing current requires taking the shape of the B-H loop into account.

In addition, the correct representation of the hysteresis is important so that it handles long term remanence and recoil loops [17]. This is due to the fact that the extent of the half cycle saturation depends on the history of the state of the magnetic core. Hence an accurate representation of the status of the magnetic core cannot be modelled without taking the history into account.

1.5 Objectives of this dissertation

A general difficulty in modelling the magnetization curves of ferromagnets arises due to the possibility of having a large number of magnetizations depending on the history of a sample. Therefore in order to characterize the material behaviour, a model has to include not only the major loop, but also the associated curves such as minor loops.

During the past decade a considerable effort has been devoted to the development of simulation models of power transformers [26]-[30]. These models contain a wide range of modelling details of the iron core of the transformer with varying degree of complexities. Many of these attempts are curve fits, which ignore the underlying physics of the material behaviour. In short time simulations, these piecewise linear

solutions of saturation can give the impression that they handle remanence because the system time constants maintain the magnetization over several hundreds of milliseconds. However, over time scales of seconds the flux will decay to zero. Hence, the need exists for a transient simulation model of a power transformer for use in GIC studies, that accurately represents the magnetizing characteristics, including the long term remanence and recoil loops of the iron core.

Objectives

The main objective is to develop a new transformer model, and to use that in simulation studies to analyse the effects of GIC on a power system. This can be divided into the following tasks.

1. Development of the new model.

- Develop a new simulation model of a power transformer for use in electromagnetic transient simulation studies. The new model will address the requirements of carrying out a GIC study, such as an accurate representation of hysteresis characteristics that includes recoil loops and long term remanence. In a typical transformer model, it is usually possible to initialize the remanence, however it requires outside intervention whereas the new model presented here will do it automatically.

- Develop an algorithm to incorporate this new model into an electromagnetic transient simulation programme such as EMTP, PSCAD/EMTDC. This enables the new model to be used along with existing models such as transmission line models to carry out system studies.

- Develop a methodology to determine the parameters of the model to represent a given transformer using measured and name plate data.

- Validate the new model by comparing simulation results with recorded waveforms.

2. GIC studies using the new model.

- Model a section of a power system using an electromagnetic transient simulation programme.

- Validate the simulation model by comparing simulation results with recorded data. This involves proper initialization of the simulation model to represent the conditions of the actual system.

- Determine the sensitivity of the simulation results to (a) the remanent flux in the core, (b) the history of the quasi dc current, and (c) the parameters in the simulation model of a power system.

1.6 Overview of this dissertation

This dissertation consists of six Chapters. Chapter 2 describes the development of the new transformer model. A mathematical model based on the physics of ferromagnetism is used as the basis to represent the magnetization characteristics of the transformer. Eddy current effects are also incorporated into the same model, so that the simulated B-H loop exhibits frequency dependency. This discussion presents the theory behind this model and describes how it is incorporated into a transient simulation model of a power transformer. The new model is implemented with PSCAD/EMTDC

to show how this model could be incorporated into an existing model of an electromagnetic transient simulation programme.

Chapter 3 focuses on the validation of the new model, where the simulation results are compared with laboratory recordings. A good agreement is achieved between recorded and simulated data.

Once the simulation model is validated, simulation studies are carried out to analyze a GIC event using the new transformer model. A power system simulation model of Manitoba Hydro's Dorsey substation and the 500 kV transmission line from Dorsey, Manitoba to Forbes and Chisago in Minnesota is considered for this study.

Effects of GIC on this long transmission line dates back to 1980 [31]. However, with the introduction of series compensation, the present vulnerability of this line could be considered as low. Meanwhile, in the absence of recent recordings during a GIC event, simulation studies carried out in reference [17] and [32] are used as the basis of this analysis. The GIC event of 5^{th} October 1993 was considered for validating a recorded event using the new transformer model. Chapter 4 describes the comparisons carried out using the recorded waveforms of this event.

Chapter 5 focuses on determining the sensitivity of the simulation results to the remanent flux in the core, and to the history of the quasi-dc current. In addition, the sensitivity of the simulation to parameter variation in the model of the power system is also considered.

Finally, Chapter 6 presents general conclusions on the work presented in this dissertation highlighting the major contributions.

Chapter 2

A New Transformer Model for GIC Studies

Development of a new transient simulation model of a power transformer for use in GIC studies is presented in this chapter. A mathematical model based on the physics of ferromagnetism is used as the basis of this model to represent the magnetization characteristics of the iron core of a transformer.

2.1 Background

There have been numerous approaches to modelling ferromagnetic hysteresis loops in simulation models of power transformers. A bibliographic review of the hysteresis models presented during the past three decades is given in reference [33]. Many of these attempts are curve fits, which ignore the underlying physics of the material behaviour. At the other extreme, micromagnetic methods consider all known energies on a very small scale and find the domain configuration that gives the minimum energy. In general intermediate solutions models, which can relate micro-structural

parameters to the macroscopic responses of the material to outside fields are more suitable for time domain simulations [34]. Four magnetization models are now considered as classical. They are the Stoner-Wolhfarth model, the Jiles-Atherton model, the Globus model, and the Preisach model. The methods each model uses to simulate the magnetization mechanisms, their advantages and disadvantages are discussed in reference [34].

A hysteresis model based on the Jiles-Atherton (JA) phenomenological model of a ferromagnetic material [35] is presented here. This has been used in reference [36] in the simulation of current transformers, and it has been shown that the hysteresis model based on the JA theory accurately represents the long term remanence and recoil loops in the transformer cores.

There exists a wide variety of representations for hysteresis and eddy current losses in transformer models used for power system transient studies. The most commonly used method to represent losses is to add a shunt resistance across one winding as in reference [29]. A frequency dependent resistance matrix is used in reference [37] to model the effects produced by eddy currents. A different approach is used in reference [27], where the relationship between an equivalent eddy current field and the rate of change of flux density has been experimentally obtained to represent losses in current transformers. In the new model, we have extended the hysteresis model based on the JA theory to incorporate the effects of classical eddy current loss and excess or anomalous loss [38]-[40].

In the present study, the winding capacitance is neglected, because the GIC phenomena studied are of low frequency. Thus, the transformer core model presented in reference [30] was used as the basis of this work. The simulation model of a single phase two winding transformer is considered in section 2.2 to describe how a

typical transformer model is implemented in an electromagnetic transient simulation programme. In addition, its representation of saturation is described to show how the new hysteresis model can be incorporated into an existing model. Even though this discussion focuses on a single phase two winding transformer, this algorithm is capable of representing the hysteresis characteristics of a multi-limb, multi-winding transformer model in an electromagnetic transient simulation programme.

A brief description of the Jiles - Atherton phenomenological model of a ferromagnetic material is presented in section 2.3. The hysteresis model based on the JA theory is extended in section 2.4 to incorporate the eddy current effects, and section 2.5 describes the simulation algorithm of the new transformer model that is implemented in the electromagnetic transient simulation program EMTDC.

2.2 Review of the Transformer Core Model

A brief review of the transformer core model described in reference [30] is presented in this section, and it also explains how the new hysteresis model is incorporated into this core model.

The core model of a single phase two winding transformer uses the magnetic circuit shown in Fig.2.1. The two windings of the transformer are drawn on separate limbs of the core for clarity whereas, in reality, both windings are wound on the same limb. The magnetic equivalent circuit of the transformer is given in Fig.2.2.

The branches of the magnetic equivalent circuit represent the assumed paths of flux, i.e. the transformer winding limbs (ϕ_1 and ϕ_2), the leakage (ϕ_3 and ϕ_4), and the yokes (ϕ_5). The two winding transformer has two MMF sources, $N_1 i_1(t)$ and $N_2 i_2(t)$ to represent individual windings. P_1 and P_2 represent the permeance of the transformer winding limbs, and P_5 represents the permeance of the transformer yokes.

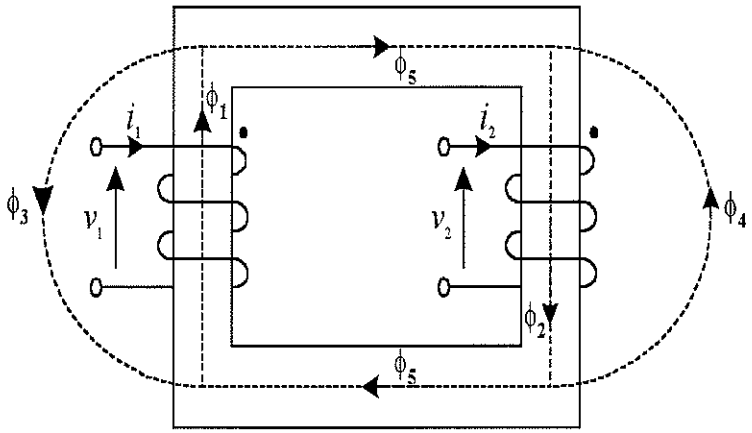

Figure 2.1: Single phase two winding transformer flux paths

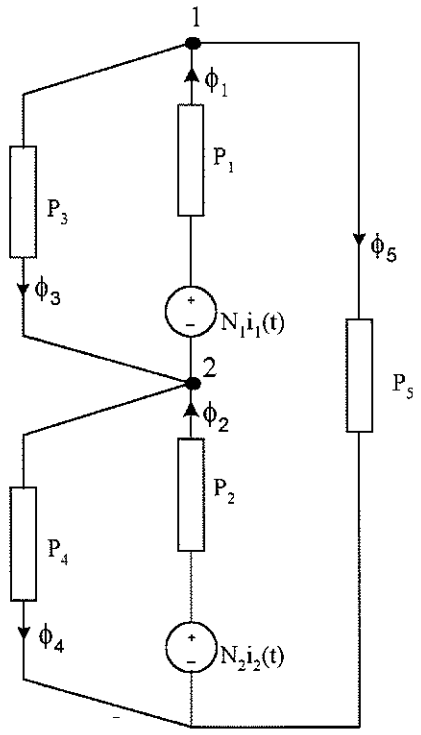

Figure 2.2: Magnetic equivalent circuit for a single phase two winding transformer

P_3 and P_4 represent the permeances of the leakage paths.

In an electromagnetic transient simulation program, the representation of a transformer begins with the calculation of the transformer inductance matrix (**L**). In this model, the transformer inductance matrix has been derived using the magnetic equivalent circuit in Fig.2.2. The following section describes how the transformer inductance matrix (**L**) is calculated using this magnetic equivalent circuit.

2.2.1 Calculation of the transformer inductance matrix

The transformer inductance matrix is calculated based on the magnetic equivalent circuit of a given transformer. The description of the single phase two winding transformer presented in the previous section is considered to describe the calculation of the inductance matrix (**L**).

It is assumed that the total length of core surrounded by windings (l_w) has a uniform cross-sectional area A_w. It is also assumed that the upper and lower yokes have the same length (l_y)and cross-sectional area (A_y). Both yokes are represented by a single equivalent branch of length $l_3 = 2l_y$, and area $A_3 = A_y$.

The branch node connection matrix $[A]$ describes the sum of the flux at each node, i.e. the total flux at each node must add up to zero (2.1 - 2.3). Therefore, this representation includes information about the configuration of the core of transformers; i.e. single phase, three phase three limb, or three phase five limb transformers.

$$\text{at node } \mathbf{1}, \qquad \phi_1 - \phi_3 - \phi_5 = 0 \tag{2.1}$$

$$\text{at node } \mathbf{2}, \qquad -\phi_1 + \phi_2 + \phi_3 - \phi_4 = 0 \tag{2.2}$$

These equations can be represented as in (2.3), where $[A]$ is the branch node

connection matrix, and $\boldsymbol{\phi}$ is the vector of branch flux.

$$[A]^T \boldsymbol{\phi} = \mathbf{0} \tag{2.3}$$

$$\text{where} \quad [A]^T = \begin{bmatrix} 1 & 0 & -1 & 0 & -1 \\ -1 & 1 & 1 & -1 & 0 \end{bmatrix} \tag{2.4}$$

$$\boldsymbol{\phi} = \begin{bmatrix} \phi_1 \\ \phi_2 \\ \phi_3 \\ \phi_4 \\ \phi_5 \end{bmatrix} \tag{2.5}$$

The MMF across each branch of the circuit is written in the vector form as in (2.6), where $\boldsymbol{\theta}$ is the vector of branch MMFs, $[N]$ is a diagonal matrix containing the number of turns in each winding, $[R]$ is a diagonal matrix containing the reluctance in each branch and $\boldsymbol{\phi}$ is the vector of the branch flux. The MMF across each branch (θ_i) of the magnetic equivalent circuit is shown in Fig.2.3.

$$\boldsymbol{\theta} = [N]\mathbf{i} - [\ R]\boldsymbol{\phi} \tag{2.6}$$

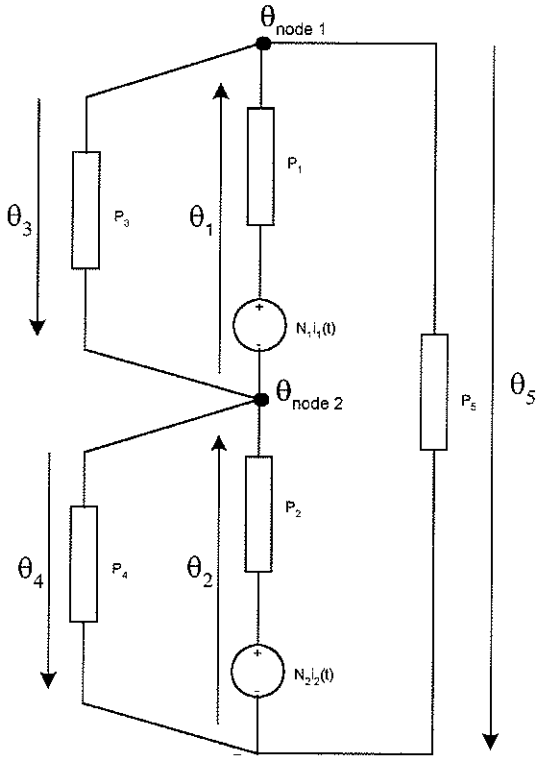

Figure 2.3: Branch MMFs

In addition, the vector of nodal MMF ($\boldsymbol{\theta}_{node}$) is related to the vector of branch MMF ($\boldsymbol{\theta}$) as in (2.7).

$$[A]\,\boldsymbol{\theta}_{node} = \boldsymbol{\theta} \tag{2.7}$$

$$\text{where} \quad \boldsymbol{\theta}_{node} = \begin{bmatrix} \theta_{node1} \\ \theta_{node2} \end{bmatrix} \tag{2.8}$$

$$\boldsymbol{\theta} = \begin{bmatrix} \theta_1 \\ \theta_2 \\ \theta_3 \\ \theta_4 \\ \theta_5 \end{bmatrix} \tag{2.9}$$

Then (2.6) can be rewritten as in (2.10) where $[P]$ is the branch permeance matrix and, using these relationships, the transformer admittance matrix and the magnitudes of the current injected can be calculated as follows.

$$\boldsymbol{\phi} = [P]\left([N]\mathbf{i} - \boldsymbol{\theta}\right) \tag{2.10}$$

$$\underbrace{[A]^T\boldsymbol{\phi}} = [A]^T[P][N]\mathbf{i} - [A]^T[P]\underbrace{\boldsymbol{\theta}} \tag{2.11}$$

$$\mathbf{0} = [A]^T[P][N]\mathbf{i} - [A]^T[P]\ [A]\,\boldsymbol{\theta}_{node} \tag{2.12}$$

$$\boldsymbol{\theta}_{node} = \left([A]^T[P]\ [A]\right)^{-1}[A]^T[P][N]\mathbf{i} \tag{2.13}$$

Multiplying (2.13) by $[A]$ gives;

$$\boldsymbol{\theta} = [A]\left([A]^T[P]\ [A]\right)^{-1}[A]^T[P][N]\mathbf{i} \tag{2.14}$$

substituting (2.14) in (2.10) gives;

$$\boldsymbol{\phi} = [M][N]\mathbf{i} \tag{2.15}$$

$$\text{where } [M] = [P] - [P][A]\left([A]^T[P]\ [A]\right)^{-1}[A]^T[P] \tag{2.16}$$

The vector of branch flux ($\boldsymbol{\phi}$) is partitioned into the set that contains the branches associated with each transformer winding as some of the elements in the vector of winding current $\mathbf{i}$ are zero. Therefore (2.15) becomes (2.20), where $\boldsymbol{\phi}_{ss}$ is the vector containing the winding flux (2.17), $\mathbf{i}_{ss}$ is the vector containing the winding current (2.18), $[N_{ss}]$ is a diagonal matrix of winding turns (2.19), and $[M_{ss}]_{2x2}$ is a square

permeance matrix.

$$\boldsymbol{\phi}_{ss} = \begin{bmatrix} \phi_1 \\ \phi_2 \end{bmatrix} \tag{2.17}$$

$$\mathbf{i}_{ss} = \begin{bmatrix} i_{s1} \\ i_{s2} \end{bmatrix} \tag{2.18}$$

$$[N_{ss}] = \begin{bmatrix} N_1 & 0 \\ 0 & N_2 \end{bmatrix} \tag{2.19}$$

Thus the transformer inductance matrix is obtained as in (2.21). Similarly, the transformer admittance matrix ($\mathbf{Y}_{ss}$) is calculated from the transformer inductance matrix, $Y_{ss} = \frac{\Delta t}{2L}$, where Δt is the time step and $\mathbf{L}$ is the transformer inductance matrix (2.22).

$$\boldsymbol{\phi}_{ss} = [M_{ss}][N_{ss}]\mathbf{i}_{ss} \tag{2.20}$$

$$\mathbf{L} = [N_{ss}][M_{ss}][N_{ss}] \tag{2.21}$$

$$\mathbf{Y}_{ss} = \frac{\Delta t}{2}\left([N_{ss}][M_{ss}][N_{ss}]\right)^{-1} \tag{2.22}$$

A further development to this transformer model has been presented [41], in which the necessity to input detailed core data such as the length (l) and the cross-sectional area (A) of each limb, and the actual number of turns (N) in each winding has been eliminated. In this method, instead of calculating the transformer inductance matrix using the actual values of N, A, and l, an equivalent inductance matrix is calculated by fixing the value of N, and calculating the appropriate values of A and l, such that the original inductance matrix is obtained. In order to illustrate this method let us consider two inductors, L_1 and L_2 given in Fig.2.4. The permeance P_1 of the

inductor L_1 is different from the permeance P_2 of the inductor L_2 because of the different number of turns (N_1 and N_2), different cross sectional areas (A_1 and A_2), and different lengths (l_1 and l_2). However, the two inductors can exhibit the same inductance if the both inductors have the same values for the product of NA and the ratio of $\frac{N}{l}$ (2.25 - 2.27). Thus, in this representation, the number of turns have been assigned the values of the primary and secondary winding voltages and the corresponding values of A and l are calculated appropriately.

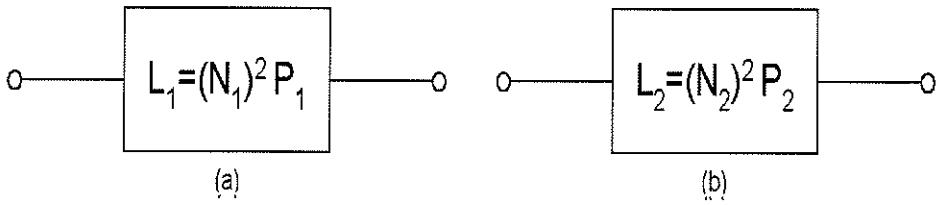

Figure 2.4: Matched Inductors

$$L_1 = N_1^2 P_1 = \mu \; N_1 A_1 \frac{N_1}{l_1} \tag{2.23}$$

$$L_2 = N_2^2 P_2 = \mu \; N_2 A_2 \frac{N_2}{l_2} \tag{2.24}$$

$$\text{if} \quad N_1 A_1 = N_2 A_2 \tag{2.25}$$

$$\text{and} \quad \frac{N_1}{l_1} = \frac{N_2}{l_2} \tag{2.26}$$

$$\text{then} \quad L_1 = L_2 \tag{2.27}$$

2.2.2 Existing model

The representation of saturation in a transformer model of EMTDC is considered to show how a typical transient simulation programme implements saturation [41]. A detailed review of this model was presented in the previous section. The same model is considered as an example in the following section to describe how the Jiles

-Atherton theory is incorporated into a power transformer model of a typical transient simulation programme.

In this model, saturation is represented with a current source connected across each winding as in Fig.2.5. The current source representation is used since it does not involve change to and inversion of the subsystem matrix during saturation [42]. Meanwhile, a piece-wise linearly interpolated B-H characteristic curve has been used to model saturation in the transformer core (Fig.2.6).

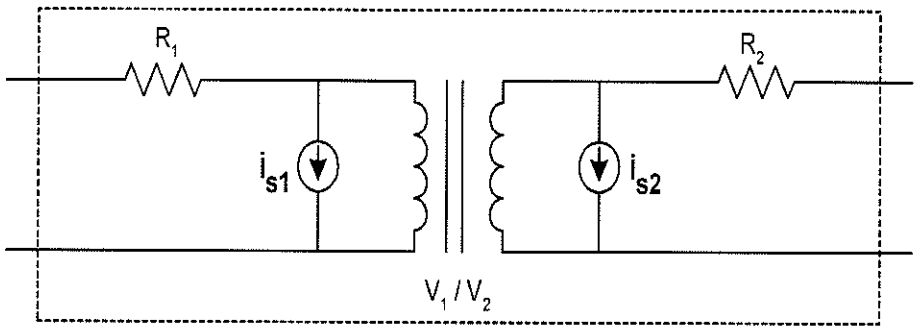

Figure 2.5: Representation of saturation in EMTDC

The simulation algorithm begins with calculation of the winding-limb fluxes (ϕ_i) using the winding voltages (v_i), where $i = 1$ .. number of windings. The fluxes in each branch, and the flux densities (B_i) of winding limbs and the yoke are calculated using the calculated values of the flux (ϕ_i). The differential permeability (μ_{dif_i}) and the magnetic field strength (H_i) of the branches that represent the iron core are calculated using the piece-wise linearly interpolated B-H curve at the flux density B_i (2.28). Then the permeance of these branches is calculated to update the branch

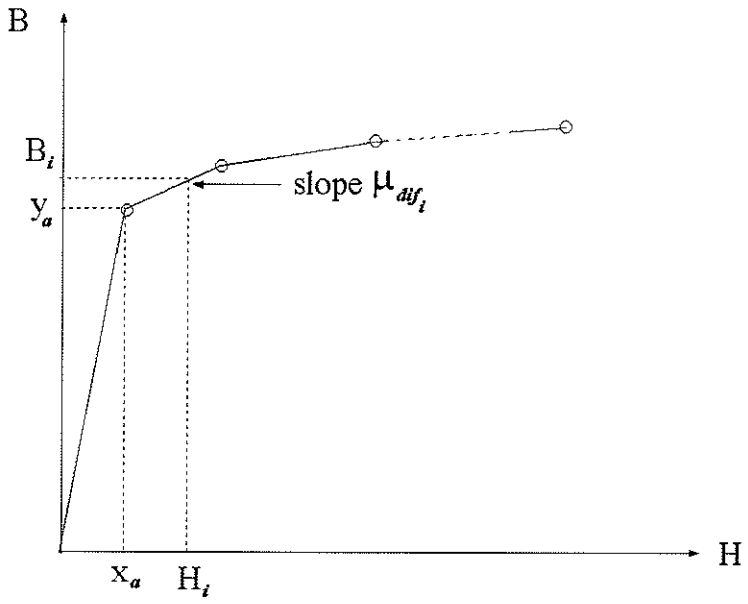

Figure 2.6: Saturation curve of the existing model

permeance matrix $\mathbf{P}$ (2.29). Furthermore

$$H_i = \frac{B_i - y_a}{\mu_{dif_i}} + x_a \tag{2.28}$$

$$P_i = \frac{\phi_i}{H_i l_i} \text{ or } P_i = \frac{\mu_i A_i}{l_i} \tag{2.29}$$

In addition, matrix $[M_{ss}]$ is updated, and finally $\boldsymbol{\phi}_s$ and $([M_{ss}][N_{ss}])^{-1}$ are multiplied to obtain $\mathbf{i}_s$. Thus, the magnitudes of the current injected for the present time step are calculated as in (2.30). The elements of $\mathbf{i}_s$ contain the magnitudes of the current injected across each winding (2.18). In an n winding transformer, $\mathbf{i}_s$ contains the magnitudes of the n current sources, that are injected across the corresponding windings.

$$\mathbf{i}_s = \boldsymbol{\phi}_s \left(\mathbf{M}_{ss}\mathbf{N}_{ss}\right)^{-1} \tag{2.30}$$

2.2.3 The new model : Incorporating the JA Theory

The aim of this work is to develop an improved transformer model to be used in GIC studies. The piece-wise linear representation of saturation does not properly represent the increased levels of harmonic current when the transformer undergoes half cycle saturation. In addition, this representation does not model the long term remanence and recoil loops in the core.

The new model presented here uses the Jiles - Atherton theory of a ferromagnetic material to represent the hysteresis characteristics of the transformer core. Instead of using a piece-wise linearly interpolated curve to model the B-H characteristics, we have incorporated the differential equations described in the JA theory to model the hysteresis characteristics of the transformer core.

The saturation model described in the previous section uses a piece-wise linear B-H characteristic to calculate the differential permeability (μ_{dif_i}) and magnetic field strength (H_i) of the branches that represent the iron core. In the new model, values of these variables are calculated using the JA theory. This is followed by the calculation of branch MMFs and branch permeances. Then the simulation algorithm continues to follow the main algorithm of the existing model, where the transformer inductance matrix is calculated using (2.21). Similarly, the transformer admittance matrix can be calculated using (2.22), and the magnitude of the currents injected is calculated using (2.30). Therefore an interface between the JA theory and the existing transformer model is established.

A brief review of the Jiles-Atherton theory is presented in the following section. This also describes the basis of the two differential equations used in this simulation model. The simulation model based on these equations is extended in section 2.4 to incorporate eddy current effects, and section 2.5 describes the simulation algorithm

that was outlined in this section.

2.3 Jiles - Atherton Theory

The Jiles Atherton (JA) theory is as an attempt to create a quantitative model of hysteresis based on a macromagnetic formulation. The model describes isotropic polycrystalline materials (multi-domain grains) with domain wall motion as the major magnetization process. If the grains are randomly oriented in space it is known as an isotropic material. The more common case is when the crystals have a preferred orientation, known as anisotropy.

Considering the domain wall motion, two differential equations have been derived. They represent the irreversible differential susceptibility and reversible differential susceptibility. The solution of the two differential equations, combined with an appropriate choice of function for the anhysteretic magnetization, leads to a normal sigmoid shaped hysteresis curve [35].

2.3.1 Background

If a specimen of iron or steel is subjected to a magnetic field that is increased from zero to a higher value and then decreased again, it was observed that the plot of flux density, also known as magnetic induction (B) vs magnetic field strength (H) will not retrace the original curve. This phenomenon was named hysteresis by Ewing in 1881 [43]. This was one of the first attempts to explain ferromagnetic phenomena in terms of forces between atoms. Assuming each atom was a permanent magnet free to rotate in any direction, he described how the orientation of the various magnets, with respect to the field and to each other, was entirely due to mutual magnetic forces [44][45].

Some years after Ewing's work, one of the most important advances in the understanding of ferromagnetism was made by Weiss in 1907 [46]. This theory was based on the earlier work of Ampere, Weber and Ewing, in which Weiss suggested the existence of magnetic domains in ferromagnets. He also established that (a) atomic moments were in permanent existence, (b) the atomic moments were ordered (aligned) even in the demagnetized state, (c) it was the domains that were randomly oriented in the demagnetized state, and (d) the magnetization process consisted of reorienting the domains so that either more domains were aligned with the field, or the volume of domains aligned with the field was greater than the volume of domains aligned against the field. Subsequent studies have confirmed that the magnetization of a ferromagnetic material is changed by a change in the direction of magnetization of the domain (domain rotation) or a change in the volume of the domain (moving boundary) [47][48][49].

The boundary between domains is not sharp on an atomic scale. A transition layer separates adjacent domains magnetized in different directions. Therefore, two domains can have magnetic moments in different directions on either side of the domain boundary, with the transition region in which the magnetic moments realign between the domains belonging to neither domain (Fig.2.7)[47]. This transition layer is named after Bloch, who was the first person to study the nature of this layer in 1932.

The changes in magnetization arising from the application of a magnetic field to a ferromagnetic material can be either reversible or irreversible depending on the domain process involved. A reversible change occurs when the magnetization returns to its original value on the removal of a magnetic field. In ferromagnetic materials this usually occurs during small increments of the field. More often, both reversible

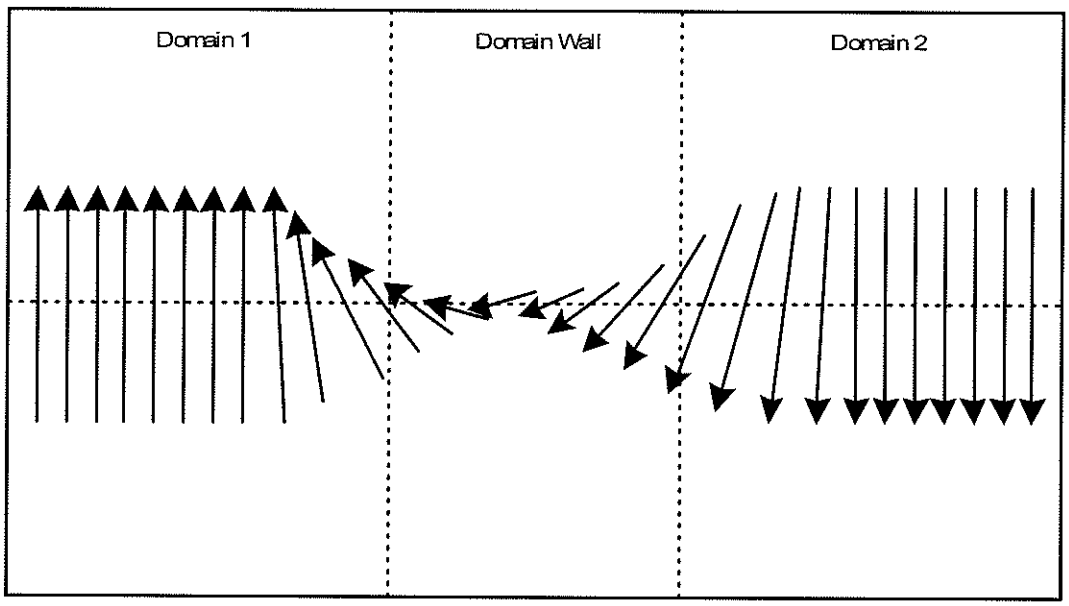

Figure 2.7: Alignment of individual magnetic moments within a 180^0 domain wall

and irreversible changes occur, so that on the removal of the field, the magnetization does not return to its initial value. Thus under these conditions, hysteresis is observed if the field is cyclic.

2.3.2 Hysteresis and related properties

A number of magnetic properties of the material characterize the general features of the hysteresis loop. It has been observed that if a specimen of iron or steel is subjected to cold working, the hysteresis loss and the coercivity increase. In addition, the introduction of other non-magnetic elements to iron, such as carbon in making steel, also increases the hysteresis loss and coercivity. Therefore, it appears that imperfections in the material cause an increase in the energy lost during the magnetization process in the form of an internal friction. Another mechanism which gives rise to hysteresis is caused by magnetocrystalline anisotropy[47], i.e., a crystal is characterized by the

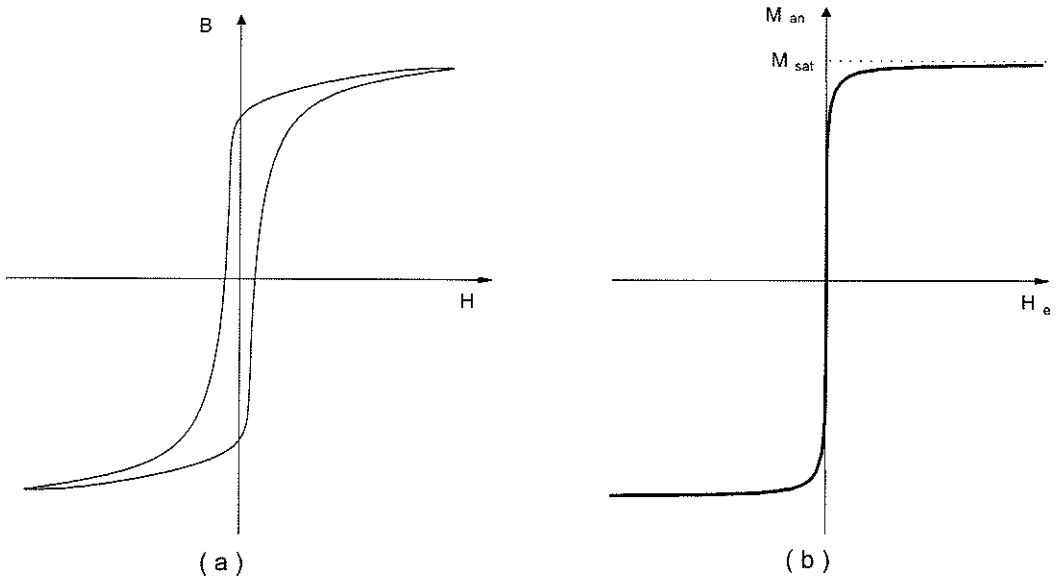

Figure 2.8: (a) Major loop; (b) Anhysteretic magnetization curve.

periodic arrangement of its elements (atoms, ions) in space. The anisotropy energy tends to make the magnetization of domain line up along certain crystallographic axes.

Based on the hypothesis that the imperfections cause hysteresis, if the material was free of all the imperfections it would be hysteresis free (ignoring the anisotropic effects). Then the magnetic induction would be a single valued function of the magnetic field called the anhysteretic magnetization curve (Fig.2.8b) [48]. The magnetization would be reversible, thus each point on the anhysteretic curve corresponds to the domain configuration that gives the lowest possible energy (global minimum) for a given external field.

Parameter Characterization

The coercive force is one of the most sensitive properties of ferromagnetic materials that can be controlled. Therefore the width of the loop across the H axis, (which is twice the coercivity H_c) is an independent parameter since this can be altered during manufacturing process. In addition, the saturation magnetization defines the upper limit to the magnetization that can be achieved. The height of the curve along the B axis (remanence B_R) is also an independent parameter. The orientation of the entire hysteresis curve, that is the slope of the curve at the coercive point, can be changed independently of the other parameters. In addition, hysteresis loss and the initial permeability may also be independent parameters.

The above description has highlighted some of the most important parameters that characterize the general features of the hysteresis loop. However, there is no general form of hysteresis loop for ferromagnetic materials. There does exist a shape of hysteresis loop that occurs frequently in practice, which is known as the 'Sigmoid' shape Fig.2.8a. The Jiles Atherton theory describes a hysteresis model that generates the familiar sigmoid shaped hysteresis loops by considering impedances to domain wall motion caused by pinning sites encountered by the domain walls as they move. [35].

2.3.3 Review of the mathematical model

The Jiles - Atherton theory describes the relationship between the magnetization, M, and the magnetic field intensity, H, for the core material. The flux density B, also called the magnetic induction, consists of two contributions. The magnetic induction in free space ($\mu_0 H$), and the contribution to the induction from the magnetization of a material ($\mu_0 M$). The relationship between the flux density B, M and H is given by

(2.31), where B is in Tesla and H and M[1] are in Amperes per meter.

$$B = \mu_0(M + H) \tag{2.31}$$

Considering the domain wall motion, two differential equations have been derived in the Jiles - Atherton theory. These represent the irreversible and reversible magnetization processes. The anhysteretic magnetization curve is derived using a mean field approach, in which the magnetization of any domain is coupled to the magnetic field intensity, H, and the bulk magnetization, M. The solution of the two differential equations, combined with an appropriate choice of function for the anhysteretic magnetization, leads to a normal sigmoid shaped hysteresis curve [35].

The basis of this model is the fact that the anhysteretic magnetization is the lowest energy state of domain configuration. Thus, for a given field, if the magnetization M is greater than the anhysteretic magnetization M_{an}, then the domain walls will experience a force which tends to reduce the magnetization. Similarly, if the magnetization M is less than the anhysteretic magnetization M_{an}, then the domain walls will experience a force which tends to increase the magnetization [35].

Irreversible Magnetization

The change in energy of a ferromagnet could be considered as a change in the magnetization or as a hysteresis loss. In the case where there is no hysteresis loss, the magnetization follows the anhysteretic curve, M_{an}. In general the changes in the irreversible magnetization can be expressed as in (2.32). This shows that the rate of change of magnetization with the field is proportional to the displacement from the

[1]The magnetic polarization or intensity of magnetization (I) is a related quantity used in the Kennelly convention with units of Tesla, whereas the Sommerfeld system of units uses magnetization (M) with units of A/m. Therefore $I = \mu_0 M$.

anhysteretic $M_{an}(H_e) - M_{irr}(H_e)$ [35].

$$\frac{dM_{irr}}{dH_e} = \frac{M_{an}(H_e) - M_{irr}(H_e)}{\frac{\delta k}{\mu_0} - \alpha[M_{an}(H_e) - M_{irr}(H_e)]} \tag{2.32}$$

Reversible Magnetization

The reversible magnetization reduces the difference between the prevailing irreversible magnetization, M_{irr}, and the anhysteretic magnetization, M_{an}, at the given field strength. This can be expressed as in (2.33) [35].

$$M_{rev} = c(M_{an} - M_{irr}) \tag{2.33}$$

$$\frac{dM_{rev}}{dH} = c(\frac{dM_{an}}{dH} - \frac{dM_{irr}}{dH}) \tag{2.34}$$

The coefficient c represents the reversible wall motion. This can be calculated from the ratio of the initial normal susceptibility to the initial anhysteretic susceptibility.

Total Magnetization

The total magnetization is an addition of the reversible and irreversible magnetizations. The JA theory describes an expression for the change in the total magnetization with the field ($\frac{dM}{dH}$) using the anhysteretic magnetization curve of the material.

The anhysteretic magnetization M_{an} at a given field H_e represents the global minimum energy state where H_e is the effective field (2.35). The α is the mean field parameter which represents interdomain coupling. The anhysteretic magnetization M_{an} can be expressed in the form as in (2.36), where M_{sat} is the saturation

magnetization and f is an arbitrary function of the effective field [35].

$$H_e = H + \alpha M \tag{2.35}$$

$$M_{an} = M_{sat} \;\; f(H_e) \tag{2.36}$$

The function f must have the following properties.

$$\lim_{H_e \to 0} f(H_e) = 0 \tag{2.37}$$

$$\lim_{H_e \to \infty} f(H_e) = 1 \tag{2.38}$$

$$\frac{dM_{an}}{dH_e} \geq 0 \text{ for all } H_e \tag{2.39}$$

The function given in (2.40) has been used in [36] in the simulation of current transformers, where a_1, a_2 and a_3 are constants. The same function is used to represent the anhysteretic characteristic of the core of the power transformer model, on the basis that the characteristics of the material is likely to be the same, i.e. grain oriented silicon steel. This function satisfies the conditions given in (2.37)-(2.39), provided that $a_1, a_3 > 0$ and $a_2 \geq a_1$

$$M_{an} = M_{sat} \frac{a_1 \; H_e + H_e^2}{a_3 + a_2 H_e + H_e^2} \tag{2.40}$$

$$\frac{dM_{an}}{dH_e} = M_{sat} \frac{a_1 a_3 + 2a_3 H_e + (a_2 - a_1) H_e^2}{(a_3 + a_2 H_e + H_e^2)^2} \tag{2.41}$$

The change in the total magnetization with field can be expressed as in (2.42). This can be expressed in terms of $\frac{dM_{an}}{dH_e}$ as in (2.43) . The parameters c, α and k are constants for the material being used and δ takes the value 1 or -1 based on the sign of $\frac{dH}{dt}$. The parameter k represents the coercivity.

The function $\frac{dM}{dH}$ in (2.43) can take some non-physical solutions when the magnetic field is reduced from the tip of the loop, when the magnetization M_{irr} is below the anhysteretic M_{an} in the first quadrant or above the anhysteretic in the third quadrant. Under these circumstances, the domain walls remain pinned on the defect sites and hence $\frac{dM_{irr}}{dH} = 0$. Therefore this function takes a modified form when the $(M_{an} - M)\delta$ becomes negative, as in (2.44) [36][50].

$$\frac{dM}{dH} = \frac{dM_{irr}}{dH} + \frac{dM_{rev}}{dH} \tag{2.42}$$

$$\frac{dM}{dH} = \frac{c\,\frac{dM_{an}}{dH_e} + \frac{M_{an}-M}{\frac{\delta k}{\mu_0} - \frac{\alpha(M_{an}-M)}{1-C}}}{1 - \alpha c\frac{dM_{an}}{dH_e}} \quad for\ all\ (M_{an} - M)\delta > 0 \tag{2.43}$$

$$\frac{dM}{dH} = \frac{c\,\frac{dM_{an}}{dH_e}}{1 - \alpha c\frac{dM_{an}}{dH_e}} \quad for\ all\ (M_{an} - M)\delta < 0 \tag{2.44}$$

The new transformer model uses the above equations to model the hysteresis characteristics of the iron-core. Therefore this representation properly represents the long term remanence, recoil loops and the hysteresis losses. This model can be extended to include the eddy current effects as described in the following section.

2.4 Core Loss

One of the most important parameters of a magnetic material used in ac applications is its losses. There are two forms of losses which occur in a transformer core. They are the hysteresis loss and eddy current loss. Hysteresis arises due to domain wall motion in the material. Eddy currents are induced in transformer core laminations by an alternating flux in the core and the losses arising from these eddy currents are frequency dependent [35][38]. The modelling of eddy current loss in a laminated iron

core is at least as important as modelling of hysteresis, as the eddy current losses are significantly greater than the hysteresis losses in a core material [51].

This section describes how the eddy current losses are incorporated into a simulation model of a transformer based on the Jiles-Atherton theory of ferromagnetic hysteresis. The hysteresis model presented in the previous section is extended to incorporate the effects of classical eddy current loss and excess or anomalous loss [38][40].

2.4.1 Background

The area of the hysteresis loop has an important physical meaning. It represents the amount of energy transformed into heat during one cycle of magnetization as given in (2.45), where P is the power loss per unit volume and f is the frequency of magnetization. If the area of the loop is measured on the same specimen for different magnetization frequencies f, a substantial increase in the area and change in the shape of the loop can be observed with increasing f.

$$\frac{P}{f} = \oint H \, dB \tag{2.45}$$

The most important advancement in understanding of losses in a ferromagnetic material dates back to the 1940s. During this period, it was generally recognized that the domains exist in an magnetized material and, when a magnetic field is applied, the change in the magnetization takes place by movement of boundaries between domains. However the shapes of domains, the ways in which the boundaries form and move with field and stress was first established experimentally by Williams, Bozorth, and Shockley in 1949 [52][53]. Since then all attempts to deal with the physical origin

of magnetic losses have taken domain wall motion explicitly into account.

The loss for a single moving wall was experimentally evaluated with a single domain boundary in a crystal of silicon iron by Williams, Shockley, and Kittel [54]. The results showed that the total losses in a ferromagnetic material are often several times greater than the eddy current and hysteresis losses calculated assuming a uniform and isotropic permeability. It was also reported that the difference between calculated and measured losses, which was known as the 'eddy current anomaly', could in principle be accounted for if the domain structure of the magnetic material was considered in the calculation of losses.

Pry - Bean calculated energy losses from eddy currents for magnetic sheet materials with a simple domain configuration [55]. Since then, this model has served as the foundation for most of the work in this field.

2.4.2 Loss separation

The concept of loss separation describes the total power loss at a given magnetizing frequency as in (2.46), where the total losses are divided into three parts, P_{hys}, P_{cls} and P_{exc}. P_{hys} is the hysteresis loss and P_{cls} is known as the classical eddy current loss that is calculated assuming a uniform magnetization. When the calculated values of hysteresis and classical eddy current losses are added, their sum is significantly less than the measured losses. This difference is known as the excess or anomalous losses (P_{exc}).

With a sinusoidal excitation, P_{cls} takes the general form as in (2.47), where f is the frequency, D is the thickness of the laminations, $B_{\max}$ is the peak flux density, ρ is the resistivity and k_o is a constant [38][56] [57].

$$P_{total} = P_{hys} + P_{cls} + P_{exc} \tag{2.46}$$

$$P_{cls} = \frac{k_o\ f^2 D^2 B_{\max}^2}{\rho} \tag{2.47}$$

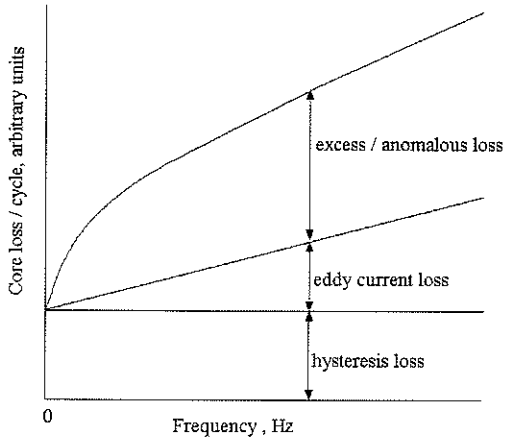

Figure 2.9: Comparison of loss for a grain-oriented steel.

Excess Loss

Excess loss arises due to the fact that any ferromagnetic material is made up of self-saturated domains, thus the microscopic magnetic flux pattern in the material is not smooth and continuous as assumed in calculating the classical eddy current losses. Magnetization proceeds by a movement of domain boundaries and, if the domains are relatively large, the eddy currents induced in the neighbourhood of the moving boundaries will differ from the simple classical pattern assumed [38][39][57].

2.4.3 Incorporating Losses

In the transformer model proposed here, the JA model is used to represent the hysteresis characteristics of the core and hence it properly represents the hysteresis loss of a transformer core. We have extended this model to incorporate the effects of classical eddy current and excess losses as described below.

The total magnetic field intensity, H_{tot}, can be expressed as in (2.48), where H_{hyst} is calculated with the JA model and, the sum of H_{cls} and H_{exc} is added to represent the eddy current effects [58][59].

$$H_{tot} = H_{hyst} + H_{cls} + H_{exc} \tag{2.48}$$

The instantaneous power loss per unit volume due to classical eddy currents is proportional to the rate of change of magnetization [60]. This can be expressed as in (2.49), where W_{cls} is the energy lost per cycle per unit volume, B is the flux density, D is the thickness of the laminations, ρ is the resistivity and β is a constant ($\beta = 6$ for laminations)[40]. In our model, H_{cls} represents a magnetic field intensity equivalent to the classical eddy current losses. Equation (2.50) represents the energy lost due to classical eddy currents per cycle per unit volume. From (2.45) and (2.49) it is clear that the energy lost due to classical eddy currents per cycle per unit volume can be represented in the model with an equivalent magnetic field proportional to $\frac{dB}{dt}$. In our model, H_{cls} represents a magnetic field intensity equivalent to the classical eddy current losses. Therefore H_{cls} in (2.48) can be expressed as $H_{cls} = k_1 \frac{dB}{dt}$ where k_1 is

a constant.

$$\frac{dW_{cls}}{dt} = \frac{D^2}{2\rho\beta}\left(\frac{dB}{dt}\right)^2 \tag{2.49}$$

$$W_{cls} = \oint \frac{D^2}{2\rho\beta}\frac{dB}{dt}dB \tag{2.50}$$

The instantaneous excess power loss can be expressed as in (2.51), where G is a constant, S is the cross sectional area of laminations and, H_o is a parameter representing the internal potential experienced by domain walls [40][61]. Equation (2.52) represents the excess losses per cycle per unit volume. From (2.45) and (2.49) it is clear that this energy loss can be represented by an equivalent magnetic field proportional to $(\frac{dB}{dt})^{\frac{1}{2}}$. Thus H_{exc} in (2.48) can be expressed as $H_{exc} = k_2(\frac{dB}{dt})^{\frac{1}{2}}$ where k_2 is a constant.

$$\frac{dW_{exc}}{dt} = \left(\frac{GSH_o}{\rho}\right)^{\frac{1}{2}}\left(\frac{dB}{dt}\right)^{\frac{3}{2}} \tag{2.51}$$

$$W_{exc} = \oint \left(\frac{GSH_o}{\rho}\right)^{\frac{1}{2}}\left(\frac{dB}{dt}\right)^{\frac{1}{2}} dB \tag{2.52}$$

Therefore in time domain simulations, the total magnetic field intensity H_{tot} can be expressed as in (2.53), where the values of constants k_1 and k_2 are tuned to simulate the core loss of the transformer at power frequencies. The initial values of k_1 and k_2 are calculated using (2.49) and (2.51), respectively. The k_1 and k_2 are tuned to simulate the core loss at power frequencies using measured data. (See Appendix A.) Then

$$H_{tot} = H_{hyst} + k_1 \frac{dB}{dt} + k_2 \left(\frac{dB}{dt}\right)^{\frac{1}{2}} \tag{2.53}$$

The following section describes the new simulation algorithm, that incorporates all the equations described so far.

2.5 Simulation Model

2.5.1 The existing model

The existing model considered is based on the core model presented in section 2.2. A single phase two winding transformer model was shown in Fig.2.1, and its magnetic equivalent circuit was shown in Fig.2.2. In this magnetic equivalent circuit, branches 1 and 2 represent transformer winding limbs.

The simulation algorithm of the existing transformer model begins with the calculation of the flux in each branch in the magnetic equivalent circuit that contains a winding, i..e. branches 1 and 2 (2.55).

$$\phi_i^{new} = \phi_i^{old} + \Delta\phi_i \tag{2.54}$$

$$\phi_i^{new} = \phi_i^{old} + \left(\frac{v_i^{new} + v_i^{old}}{2}\right) * \frac{\Delta t}{N_i} \tag{2.55}$$

where i = 1, 2 ; for single phase two winding transformer

ϕ_i^{new} = present value of flux in the i^{th} branch

ϕ_i^{old} = value of flux in the i^{th} branch in previous time step

$\Delta\phi_i$ = incremental flux in the present time step

v_i^{new} = present value of voltage in the i^{th} winding

v_i^{old} = value of voltage in the i^{th} winding in previous time step

N_i = Number of turns in the i^{th} winding

Δt = time step

Then the flux density of branches 1 and 2 are calculated from (2.56). If the flux density $|B_i|$ is greater than y_a and smaller than y_b, then the piece-wise linear segment that corresponds to this flux density determines the differential permeability of the core. This piece-wise linear segment in the saturation curve can be described with the points (x_a, y_a) and (x_b, y_b). Once the magnitude of the differential permeability (μ_{dif_i}) is found, the magnetic field strength (H_i) is calculated using B_i and μ_{dif_i}.

$$B_i = \frac{\phi_i^{new}}{Area} \tag{2.56}$$

$$\text{if } y_a < B_i < y_b \tag{2.57}$$

$$\mu_{dif_i} = \frac{y_b - y_a}{x_b - x_a} \tag{2.58}$$

$$H_i = \frac{B_i - y_a}{\mu_{dif_i}} + x_a \tag{2.59}$$

Using these values, the new value of the branch permeance (P_i) is updated, where l_i is the length of the branch i.

$$P_i = \frac{\phi_i^{new}}{H_i l_i} \tag{2.60}$$

The present value of the branch $MMFs$ are used in the calculation of the flux in the leakage paths, i.e. branches 3 and 4 shown in Fig.2.2. N_i is the number of turns in the i^{th} winding, i_i is the current in the i^{th} winding.

$$\phi_{i+2} = (N_i i_i - H_i l_i) * P_{i+2} \tag{2.61}$$

This is followed by the calculation of flux in the yoke, i.e. branch 5 in Fig.2.2;

$$\phi_5 = \phi_1 - \phi_3 \tag{2.62}$$

Once the magnitude of the flux in yoke is known, this value is substituted in (2.56) - (2.60), and hence the new value of the branch permeance (P_5) is found. Therefore, at this stage, the branch permeance matrix has been updated with the new values for the present time step. Then the simulation algorithm continues to follow the main algorithm, where the transformer inductance matrix is calculated using (2.21). Similarly, the transformer admittance matrix can be calculated using (2.22), and the magnitudes of the current injected are calculated using (2.30). These new values of the current are injected across each winding.

2.5.2 The new model

In the simulation algorithm discussed in the previous section, the transformer model uses the slope of the B-H curve (μ_{dif}) to update the branch permeance matrix, and the transformer inductance matrix, and hence to calculate the magnitudes of the current injected. However, the slope of the M -H loop described in the JA model is related to the slope of the B-H loop. Equation (2.31) is reproduced here as (2.63), which by taking the derivative with respect to H, gives (2.65).

$$B = \mu_0 (M + H) \tag{2.63}$$

$$\underbrace{\frac{dB}{dH}} = \mu_0 \left(\frac{dM}{dH} + 1 \right) \tag{2.64}$$

$$\mu_{dif} = \mu_0 \left(\frac{dM}{dH} + 1 \right) \tag{2.65}$$

Hence, the M-H relationship given in the JA theory, that describes $\frac{dM}{dH}$ (2.43) can be used for this purpose. Therefore during each time step, the slope of the M-H loop is used in the process of updating the branch permeance matrix. Thus, the new hysteresis model is incorporated into the simulation algorithm of the power transformer as described below.

During each time step, the transformer model calculates the flux (ϕ_i) and the incremental flux ($\Delta\phi_i$) in winding limbs as in (2.55). The input to the hysteresis model are the flux (ϕ_i), and the incremental flux ($\Delta\phi_i$) of the winding limbs, and the yoke. For each magnetic branch under consideration, the increment in H_i (ΔH_i) and the increment in M_i (ΔM_i) are estimated using $\Delta\phi_i$ as in (2.66) and (2.68) respectively. Using the estimates of ΔH_i and ΔM_i, the new values of M_i and H_i are updated as in (2.69) and (2.70). H_{old_i} and M_{old_i} are the H_i and M_i values during the

previous time step. The parameter δ_i, which indicates the direction the magnetization is obtained from (2.71).

$$\Delta H_i = Q \ \Delta H_{i\,\max} \text{ where } (\ 0 \leq Q \leq 1) \tag{2.66}$$

$$\Delta H_{i\,\max} = \frac{\Delta \phi_i}{A\ \mu_0} \tag{2.67}$$

$$\Delta M_i = \frac{\Delta \phi_i}{A\ \mu_0} - \Delta H_i \tag{2.68}$$

$$H_i = H_{old_i} + \ \Delta H_i \tag{2.69}$$

$$M_i = M_{old_i} + \Delta M_i \tag{2.70}$$

$$\delta_i = sign(\Delta H_i) = sign(\Delta \phi_i) \tag{2.71}$$

Using the values obtained from (2.69), (2.70) and (2.71), the current value of $\frac{dM}{dH}$ is calculated using (2.43). A numerical iterative method is used to reduce the error in the calculated value of $\frac{dM}{dH}$ by varying Q.

In order to incorporate losses, the magnitude of H_i that is calculated in (2.69) is modified using (2.53). Therefore, the effects of excess and anomalous losses are added to this expression, as described in section 2.4.3. Finally the calculated H_{tot_i} value is used to find the branch MMF_i, and the branch permeance P_i. This process is repeated for all the branches in the equivalent circuit which represent a winding or a yoke. At this stage, the branch permeance matrix is updated with the new values for the present time step. Then the simulation algorithm continues to follow the main algorithm in the existing model. The transformer inductance matrix is calculated using (2.21), followed by the calculation of the transformer admittance matrix using (2.22), and the magnitudes of the current injected using (2.30). Finally, the new values of the current are injected across each winding.

2.6 Summary

This chapter described how the Jiles Atherton theory of ferromagnetic hysteresis is incorporated into an electromagnetic transient simulation model of a power transformer. A brief review of an existing model was presented to show how a typical transformer model represents saturation, and also to identify a methodology to interface the existing model with the JA theory. This was followed by a review of the JA theory, that described the two differential equations on which the new model is based.

Having incorporated the JA theory to represent the hysteresis characteristics of the core, the simulation model was extended to include the effects of eddy currents. An expression for excess and anomalous losses was added. Therefore, when the simulation algorithm determines the magnitude of the current injected across each winding, the eddy current effects are taken into account. Therefore, this approach becomes useful in the simulation of multi-winding transformers, such as three phase three limb or three phase five limb etc.

PSCAD/EMTDC was considered as an example to show how this model could be implemented in an electromagnetic transient simulation software package. This enables the new model to be used along with the existing models for other power system elements such as transmission line models based on travelling waves etc., to carry out system studies.

Chapter 3

Validation of the New Model

Simulation results are compared with laboratory recordings to validate the model. A series of tests were carried out using a 3kVA, 115V/2300V, 60Hz single phase distribution transformer. In order to simulate the B-H characteristics of this test transformer in EMTDC, the parameters of the new model were determined as described below.

3.1 Determination of Parameters

In order to simulate the magnetizing characteristics of a transformer with the new model, the following parameters are required;

1. Parameters of the hysteresis model.

    - The anhysteretic function has three constants a_1, a_2, and a_3 as in (2.40).
    - M_{sat}, the saturation magnetization is a constant for a given material.
    - α represents interdomain coupling, and it is used in determining the effective field H_e in (2.35)
    - k represents the coercivity, and hence determines the hysteresis loss (2.32).

- c determines the reversible component of magnetization as described in (2.33).

2a. Parameters of the eddy current representation.

- The expression given in (2.53) has two constants k_1 and k_2 that determine the contributions from excess and anomalous losses.

2b. Parameters that interface the new model with EMTDC. This requires either,

- the cross sectional area (A), length of each limb (l), and number of turns in each winding (N),

  or,

- if the actual values of the cross sectional area (A), length of each limb (l), and number of turns in each winding (N) are not known, then an equivalent inductance matrix can be used to represent the transformer. (See Appendix A.)

In a simulation model, the parameters of the first category depend on the properties of the core material, whereas the parameters of the second category are dependent on the properties of the core material and the design of the transformer. These parameters were determined such that the simulated saturation characteristics (V_{rms}/I_{rms}) closely matches the measured values.

3.1.1 Parameters for the hysteresis model

The numerical determination of the parameters for the anhysteretic magnetization curve from experimental measurements has been presented in [50]. This process has

Table 3.1: Primary data for the anhysteretic magnetization curve; core material M4

H_{anhys} (A/m)	1.7	3.0	5.3	10.5	16	28	36	52
B_{anhys} (T)	0.80	1.00	1.20	1.40	1.49	1.56	1.59	1.64

been adopted in [36] to calculate parameters for the current transformer model. The same methodology was used to derive the parameters for the power transformer model presented here.

Anhysteretic Magnetization Curve

Parameters that represent the anhysteretic magnetization curve are dependent on the core material. Therefore, in order to derive parameters for the test transformer, a measured B-H characteristic is required. The measured B-H characteristic of the core material M4 was used in this analysis (See Table 3.1) [62]. This is a typical core material used in manufacturing distribution transformers.

This calculation involves the determination of the three constants a_1, a_2, and a_3 in (2.40) and α. Typically M_{sat} is 1.71e6 A/m for iron (Table 4.1 of [49]). If the values of the α and M_{sat} are known, then the determination of a_1, a_2 and a_3 is a constrained optimization problem of minimizing the error between the reference anhysteretic characteristic and the model. Thus, an initial value of α is assumed. The initial value of α is selected by comparing the magnetization curve of the core material M4 with a known curve such as the anhysteretic magnetization curve of the current transformer core material used in [36] as in Fig.3.1. The variation of the anhysteretic magnetization curves with α is discussed in [35]. If the α value is increased, the magnitude of the anhysteretic magnetization (M_{an}) for a given effective field (H_e) also increases. Therefore, it can be expected that the α value of the core material M4 is less than the α value of the current transformer material, i.e. 1.32e-5. Therefore an initial value

Table 3.2: Parameters for the Hysteresis Model Based on the Core Material M4

α	M_{sat}	a_1	a_2	a_3
3.90e-6	1.71e6	60	96	93

of 1.0e-6 is assumed for α. Using this initial guess of α, a numerical iterative routine of least squares estimation was used and the α with the minimum error was chosen. The parameters a_1, a_2 and a_3 for this α are given in Table 3.2.

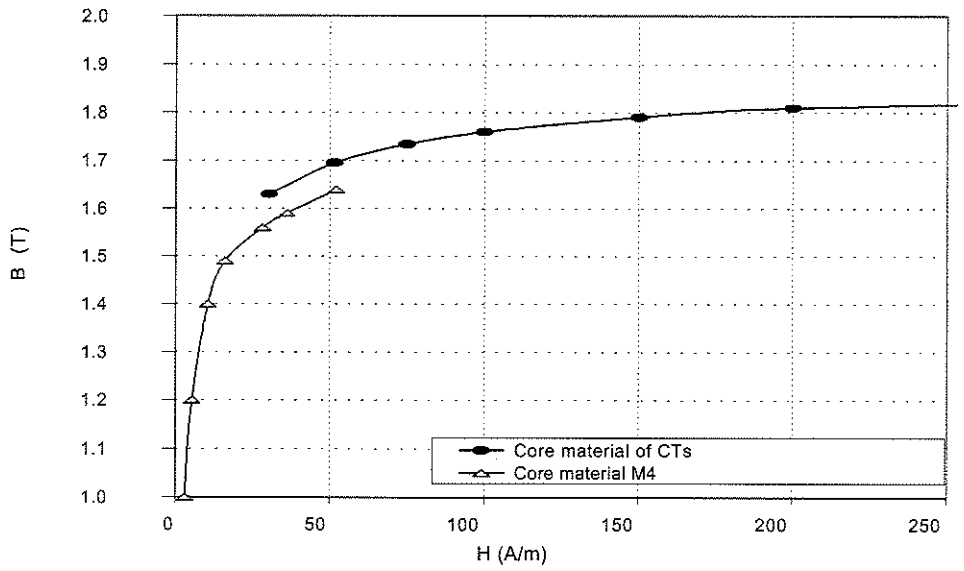

Figure 3.1: Comparison of the magnetization curves: core material of CTs and the core material M4.

Determination of parameters k and c

The value of k can be calculated considering its relationship with H_c. The general relationship between k and H_c can be expressed if the differential susceptibility at the coercive point χ'_{H_c} is known. In general $\chi'_{H_c} = \chi'_{\text{max}}$ denotes the differential susceptibility around the coercive point, which in the model is always the maximum value observed around the hysteresis loop [50]. Thus k can be found using (3.1), if

Table 3.3: Determination of parameters k and c

H_c	$\chi'_{\max}$	c	k
8 A/m	374e3	0.1	8.96e-6 A/m

H_c, c, α and $\chi'_{\max}$ are known. The values of H_c and $\chi'_{\max}$ are found from the reference $B-H$ loop of the core material M4, and are given in Table 3.3.

$$k = \frac{M_{an}(H_c)}{1-c}\left[\alpha + \frac{1}{\frac{\chi'_{\max}}{1-c} - \frac{c}{1-c}\frac{dM_{an}(H_c)}{dH}}\right] \tag{3.1}$$

The value of c can be calculated from the ratio of the initial normal susceptibility $\chi'_{in} = \left(\frac{dM}{dH}\right)_{M=0,\ H=0}$ to the initial anhysteretic susceptibility $\chi'_{an} = \left(\frac{dM_{an}}{dH}\right)_{M=0,\ H=0}$[50]. However this method could not be used due to lack of data. Typical values of c for several iron core materials are given in [50]. Thus the value of c is set to 0.1. The same value has been used in the current transformer models in [35]. The magnitudes of k and c used in this simulation model are given in Table 3.3.

3.1.2 Parameters for a given transformer

The parameters derived in the previous section are the basis of the hysteresis model. However, in order to simulate the measured magnetizing current, the hysteresis model has to be interfaced with the existing model in EMTDC. This involves the need to input detailed core data such as the length (l) and the cross-sectional area (A) of each limb, and the actual number of turns (N) in each winding so that the transformer is properly represented with its inductance matrix, as discussed in section 2.2.

If the actual core dimensions and the number of turns are known, the model can be readily implemented with EMTDC. Meanwhile, there are two constants in (2.53), that represent the effects of the excess and anomalous loss. The values of these two

constants k_1 and k_2 can be determined such that the total power loss measured at rated conditions are simulated in the model.

However, if the actual core dimensions and the number of turns are not known, interfacing of this model with EMTDC can be achieved by determining an equivalent inductance matrix as described in section 2.2.1, where (2.25) - (2.27) have shown the relationship between the length (l) and the cross-sectional area (A) of each limb, and the actual number of turns (N) in each winding.

The actual number of turns in the windings are not commonly available. Therefore the number of turns, N_1 and N_2, are set equal to the rated voltage of the windings (2.26). Then the magnitude of A is calculated by assuming a peak operating flux density (B_{max}) of 1.6 $\sim$ 1.7 T at the rated conditions, so that the actual value of the product of NA is matched by the product of NA used in the simulation model. (See Appendix A.)

Once the parameters of the anhysteretic magnetization curve, the magnitude of the cross sectional area, and the number of turns in each winding are determined, it remains to determine the length of the winding limb, l , and the constants k_1 and k_2 used in (2.53). However, all three parameters affect the waveform of the simulated magnetizing current, and hence the magnitude of the rms value of the magnetizing current and the open circuit core losses. Therefore, the length of the winding limb, l ,and the constants k_1 and k_2 in (2.53) are tuned such that the correct magnitude of the magnetizing current and the power loss are simulated at the rated conditions. The calculated values are given in Table 3.4. At this stage the measured saturation characteristic (V_{rms}/I_{rms}) and the simulated characteristic can be compared. The slope of the anhysteretic curve in the saturation region and the width of the B-H loop in the shoulder region may be slightly modified to match the particular characteristics

Table 3.4: Parameters for a 3kVA Distribution Transformer

B_{max}	A	l	k_1	k_2
1.65	2.27	0.717	3.5e-3	0.79

of a given transformer [36].

3.2 Comparisons with Recorded Waveforms

Simulation results for open circuit tests on a single phase two winding transformer model are compared with test results. Simulations were carried out with the electromagnetic transient program PSCAD/EMTDC.

The single-phase two-winding model used has a current source across each winding to represent the saturation. In the new model, the eddy current effects are also incorporated into the same algorithm. Thus, the calculated value of the saturation current injected across each winding also contains the effects of eddy currents (Fig.3.2a).

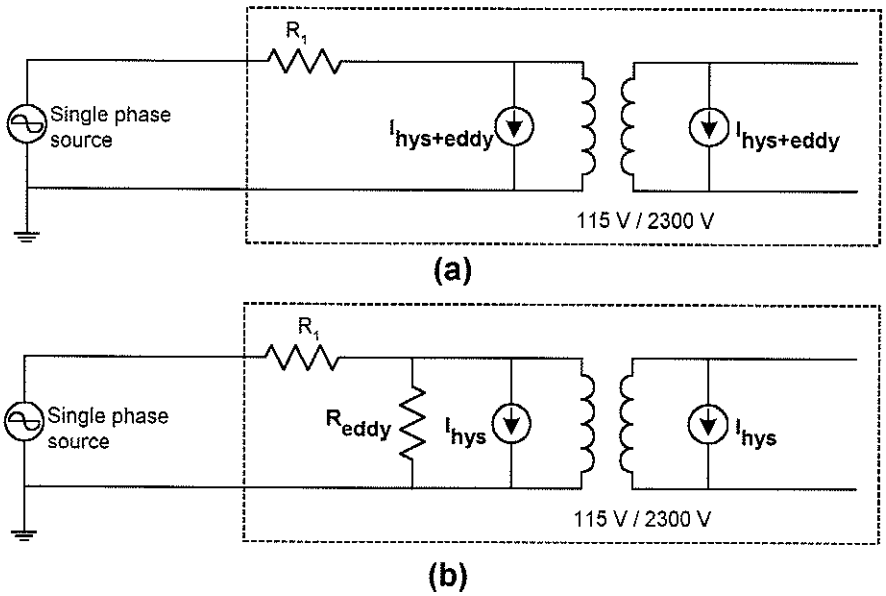

Figure 3.2: Simulation models; (a) with the new algorithm, (b) with an external resistor representing losses.

3.2.1 Comparisons : Open Circuit tests at 60 Hz

Figure 3.3 shows the comparison of the simulated waveform and the recorded waveform at the rated voltage and frequency. Figure 3.4 shows the comparison of the flux density (B) versus current (I) curve for the same conditions. A close comparison is seen between the simulation and the recorded waveforms. Figures 3.5 and 3.6 show the comparison of the magnetizing current at 0.9 pu and 1.1 pu voltages respectively, and the remaining comparisons are presented in Appendix B. A slight difference is seen between the measured and the simulated waveforms, which can be due to a slight mismatch in the simulated B-H loop.

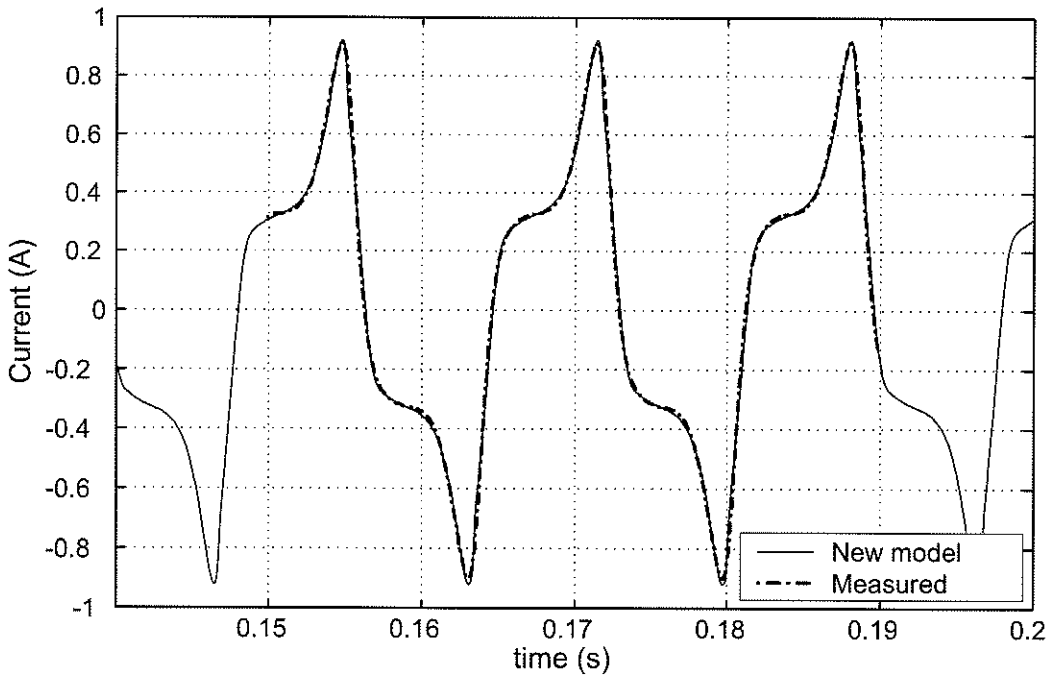

Figure 3.3: Magnetizing current at the rated conditions

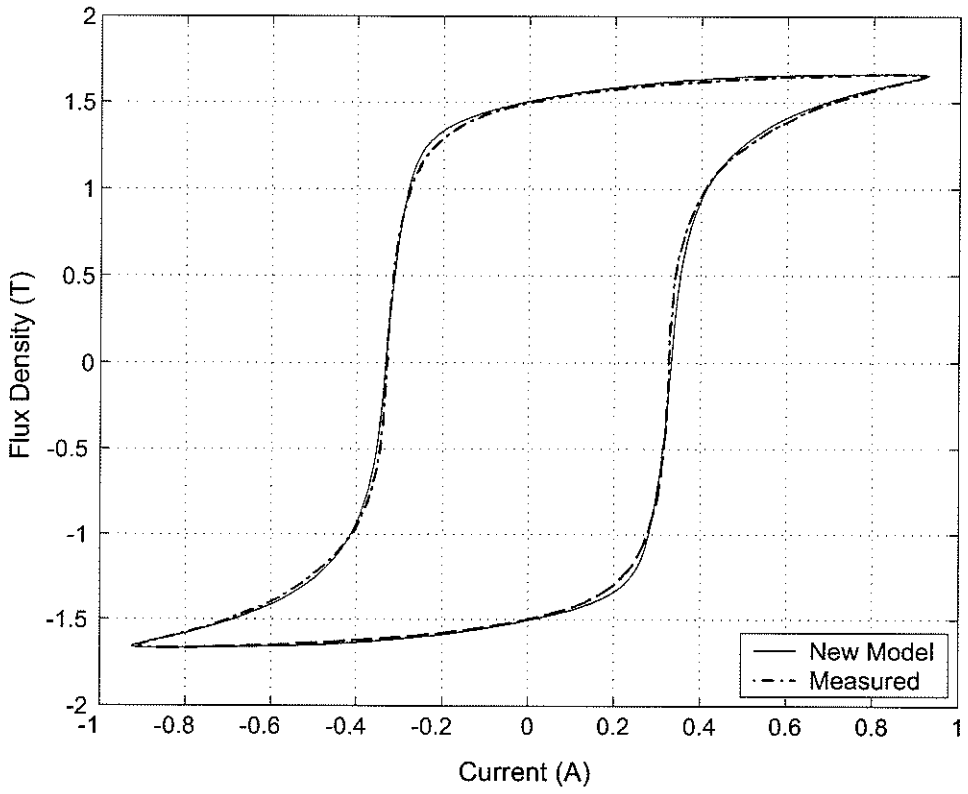

Figure 3.4: Flux density (B) vs Magnetizing current (I) at 60 Hz

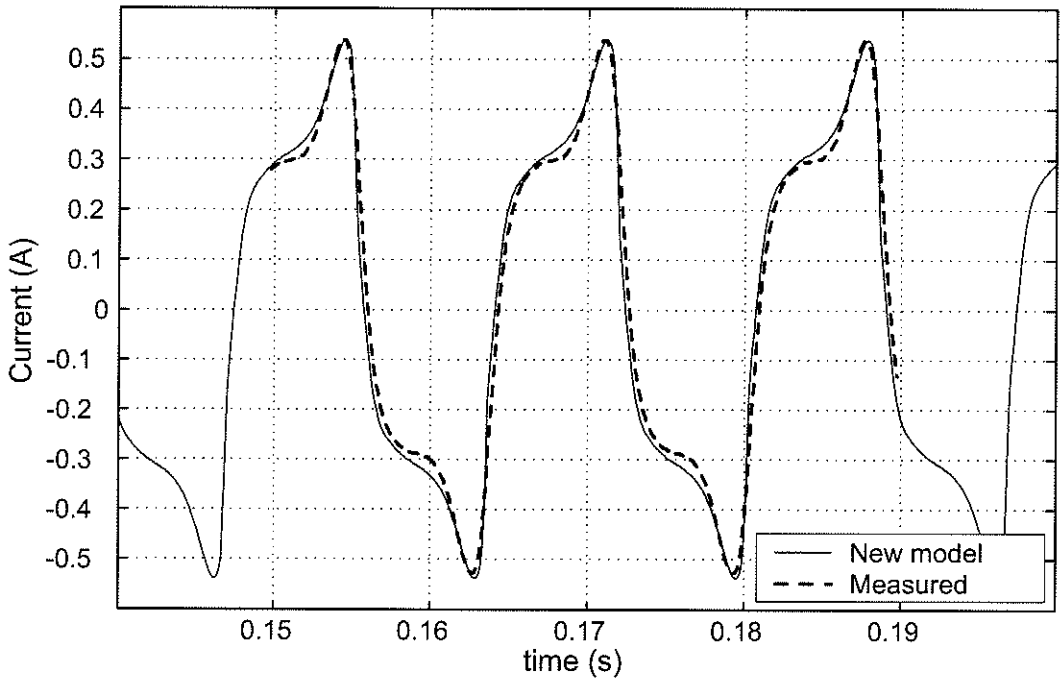

Figure 3.5: Magnetizing current at 0.9 pu voltage

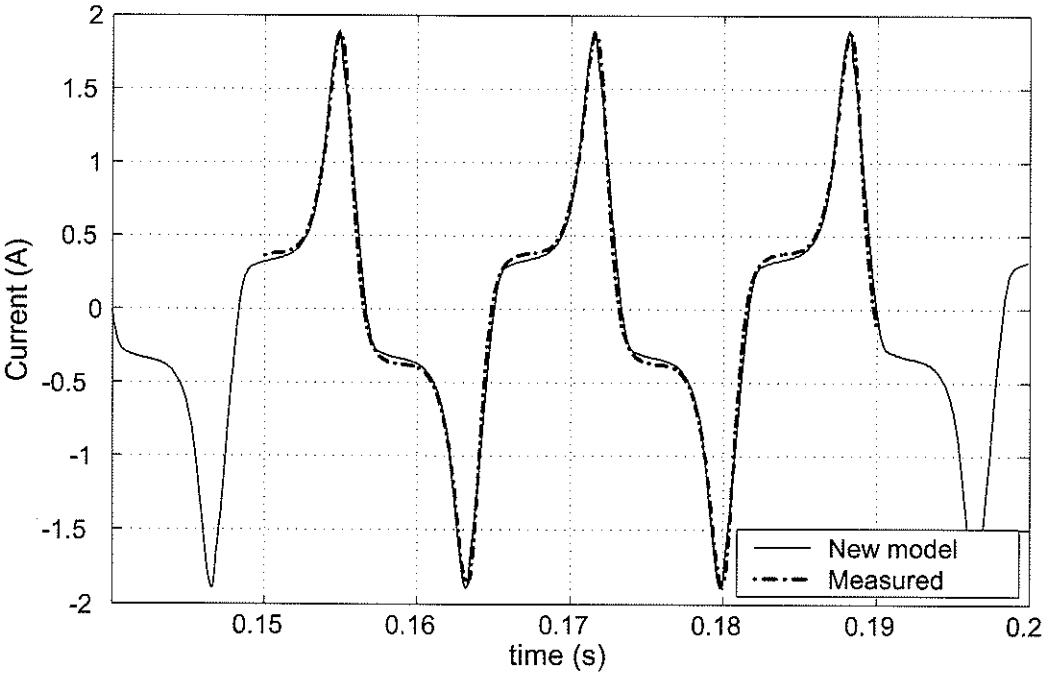

Figure 3.6: Magnetizing current at 1.1 pu voltage

Simulations were also carried out to compare the new model with a more commonly used approach of representing eddy current losses using a shunt resistor as shown in Fig.(3.2b). In this 'resistor model', hysteresis characteristics are represented by the JA theory, and the eddy current effects are represented with an external resistor connected across the terminals. The magnitude of this resistor is calculated to match the measured core loss at the nominal frequency.

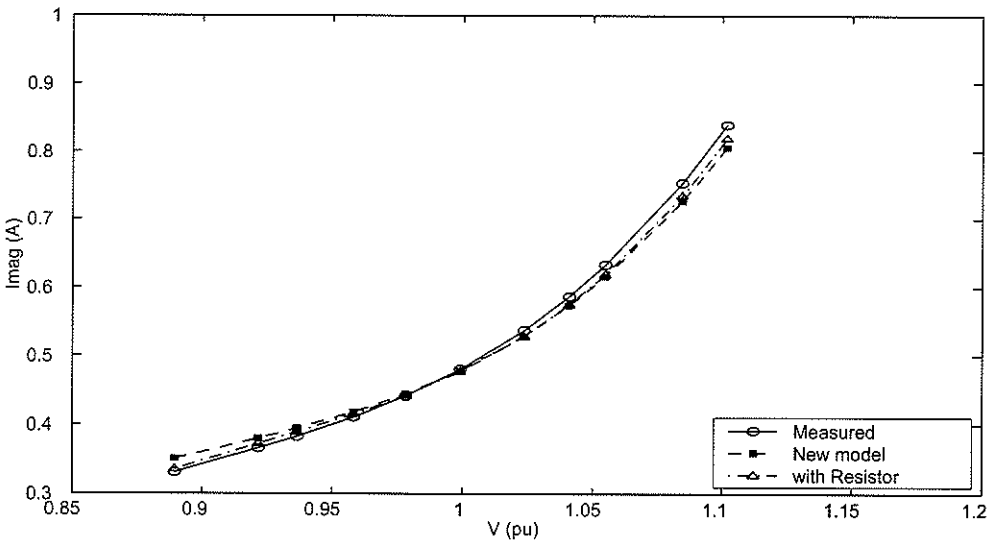

Figure 3.7: Magnetizing current at different excitation voltages at 60 Hz

Figure 3.7 shows the variation of the rms magnetizing current for different excitation voltages. The percentage error in the rms value of the magnetizing current produced by the new model is -1.0% at the rated conditions. A maximum error of 5.4% is produced by the new model at 0.9 pu voltage whereas the resistor model produced only 1.2%. The variation of the core loss (active power) is shown in Fig.3.8a. The parameters of the new model were tuned so that an accurate representation is obtained at the rated conditions. Thus the minimum error is seen at the rated conditions i.e. 2.0%. A maximum error of 13.5% is produced by the new model at 0.9

pu voltage whereas, the resistor model produced 11.3%. The variation of the reactive power consumption shows a closer match than does the variation of the active power (Fig.3.8b).

The representation of hysteresis is common for the two models discussed, and hence any mismatch in the simulated B-H loop could affect the accuracy of both models. The variation of the phase angle of the fundamental component of the magnetizing current, and the power factor are shown in Fig.3.9a and Fig.3.9b respectively. These figures explain the differences seen in the active power and reactive power consumption simulated by the new model. For example, at 1.0 pu, the magnitude of the phase angles of simulated and the recorded waveforms are 46.2^0 and 47.7^0 respectively (phase difference 1.5^0). This represents a 0.69 and 0.67 in power factors (3% error). However at 1.1 pu this phase difference increases to 2.6^0. The resulting power factors are 0.46 and 0.50 respectively (-8.0% error). With an -8.0% error in the power factor and a -4.0% error in the fundamental component of current, the total power loss simulated has an error greater than 12%. The phase angle error and hence the error in the power factor can be attributed to a mismatch in the simulated B-H loop and B-H loop of the core material.

All of the above comparisons show that the resistor model produces a closer match than does the new model. This is due to the fact that the magnitude of the core loss resistor in the resistor model was calculated at 60 Hz and all of the comparisons were carried out at the same frequency. However, the eddy current effects included in the new model are capable of representing the frequency dependency of the B-H characteristics, and the following comparisons show that it is important to model these effects accurately.

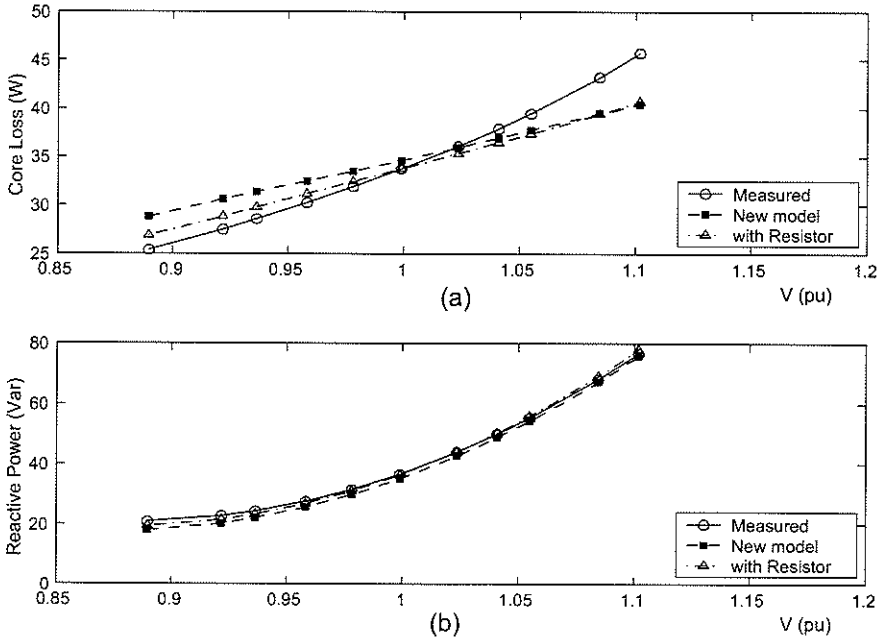

Figure 3.8: Comparison of the active power, and the reactive power at 60Hz

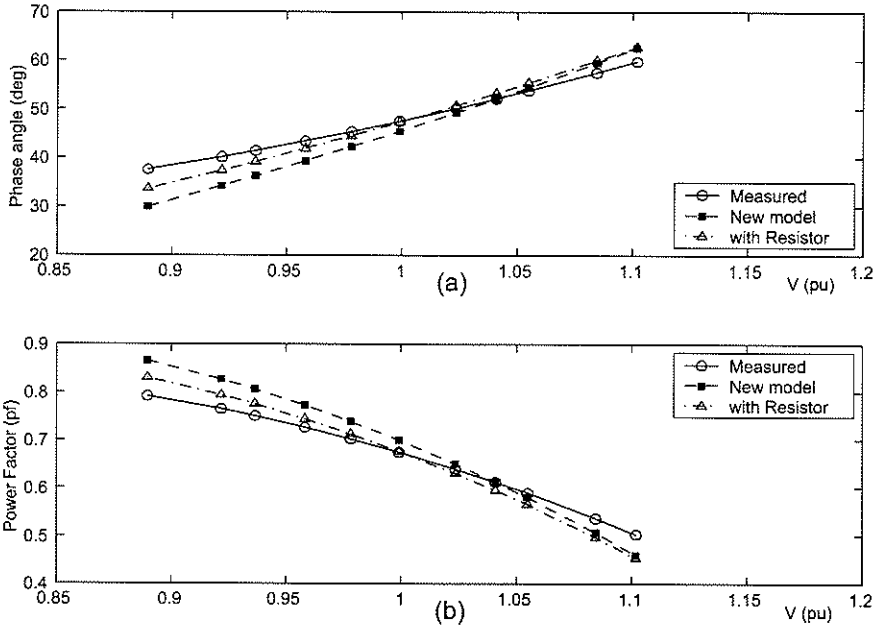

Figure 3.9: Comparison of the phase angle, and the power factor at 60Hz

3.2.2 Comparisons at different frequencies

A series of open circuit tests were carried out at different frequencies (25 $\backsim$ 60 Hz). A separately excited dc motor was used to drive a three phase generator to obtain a variable frequency, variable voltage supply. Details of the test system are given in Appendix B. The frequency of the generator voltage was adjusted using the dc motor, and the generated voltage was adjusted so that a constant $\frac{V}{f}$, thus a constant flux level is maintained in the core. Fig.3.10 shows the comparison of the simulated B-H loops produced with the new model at different excitation frequencies. It shows that the width of the B-H loop increases as the frequency is increased.

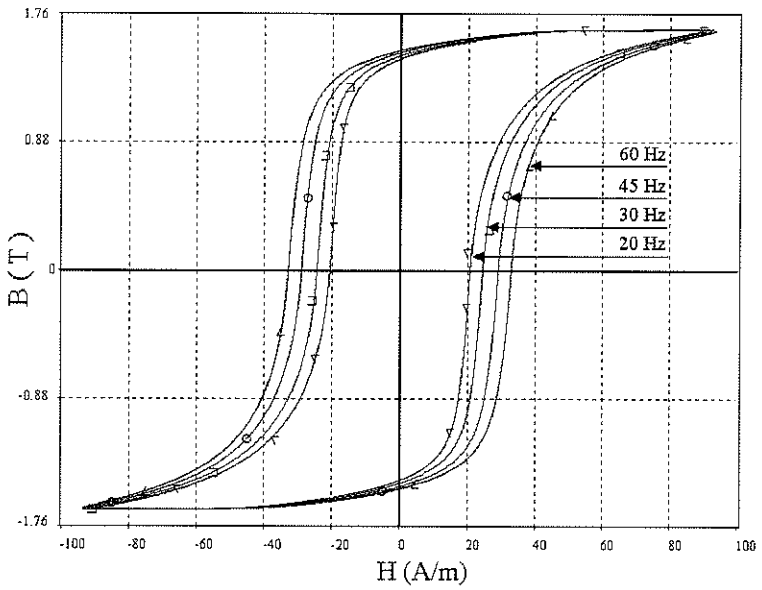

Figure 3.10: B-H loops at different frequencies

Fig.3.11a shows the comparison of the core loss at different frequencies. A maximum error of -5.6% is produced by the new model at 25 Hz whereas the resistor model showed significant deviations with the maximum error of -24.4% at 25 Hz. Similar observations can be made with the variation of core loss per cycle for frequencies 25

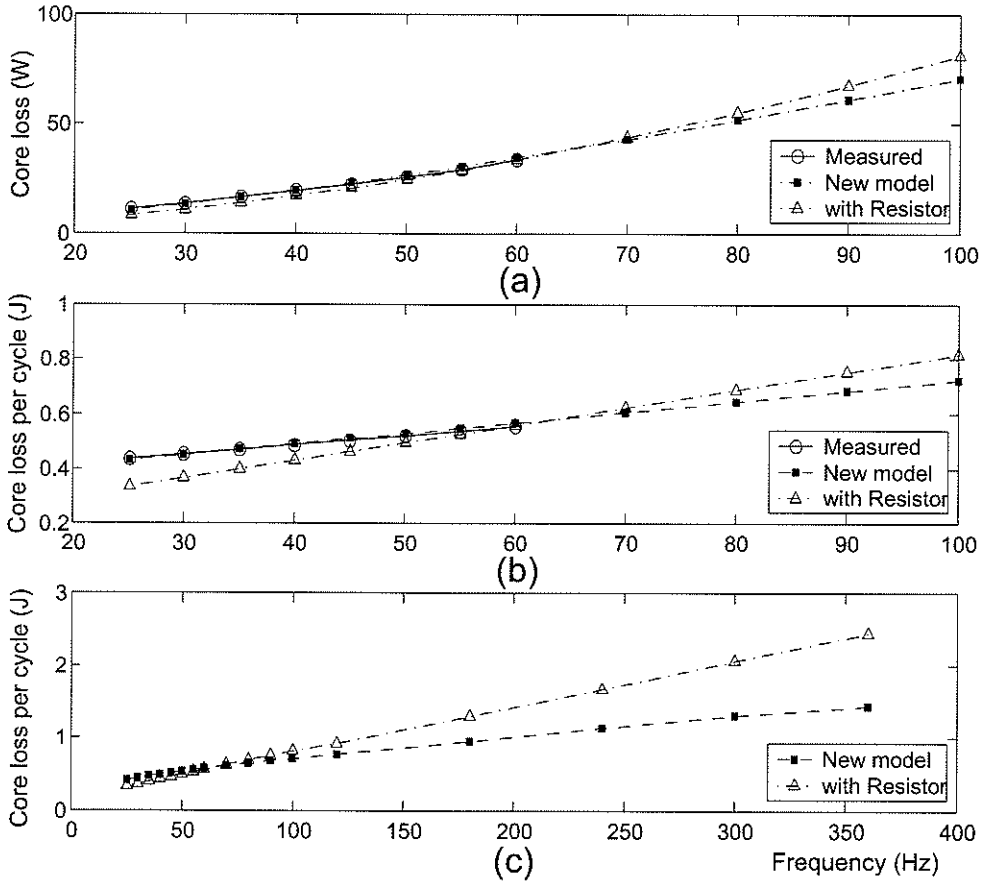

Figure 3.11: Comparison of the core loss, and the core loss per cycle at different frequencies

Hz $\sim$ 100 Hz (Fig.3.11b) and 25 Hz $\sim$ 360Hz (Fig.3.11c). Fig.3.12a and Fig.3.12b show the comparison of the magnetizing current, and the fundamental component of the magnetizing current at different frequencies.

These comparisons show that the resistor model may cause significant errors as the frequency is decreased. The same trend can be seen when the frequency is increased (70 $\sim$ 360Hz). This range could not be verified due to the lack of recorded data. However, Fig.3.11b shows that the new model has a slope much closer to the measured curve. Also previous work in this area has indicated a linear variation in this region

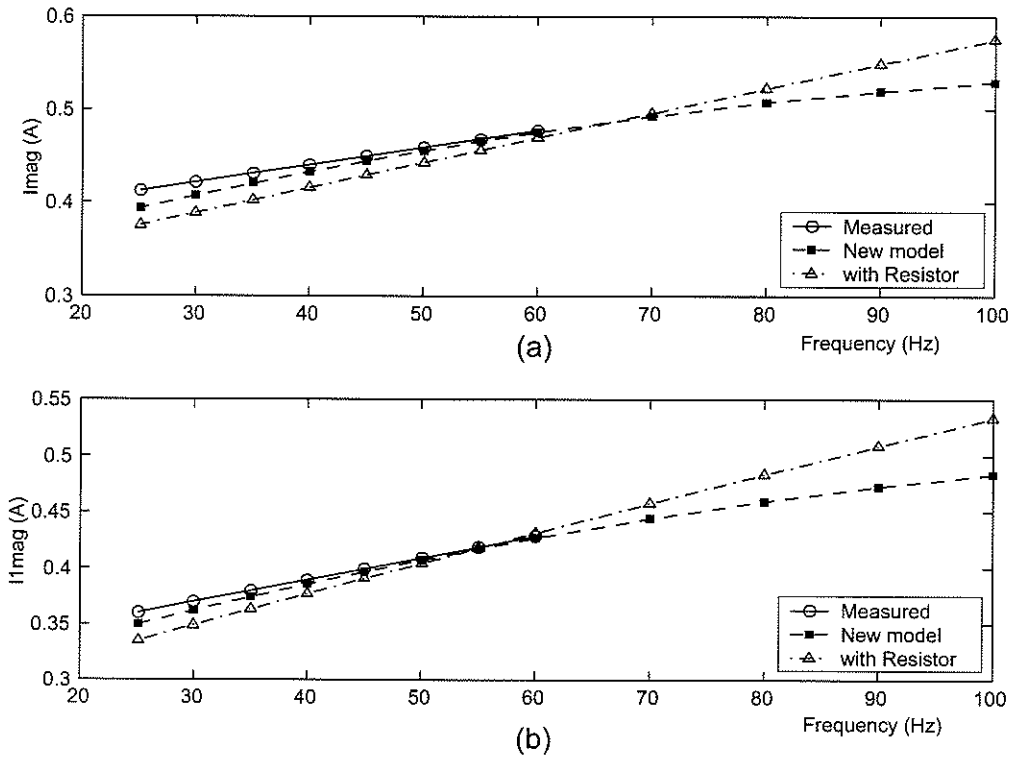

Figure 3.12: Comparison of the magnetizing current (I_{mag}) and the fundamental component of I_{mag} at different frequencies

[38][39]. This confirms that the new model is capable of simulating the magnetizing current and the power losses more accurately than does the commonly used approach of a shunt resistor. In addition, it highlights the importance of modeling the frequency dependency of the B-H loop. The comparisons at 25Hz are presented in Figs.3.13 and 3.14.

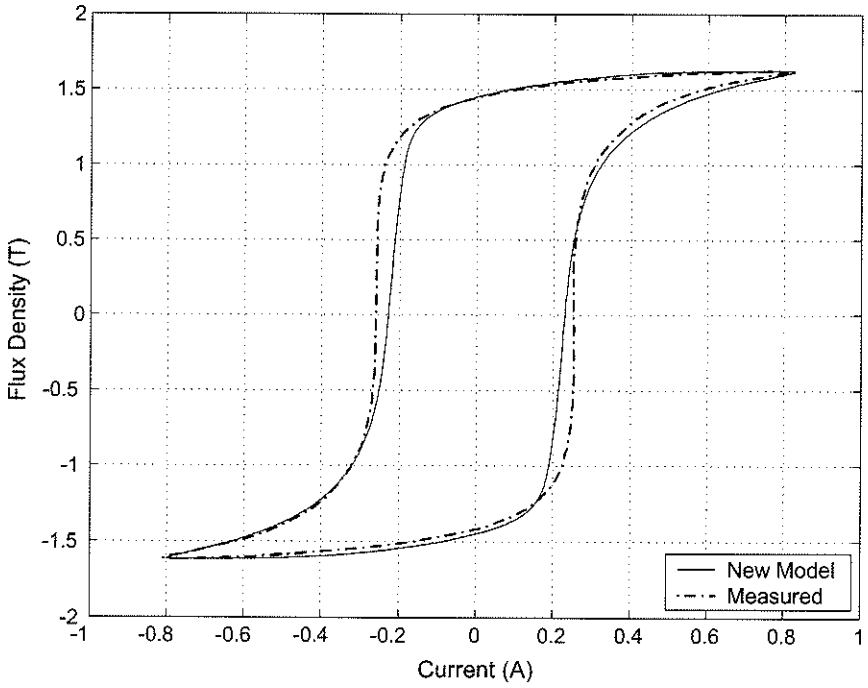

Figure 3.13: Flux density (B) vs Magnetizing Current (I) at 25 Hz

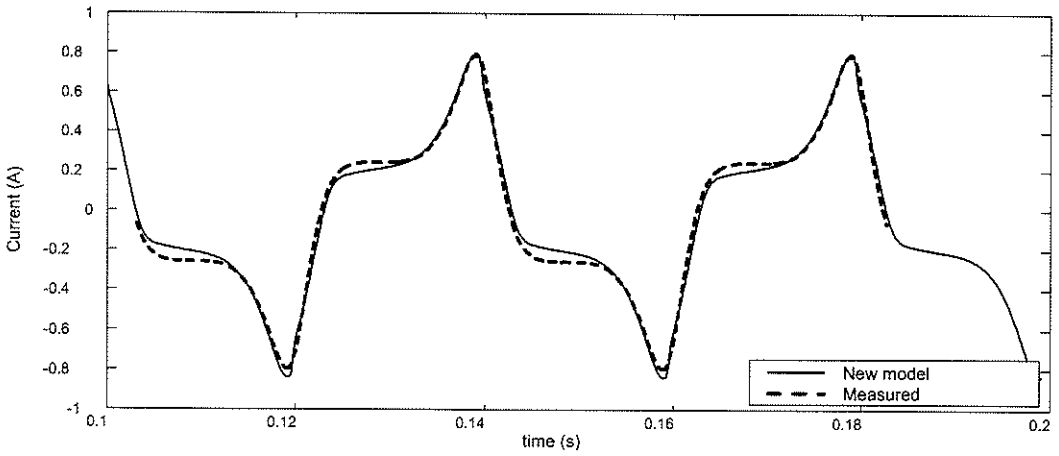

Figure 3.14: Magnetizing current at 25Hz, at the rated flux

3.3 Comparisons with an Existing Model

3.3.1 Open circuit test: magnetizing current

Simulation results of open circuit tests carried out with the new model and the existing transformer model in EMTDC are compared. The existing model has a piece-wise linear curve to represent saturation in the core. A brief overview of this model was given in section 2.2.2. This is considered as an example to show the major differences seen in the simulated waveforms of magnetizing current obtained with the new model against a typical piece-wise linear representation of saturation.

Input to the existing model are the open circuit normal magnetizing curve with excitation voltage in pu and the rms value of the magnetizing current as a percentage of the rated current. This model does not represent eddy current effects, therefore an external resistor was connected to include losses. These parameters were chosen such that the rms value of the magnetizing current, and the core loss were accurately represented at the rated conditions, which was the basis of this comparison.

Figs.3.15a and b show the comparison of the waveform of magnetizing current obtained with the new model and the existing model. The waveforms of voltage were considered as the basis of aligning the two waveforms. This allows us to compare the phase differences in the simulated waveforms of magnetizing current.

The waveform obtained with the new model has already been compared with the measured waveform in Fig.3.3. Waveforms in Fig.3.15b show that the piece-wise linear representation does not properly match the shape and magnitude of the recorded waveform.

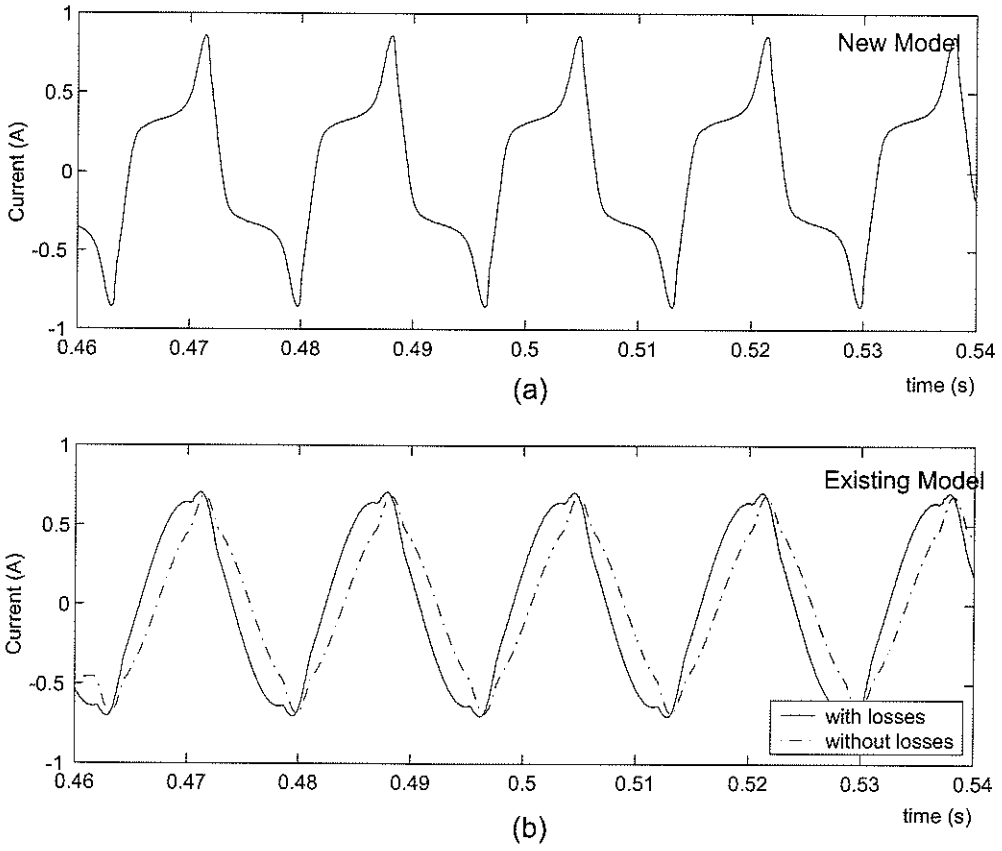

Figure 3.15: Comparison of the waveform of magnetizing current obtained with; (a) new model, (b) existing model

3.3.2 Remanence cases

During short time simulations, piecewise linear solutions of saturation can give the impression that they handle remanence because the system time constants maintain the magnetization over several hundreds of milliseconds. However, over time scales of seconds the flux decays to zero. It has been shown in reference [36] that the hysteresis model based on the JA theory accurately represents the long term remanence and recoil loops in the transformer cores. Simulations were carried out to demonstrate this effect, however these simulations could not be verified with recordings due to the limitations in the laboratory test system.

Simulations were carried out with the existing model where; (a) a resistive load of 0.01 pu is connected, (b) a resistive load of 1.0 pu is connected at the secondary terminals. The simulated system consists of a single phase source connected to the transformer through a single phase breaker. Fig.3.16 shows the simulated waveform of flux obtained when the breaker was opened. A resistive load was attached to the transformer so that it leaves maximum remanence flux in the core at the time of opening the breaker. The comparison shows that the flux in the core decays to zero after a small time duration with the existing model. This duration is dependent on the system time constant as shown in Fig.3.16 (a) and (b). In the existing model, the output waveform of flux density has been normalized to obtain a peak flux density of 1 pu., whereas the output of the new model plots the flux density in Tesla.

The same simulation was carried out with the new model. When the breaker was opened, flux in the core gradually decays and then remains at the remanent flux level as in Fig.3.17 (around -1.0 T even beyond 60 seconds). Therefore this comparison shows that a hysteresis model based on the JA theory properly represents the long term remanence in the core, whereas a piece-wise linear representation with no hysteresis would fail to maintain the remanent flux beyond several hundred milliseconds.

This simulation scheme was also used to simulate minor loops under small ac excitation. Fig.3.18 shows the simulation results of different kinds of hysteresis loops, such as a symmetrical minor loop and an asymmetrical minor loop.

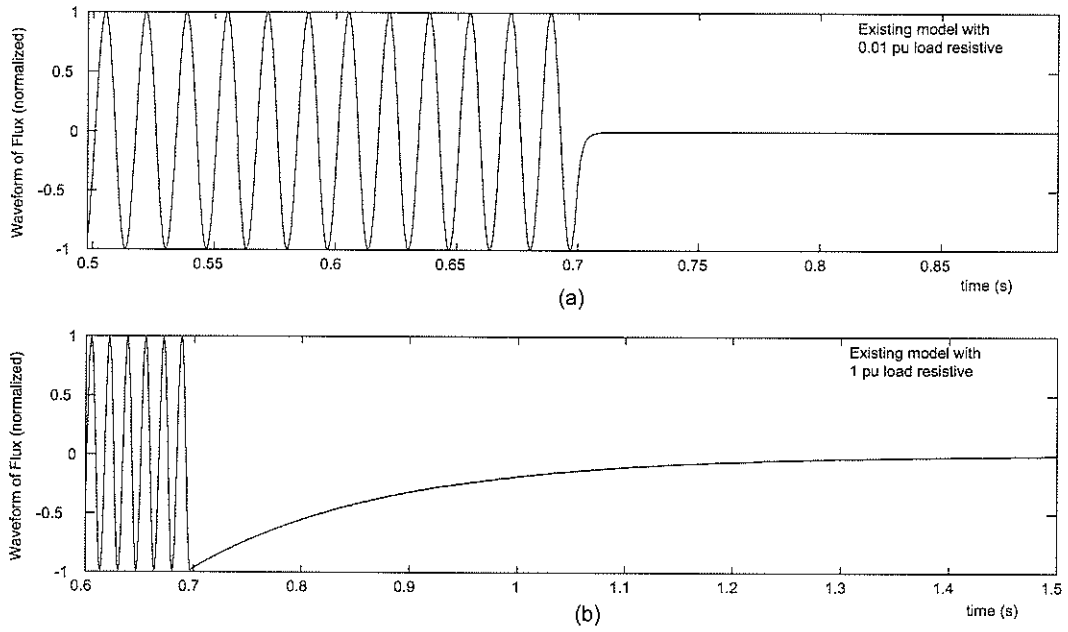

Figure 3.16: Waveform of flux density (normalized) obtained with the existing model when the breaker was opened.

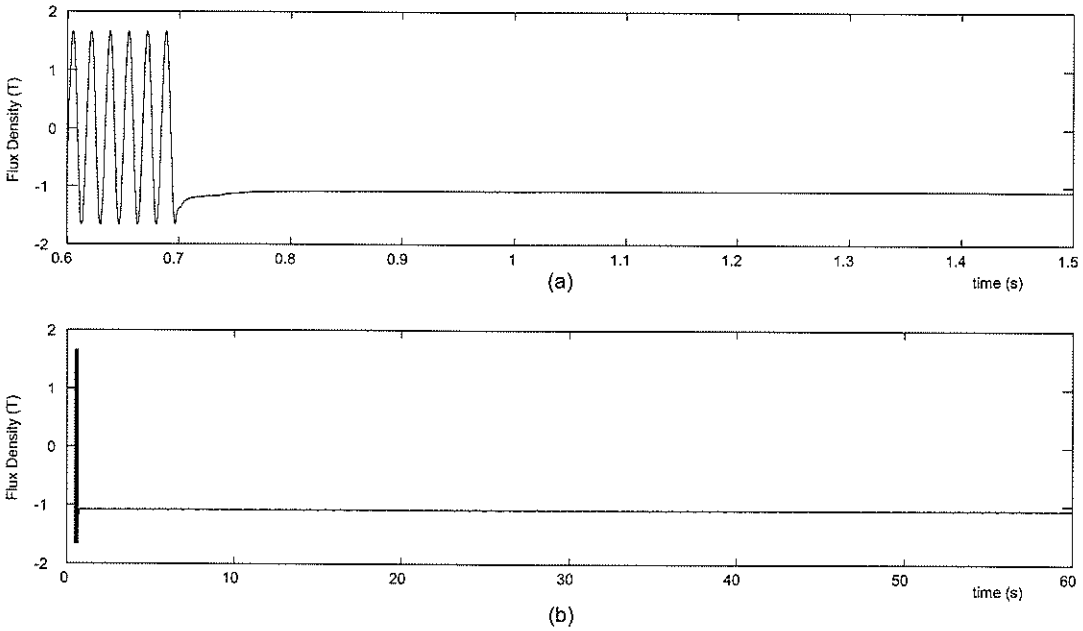

Figure 3.17: Waveform of flux density obtained with the new model when the breaker was opened.

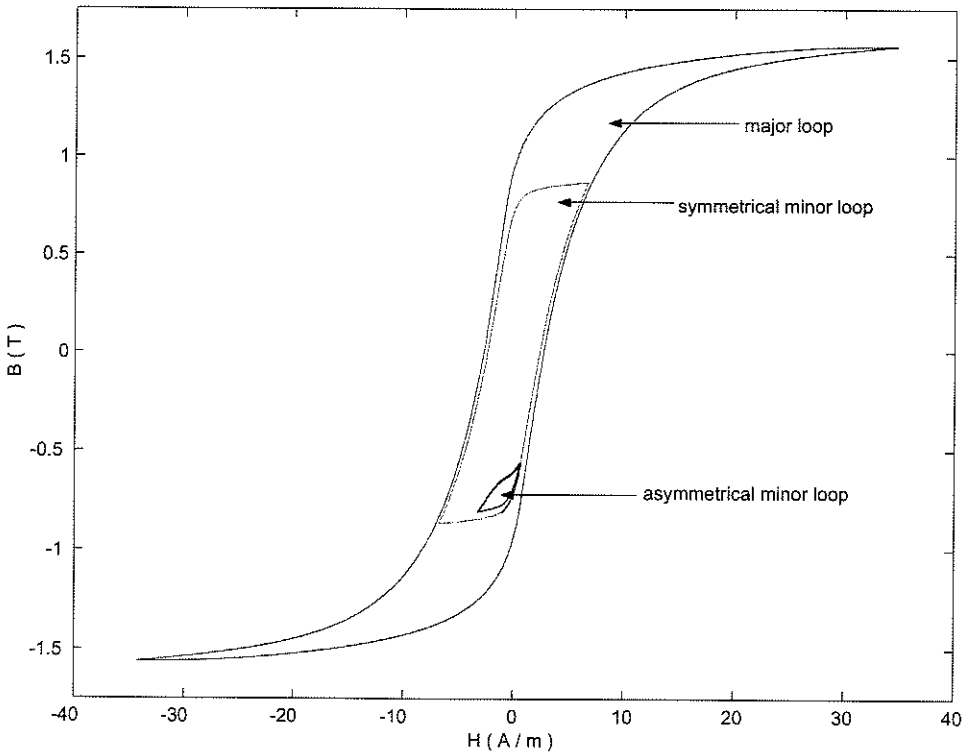

Figure 3.18: Simulation results: Different kinds of hysteresis loops

3.3.3 Inrush cases

The recorded waveforms of inrush current obtained using the 3kVA, 115V, 2300V, 60Hz single phase distribution transformer are compared with simulation results. In the laboratory test system, the low voltage winding of the transformer was energized from the demagnetized core condition by applying the rated voltage at 60Hz. The simulations are initialised by closely reproducing the point-on-wave of the recorded waveforms of voltage. Figures 3.19-3.21 show the comparison of the recorded waveforms, and the simulated waveforms obtained using the new model. Simulation results closely match the recorded waveforms.

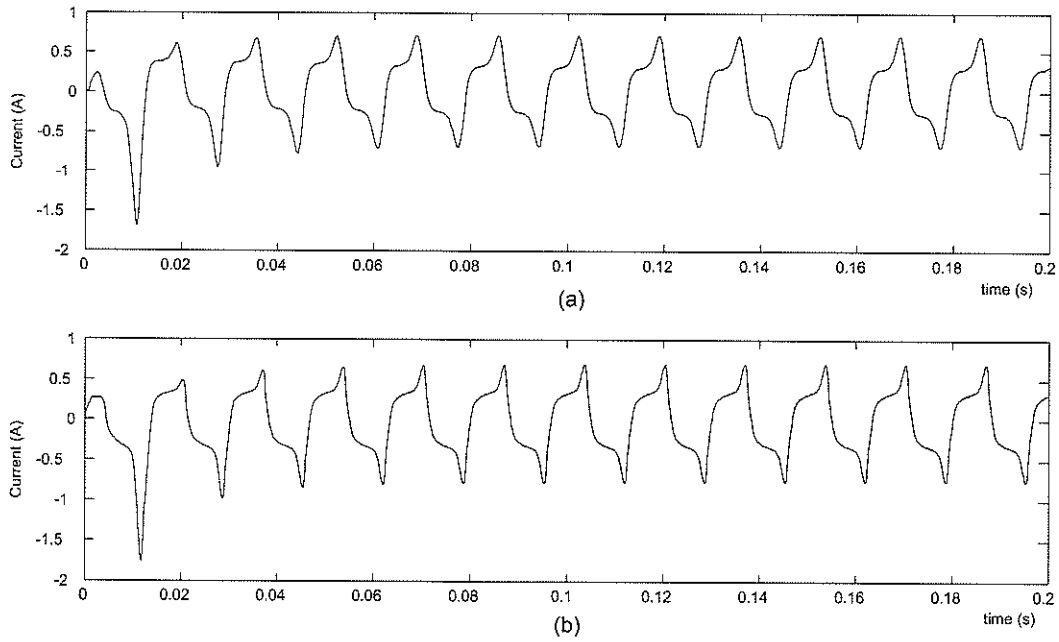

Figure 3.19: Inrush cases: Waveform of current; (a) Measured; (b) New model

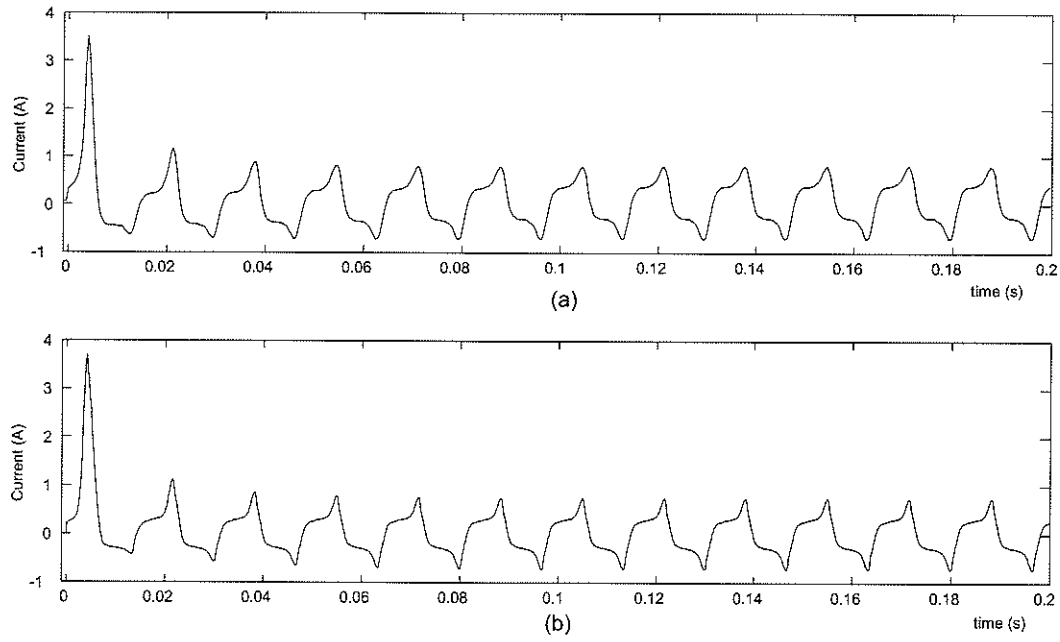

Figure 3.20: Inrush cases: Waveform of current; (a) Measured; (b) New model

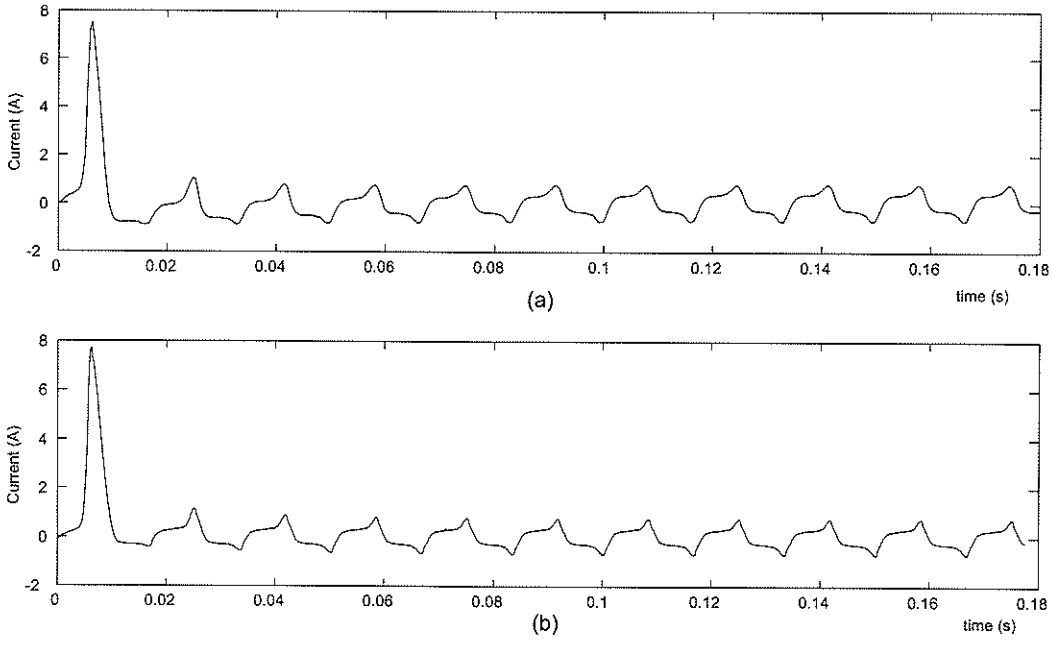

Figure 3.21: Inrush cases: Waveform of current; (a) Measured; (b) New model

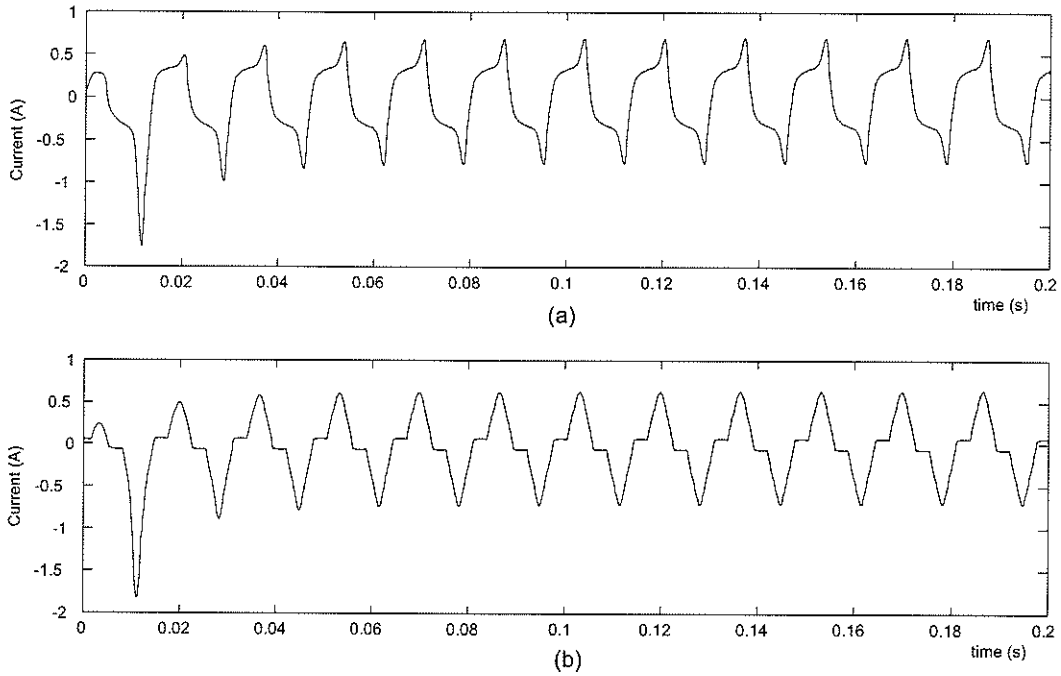

Figure 3.22: Inrush case considered in Fig.3.19a: Waveform of current; (a) New model; (b) Existing model.

The inrush condition shown in Fig.3.19a was also simulated using the existing model. Fig.3.22 shows the comparison of the simulated waveforms obtained with the new model and the existing model. Since the waveform obtained with the new model has already been compared with the measured waveform in Fig.3.19, waveforms in Fig.3.22 show that the piece-wise linear representation does not properly match the shape and magnitude of the recorded waveform.

Simulations were also carried out to analyse the inrush current during the re-closure of a circuit breaker. The simulation cases described in the previous section (section 3.3.2) were considered for this analysis. During the first case, the breaker was reclosed after 180 ms. Fig.3.23 shows the waveform of current and the waveform of flux (normalized) obtained with the existing model. Fig.3.24 shows the waveforms of current and flux density obtained with the new model. When the breaker was

reclosed, the waveform of current obtained with the existing model has a lower peak value, however it has the characteristics of a transformer inrush. The difference in the peak values is due to a decrease in the level of flux in the core at the time of reclosing.

In the second case, the breaker was reclosed after 1.0 s. Fig.3.25 shows the waveform of current and the waveform of flux (normalized) obtained with the existing mode, whereas Fig.3.26 shows the waveforms of current and flux density obtained with the new model. Comparison of waveforms of current show that the existing model does not represent an inrush during the reclosure. This is due to the fact that the remanent flux has decayed to zero, and therefore the reclosure appears as energizing the transformer from the demagnetized core condition. Meanwhile, the new model has retained the remanent flux in the core, therefore a fairly significant inrush can be seen. These results are consistent with the observations made in the previous section.

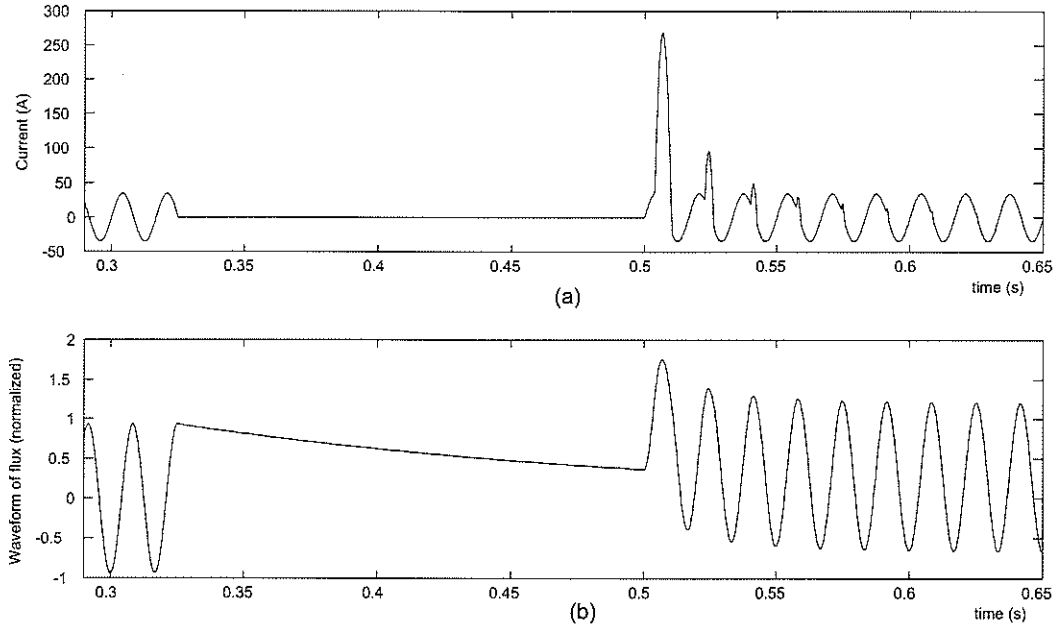

Figure 3.23: Inrush cases: Existing model with the breaker re-closed after 180ms. (a)Waveform of current; (b)Waveform of flux (normalized)

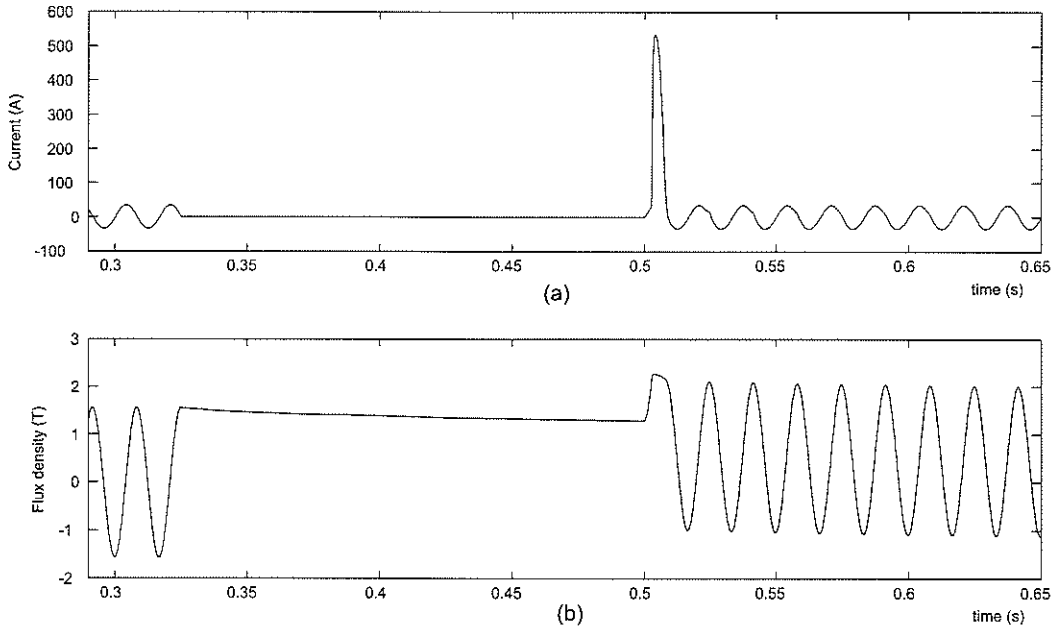

Figure 3.24: Inrush cases: New model with the breaker re-closed after 180ms. (a)Waveform of current; (b)Waveform of flux density

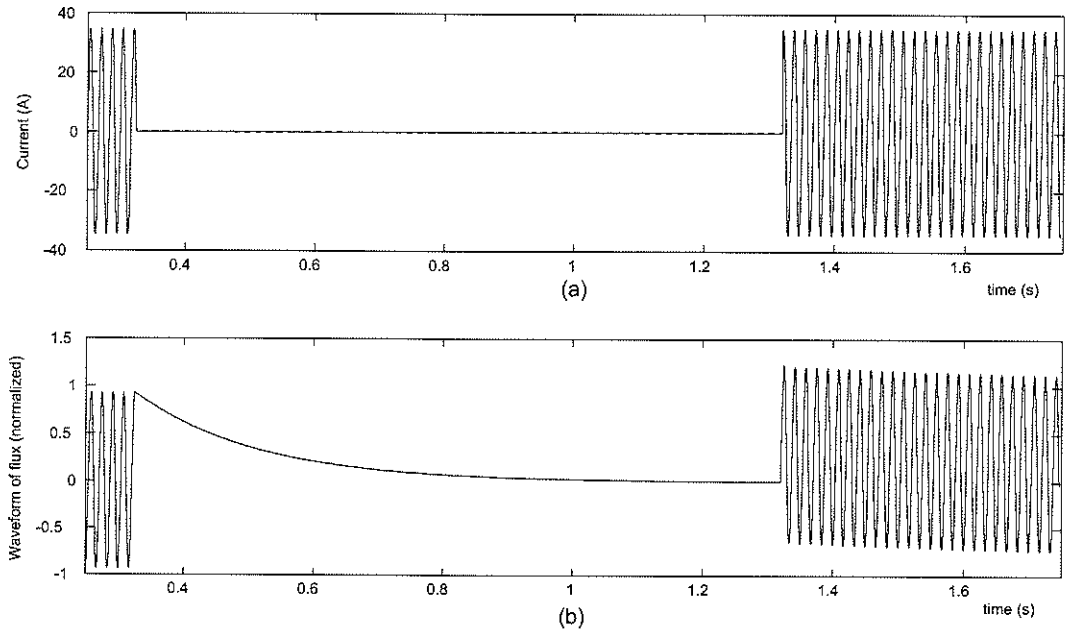

Figure 3.25: Inrush cases: Existing model with the breaker re-closed after 1.0s. (a)Waveform of current; (b)Waveform of flux (normalized)

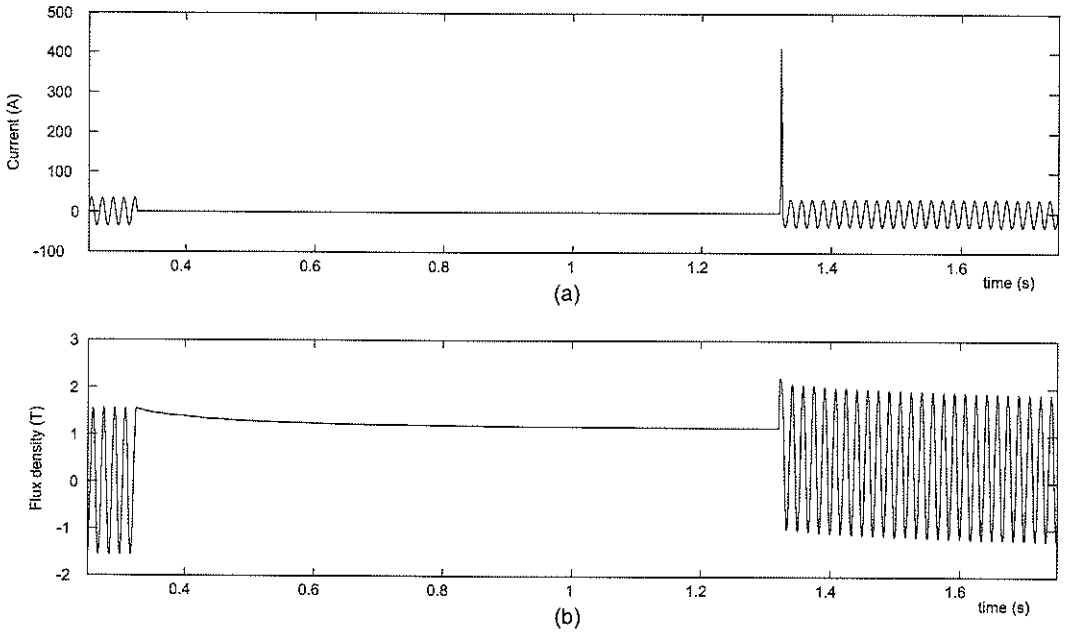

Figure 3.26: Inrush cases: New model with the breaker re-closed after 1.0s. (a)Waveform of current; (b)Waveform of flux density.

3.4 Summary

This Chapter focused on the validation of the new model using recorded waveforms. A series of tests were carried out using a 3 kVA, 115 V/ 2300 V, 60 Hz single phase distribution transformer. Simulation results for open circuit tests on a single phase two winding transformer model are compared with test results. Simulation results are in good agreement with recorded waveforms. Meanwhile, comparisons carried out at different frequencies of excitation have highlighted the importance of modeling the frequency dependency of the B-H loop.

Simulations were carried out to compare the simulated waveforms obtained with the new model against an existing transformer model, that has a piece-wise linear representation of saturation. Simulation results also show that the new model represents long term remanence and recoil loops in the core, whereas a piece-wise linear model fails to maintain the remanent flux beyond several hundred milliseconds, depending on circuit time constants.

Simulation results were also compared with the recorded waveforms of inrush current. A good agreement is seen between the simulated and recorded waveforms.

Chapter 4

GIC Studies: Comparisons

The simulation study of a GIC event involves dc superimposed on the normal ac excitation of a power system. Hence, these studies are usually based on the injection of measured or predicted values of quasi-dc current into the simulation model of power transformers. This is followed by the analysis of the effects of GIC on the simulated power system.

Validation of a simulation model using measured data allows to adjust the simulation model to correspond to actual conditions. The measured data and recorded waveforms captured during a GIC event may include the waveforms or the harmonic content of the current in transmission lines and the current at the neutral of power transformers. These data can be obtained from the SUNBURST recorders installed at different locations. SUNBURST is the name given to the monitoring system that was installed to collect data on the characteristics and effects of GIC in substations and generating stations across North America [63]. In addition to the GIC data, the power flow in transmission lines and system bus voltages across the network, before and during the event, are also essential for validations.

During the past decade, there have been numerous studies carried out to analyse

the effects of GIC on power systems, where the simulation results have been compared with measured data for validations. Most of these studies have used a piecewise linear representation to model the saturation characteristics of a transformer [64][65][66]. A curve fitting technique that represent the hysteresis effects has been used in references [17][32]. A GIC study involving a large power system that consists of over 2000 buses has been carried out using a standard load flow programme, where a finite element programme has been used to determine the earth surface potential [67][68].

The simulation results presented in chapter 3 have shown that the new transformer model developed in chapter 2 properly represents the magnetizing characteristics of a transformer, that includes the long term remanence and recoil loops. Therefore, the new model can be considered as an excellent candidate for the analysis of the effects of GIC on a power system. The following description focuses on analysing a GIC event in a power system, that includes the comparison of simulation results with recorded waveforms to validate the simulation model.

4.1 A Recorded GIC Event

Simulation studies carried out in reference [17] and [32] had compared simulation results with recorded data of a GIC event. These studies have been carried out using recordings from the SUNBURST recorder at the Dorsey converter station, and a power system model of the Dorsey substation and the 500 kV transmission line from Dorsey, Manitoba to Forbes and Chisago in Minnesota.

The SUNBURST recorder is no longer available at Dorsey, and in the absence of more recent recordings during a GIC event at this location, GIC studies carried out in reference [17] and [32] were used as the basis of the analysis presented here. There are two recorded GIC events compared in reference [32]. The event in 1993, which is the

more recent recording, was chosen for this analysis as reference [32] presents sufficient information about this event along with the recorded waveforms. The description of this GIC event is as follows.

"On the 5^{th} October 1993, the SUNBURST recorder at the Dorsey substation took a snapshot of the 500 kV line voltage and the current of the secondary side of the current and voltage transformers. The time of the recording was 04.59 GMT and the corresponding GIC in the transformer neutral was 30 A. The power flow out of Dorsey was -53.2 MW and -137.1 Mvar. The power flow out of Forbes was -100.1 MW and -34.8 Mvar" [32].

4.2 Description of the System

The 500 kV transmission line system connects three utility companies as shown in Fig.4.1. The northern section of the system is 528 km long and it connects Manitoba Hydro's Dorsey HVDC Converter station to Excel Energy's Forbes substation. The southern section of the system is 220 km long and it connects Forbes substation to Minnesota Power's Chisago substation. The simulated circuit is shown in Appendix C, Fig.C.1.

Three phase shunt reactors with sizes 225 Mvar, 300 Mvar and 150 Mvar are installed at the Dorsey, Forbes and Chisago substations respectively. Neutral reactors with sizes 425 Ω, 325 Ω, and 1250 Ω are located in Dorsey, Forbes and Chisago respectively. The Dorsey-Forbes section of the transmission line is transposed at 4 locations and Forbes-Chisago section is transposed at 3 locations.

The autotransformer at Dorsey consists of three single phase units and each separate unit is a two winding transformer. The windings are connected to form a 230/500/46 kV three phase unit with the 230 kV and 500 kV windings connected

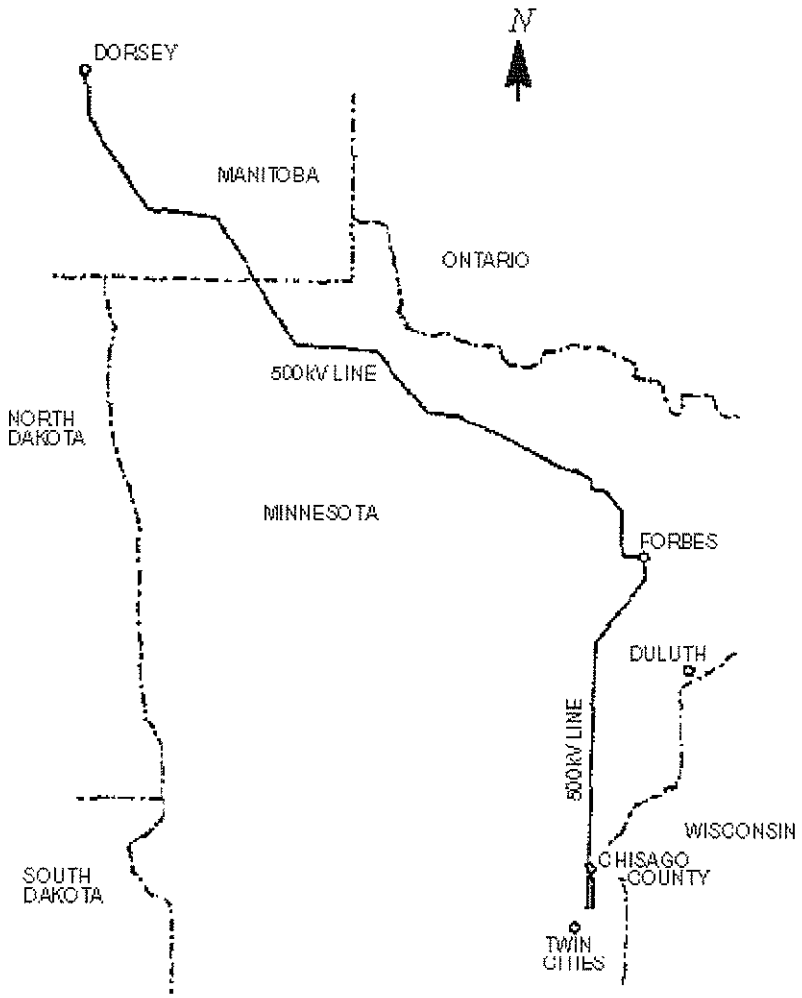

Figure 4.1: Dorsey, Forbes, and Chisago 500 kV network

as an autotransformer. The 230 kV and 500 kV windings are star connected and grounded whereas the 46 kV winding is connected as a delta winding. The transformer is rated for 720 MVA without cooling and 1200 MVA with cooling. The autotransformer at Forbes is similar with the exception that the tertiary winding is rated for only 13.8 kV. At the Dorsey Substation, filters are connected on the 230 kV side to minimize the harmonics introduced by the HVDC converter station. There is also a delta connected bank of capacitors of 15.3 μF each connected to the 46 kV

tertiary winding.

Fig.4.2a shows the recorded waveforms of three phase currents in the 500 kV line at Dorsey. Fig.4.2b shows the harmonic content of the line currents, where a high content of 2^{nd}, 3^{rd}, 4^{th}, and 5^{th} harmonics can be seen.

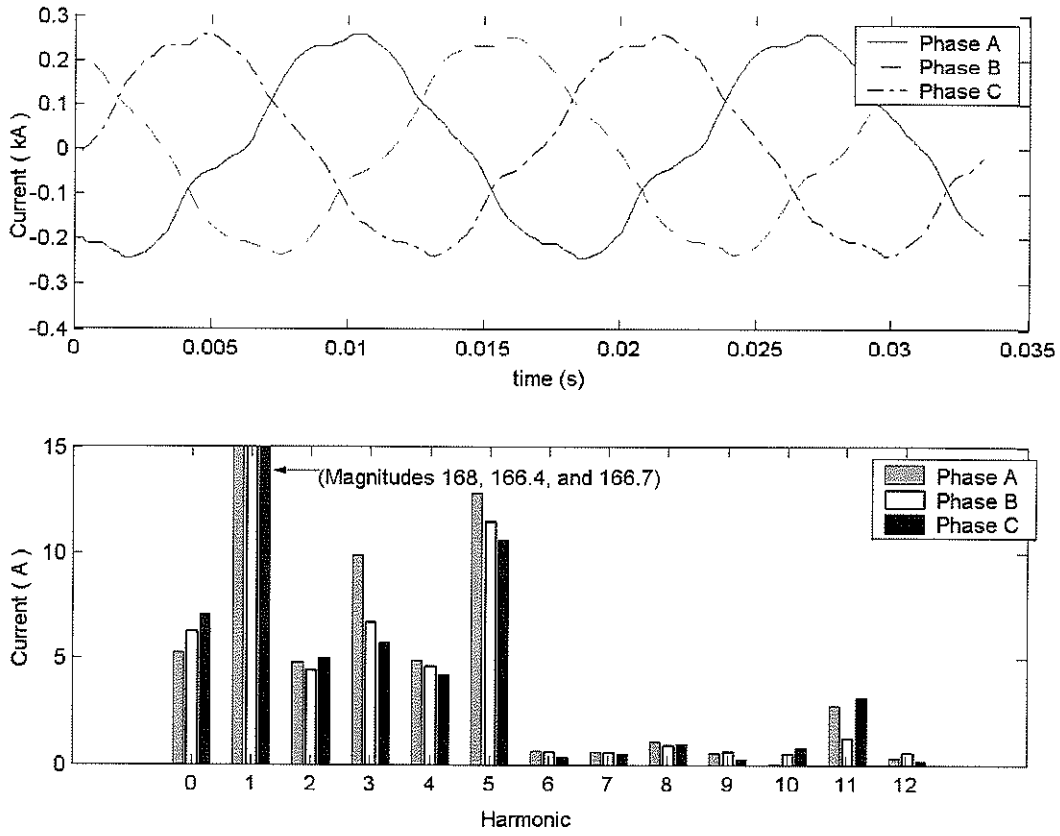

Figure 4.2: (a) Recorded waveform of current in the 500 kV line at Dorsey; (b) Harmonic content of this waveform.

The following section describes how this system could be represented in an electromagnetic transient simulation programme to analyze a GIC event.

4.3 Modelling a GIC Event in an Electromagnetic Transient Simulation Programme

The transient simulation software PSCAD/EMTDC is considered as an example to describe details of the features that are essential to be modelled. Since the new model has already been incorporated into this software package as described in Chapters 2 and 3, the power system under consideration can be represented using the existing models such as transmission line models, source models etc. Several assumptions were made in the modelling, sometimes due to lack of data and sometimes to make the system simpler.

4.3.1 Transformers

A simulation study aimed at analysing the effects of GIC in a power system requires accurate representation of magnetizing characteristics of power transformers. Thus in this study, the 230/500/46 kV, 240 MVA transformers at Dorsey and Forbes substations were represented with the new model. Meanwhile, measured data such as waveforms of the magnetizing currents, B-H loop of the core, and core dimensions were not available to derive the parameters. Therefore, open circuit test results, and name plate data were used to derive the parameters, so that the transformer is represented with an equivalent inductance matrix (Appendix C). The B-H data given in Table 3.1 were used as the basis of this calculation. This is based on the assumption that the core material is likely to be the same; i.e. grain oriented silicon steel. A peak operating flux density of 1.65 T was assumed.

Once the parameters of the anhysteretic magnetization curve are calculated, the eddy current effects can be incorporated by calculating the constants k_1 and k_2 in

(2.53). These constants were introduced as part of the expressions derived in section 2.4.3, where the effects of classical eddy current losses and excess losses were considered. In addition, the length of the core limb (2.27) can be determined to simulate the measured rms magnetizing current and the measured power loss at rated conditions. Using these calculated values, the magnitudes of open-circuit V-I characteristics are found and compared with the measured data. The slope of the anhysteretic curve in the saturation region was slightly adjusted to closely match the measured characteristics. Fig.4.3 shows the measured V-I characteristics of the transformers at Dorsey compared with the simulated V-I curve, and Fig.4.4 shows the simulated hysteresis loop at the rated conditions.

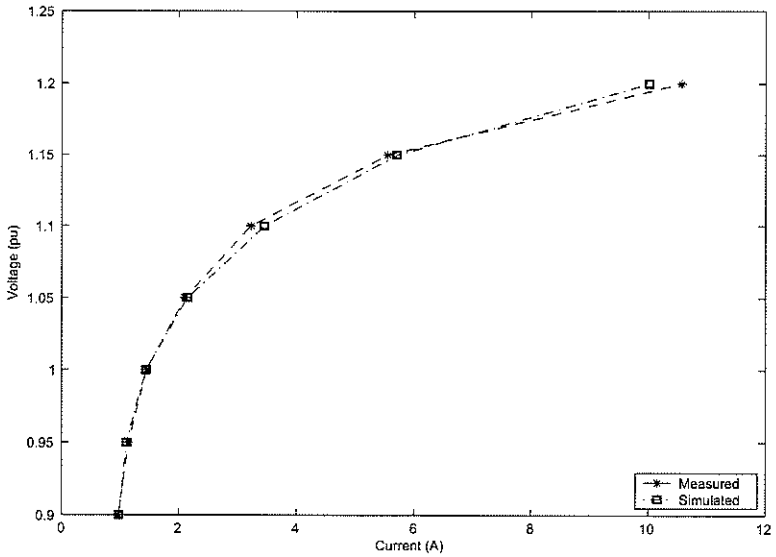

Figure 4.3: V-I characteristics of the 230/500/46 kV, 240 MVA single phase transformer

The winding resistances of transformers were represented with external resistors as they are important in a GIC study [5]. This is due to the fact that, during half cycle saturation, the dc component in the magnetizing current causes a voltage drop across the resistances that eventually leads to an equilibrium in saturation when the

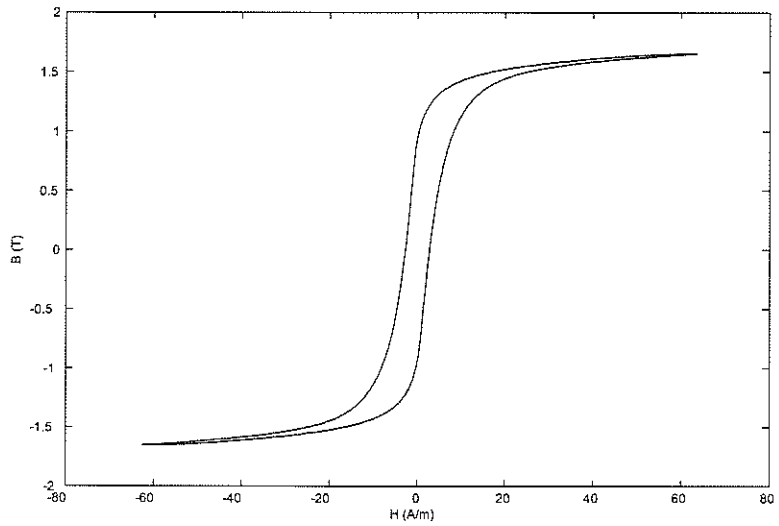

Figure 4.4: Simulated hysteresis loop at the rated conditions

voltage drop becomes equal to the dc bias that causes half cycle saturation [65].

The autotransformers at Forbes substation are similar to the autotransformers at Dorsey, with the exception that the tertiary winding is rated for 13.8 kV at Forbes, whereas it is 46 kV at Dorsey. Therefore, in the absence of measured V-I characteristics, it was assumed that the transformer at Forbes follows the same saturation characteristics as that of the Dorsey transformer.

4.3.2 Injecting GIC

GIC are quasi-dc currents that have a very slow variation in frequency. Severe GIC events can persist for several hours and can occur for several days in succession. However, a high magnitude of GIC with one polarity usually lasts for a few minutes before changing polarity [69].

If a uniform electric field is assumed during a GIC event, the resulting current can be represented with driving voltage sources that can be connected between the

grounded neutrals with a finite resistance to the remote end as in [32][68][70]. Generally each source can be modelled as either a Thevenin voltage source behind the neutral grounding resistance or a Norton current source in parallel with the neutral grounding resistance [5].

However, quite often this assumption does not correspond to actual conditions. This is due to the fact that the electric field produced at the earth's surface will have a maximum directly underneath the electrojet current and the magnitude will decay with increasing distance on either side. Considering a network of four substations [25] has shown that a source connected in the transmission line is more suitable for modelling GIC with a non uniform electric field.

Fig.4.5 shows an assumed network of four substations . It has been assumed that the transmission lines AB and CD run in a north - south direction and lines AD and BC run in an east - west direction, with each line being 100 km long having identical characteristics and grounding impedance. Assuming a non uniform electric field, it has been assumed that the electric field along lines BC and AD are 4.9 V/km and 3.2 V/km respectively. This can be represented either with a source connected in the transmission line (Fig.4.5a) or with a source connected at the grounding node (Fig.4.5b). However, due to the nature of the electric fields, sources connected at the grounding nodes also produces an electric field of 1.7 V/km along the line BA, that is not consistent with the electric fields produced by the electrojet. Therefore, in order to represent a non uniform electric field produced by the electrojet current during a GIC event, a source connected in the transmission line should be used.

In these simulation studies, a voltage source was connected in the transmission line between Dorsey and Forbes forcing a GIC to flow into the transformer neutral at Dorsey and to go through the northern section of the transmission line finally leaving

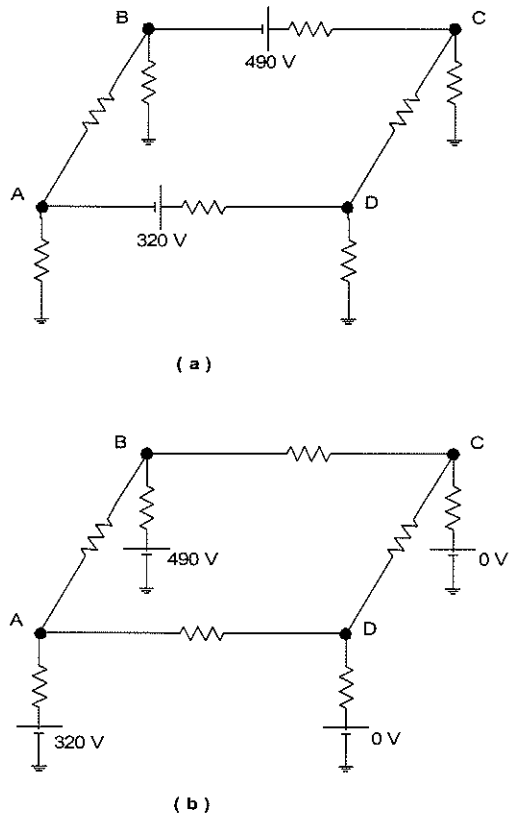

Figure 4.5: Modelling GIC due to a realistic field; (a) using a voltage source in the transmission line; (b) using a voltage source at the grounding point.

the system at Forbes transformer neutral. Meanwhile, a voltage source connected at the neutral of the transformer would have produced similar results, since the network considered has only three substations, that are connected by two transmission lines. However, a voltage source connected in the transmission line is suitable for any network configuration, and hence this representation was used.

It was also assumed that the electric field between Forbes and Chisago is negligible compared with that between Dorsey and Forbes. This is due to the fact that the northern section of the 500 kV line is much longer in length and it is closer to the north pole giving rise to a higher electric field than in the southern section. In

addition, field measurements have also shown that it is more likely to have an electric field in the east - west (E - W) direction rather than the north - south (N - S) direction [71][72]. Meanwhile, the northern section of the line runs in a north west - south east (NW - SE) direction whereas the southern section runs mainly in north - south (N - S) direction. Therefore it is reasonable to assume an electric field between the northern section (Dorsey - Forbes) and assume that the electric field in the southern section between Forbes and Chisago is negligible.

4.3.3 System Model

Modelling of transmission lines plays an important role in studying the effects of GIC in a power system. The transmission lines can be modeled using a travelling wave model in an electromagnetic transient simulation programme. Since the simulations were carried out with PSCAD/EMTDC, transmission lines were represented using the frequency dependent phase model. The phase domain frequency dependent model represents all the frequency dependent effects of a transmission line using a frequency dependent modal transformation matrix [73][74].

One section of the line was represented in two segments and it was assumed that the lines were ideally transposed. For example, the transmission line between the Dorsey and Forbes substations was represented with two segments. This representation was adopted so that the source of the quasi-dc voltage source can be connected in series with the transmission line. In addition, the ground wires were eliminated during the initialization of the transmission line model. This is due to the fact that the ground wire will carry an extremely small portion of GIC, and usually the presence of tower footing resistance further limits the current entering a grounded wire.

The model of Dorsey substation consists of the three phase autotransformer, line

reactors, ac side filters of the HVDC converter station, and an equivalent source representing the 230 kV system. The actual description of this event does not clearly indicate further information about the status of each component. Therefore simulation studies carried out in reference [32] were considered as the basis for initialization of simulations. The Forbes substation was represented with the three phase autotransformer, line reactors, and an equivalent source to represent the 230 kV system. The Chisago subsystem was represented as a 500 kV source with an internal inductance, although, in reality, transformers and reactors are present.

Once the system model is properly represented, the initial conditions can be adjusted so that the recorded power flow is simulated. This is achieved by performing a load flow analysis on the system under consideration using a load flow programme. The load flow study provides the power flow data. The same load flow information is also used to obtain the network equivalents at the required nodes of the network , so that the transient simulation can be initialized.

4.4 Comparisons

Based on the description provided for this event in reference [32], a maximum dc neutral current of 30 A has been observed during this event. However, a comparison of the magnitudes of dc neutral current shown in Fig.4.2b indicates that the total dc neutral current at the instant when the waveform was recorded was 18.75 A. Hence it is clear that the recordings have been taken when the neutral current was not at the maximum. Therefore, this recording must have been taken during an instant when the dc current was either increasing or decreasing. Without any prior knowledge about the history of the waveform of quasi-dc neutral current and the state of the transformer core, a demagnetized core was assumed as the initial condition.

In addition, in the absence of the recorded values or a predicted variation of quasi-dc current, the simulation was carried out by considering a constant dc current of 18.75 A at the neutral. Comparison of the waveform current in phase A of the 500 kV line and its harmonic content are shown in Figs.4.6 and 4.7 respectively. The magnitudes of the 2^{nd}, 3^{rd} and 5^{th} harmonics are significantly higher in the measured waveform, whereas the 8^{th} and 11^{th} harmonics are higher in the simulated waveform. In addition, it was observed that the reactive power consumption of the transformer has increased from 2.5 Mvars to 10 Mvars due to half cycle saturation.

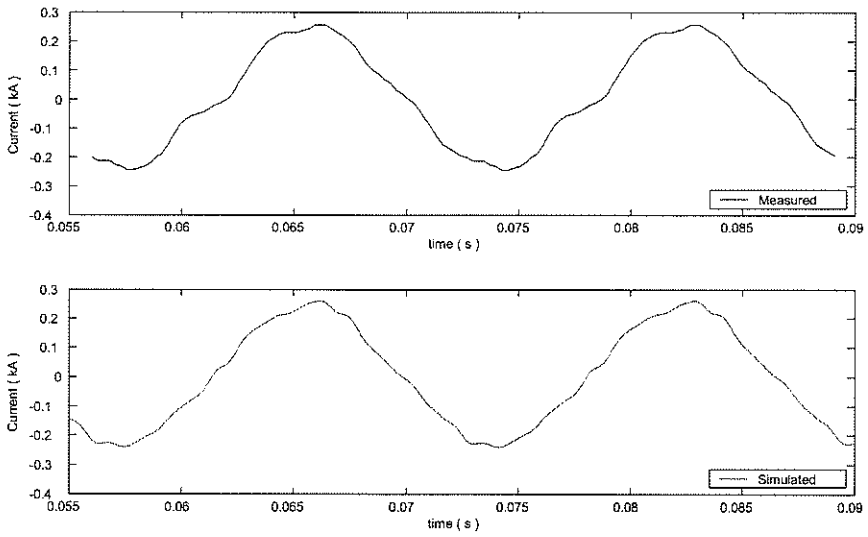

Figure 4.6: Comparison of the waveform of current in the 500 kV line ; (a) measured, (b) simulated with a constant neutral dc current of 18.75 A

The same simulation was carried out with a constant dc neutral current of 30 A to analyze the waveforms under maximum neutral dc current reported. Comparison of the waveform of currents and the harmonic contents of the recorded and simulated waveforms are shown in Figs.4.8 and 4.9 respectively. The harmonic content of the measured waveform and the simulated waveform shows a significant difference in the

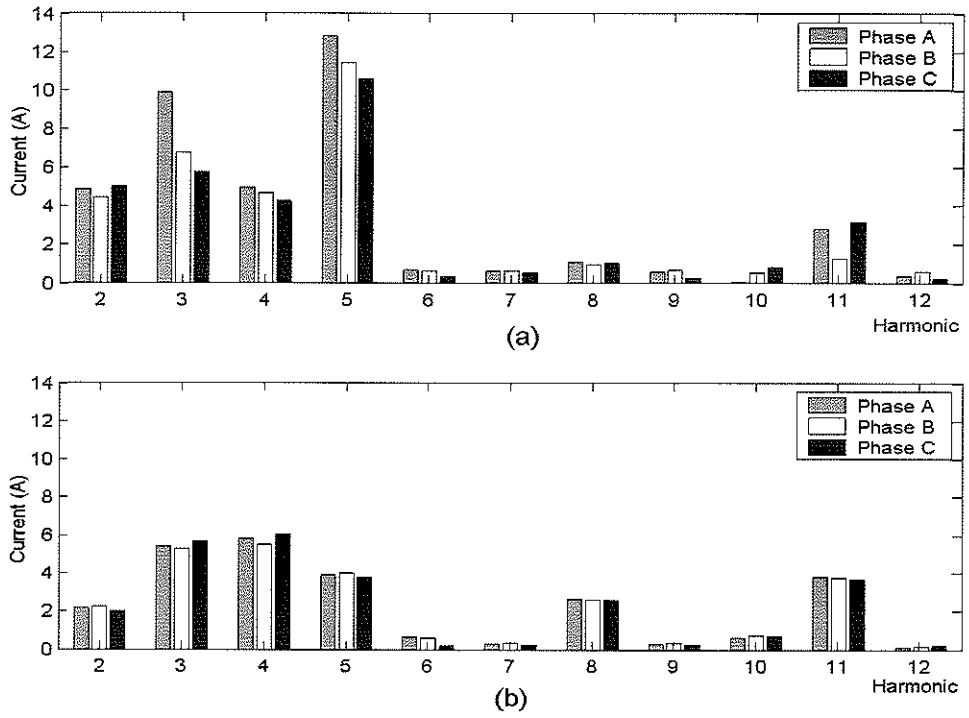

Figure 4.7: Harmonic content of the waveforms of current shown in Fig.4.6; (a) Measured, (b) Simulated

magnitudes of the 5^{th}, 8^{th} and 11^{th} harmonics. In addition, the simulated waveform shows more distortions than does the recorded waveform. These distortions can be attributed to an increased magnetizing current drawn by the transformer during half cycle saturation. The simulated hysteresis loop in Fig.4.10 shows the extent of half cycle saturation undergone in the core of the phase A transformer. Meanwhile, with an increased level of saturation in the core due to a higher neutral dc current, the reactive power consumption has increased from 2.5 Mvars to 14 Mvars.

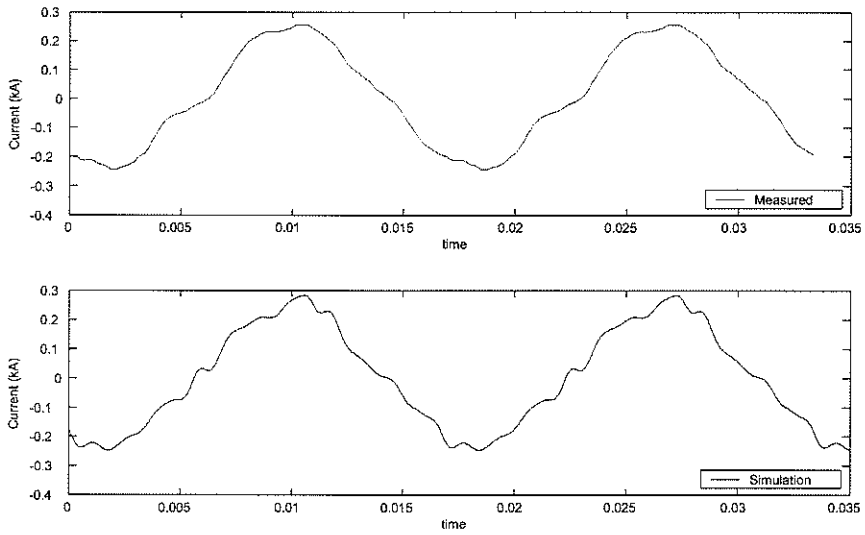

Figure 4.8: Waveform of current in the 500 kV line - phase A; measured and simulated waveforms

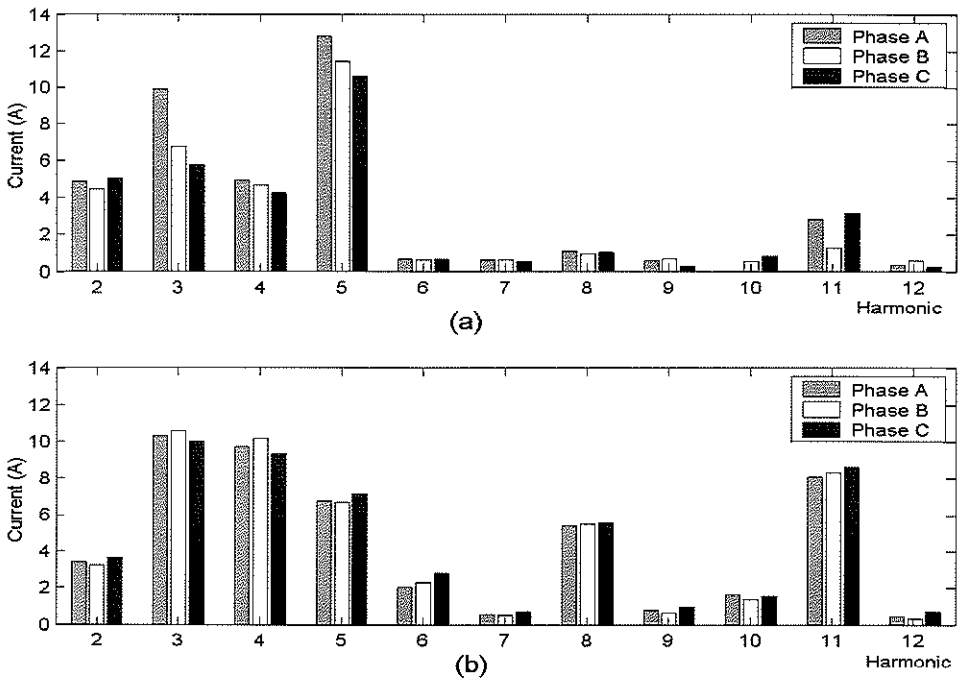

Figure 4.9: Harmonic content of the waveform of current shown in Fig.4.8; (a) Measured; (b) Simulated

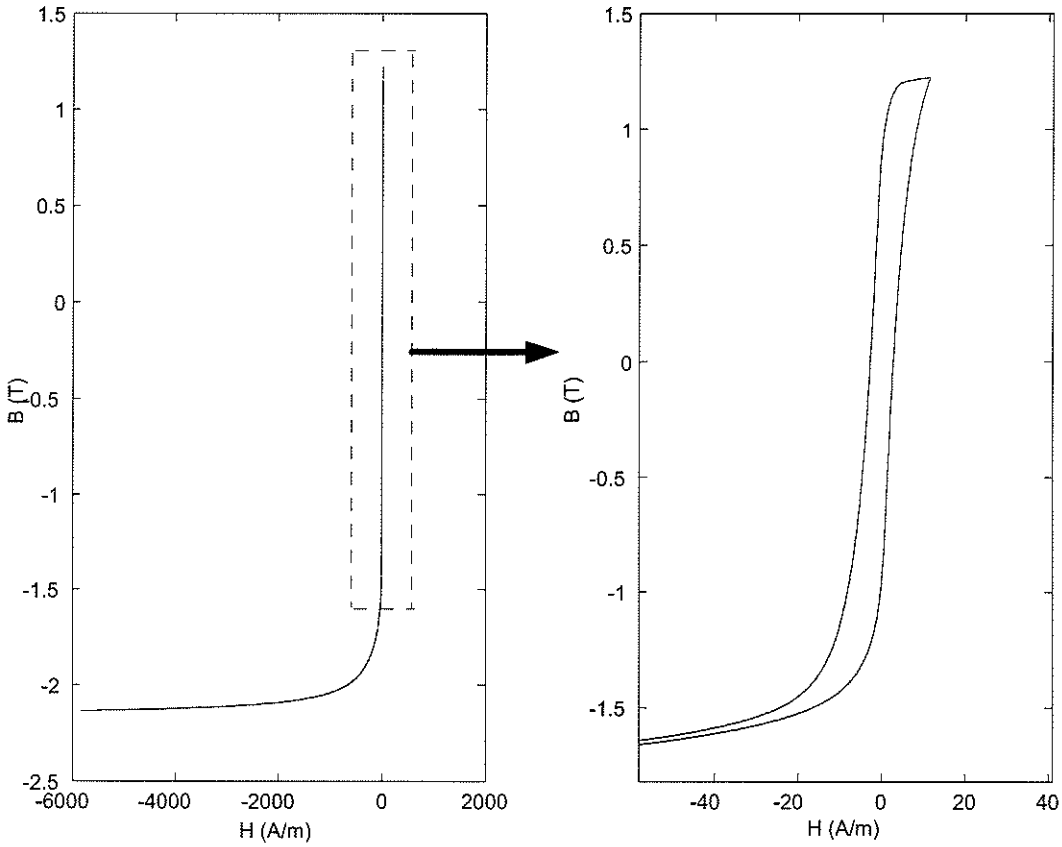

Figure 4.10: Simulated hysteresis loop during a GIC event with a constant dc neutral current of 30 A

4.5 Summary

The focus of this discussion was to show the effects of GIC on a power system, and to show how a recorded GIC event could be modelled using an electromagnetic transient simulation programme for validations and further analysis. The details of the power system model and its features that are essential to be modelled to represent a GIC event were presented. (Also see Appendix C.)

It is clear that in order to facilitate a direct comparison with the recorded data and waveforms, the simulation model should properly represent the conditions that may have prevailed at the instant when the recording was taken. The simulation studies carried out confirmed that the new transformer model represents the effects of half cycle saturation that the core undergoes in the presence of GIC. However, simulations carried out with dc neutral currents of 18.75 A and 30 A respectively, showed that some discrepancies exist between the measured and simulated waveforms.

Meanwhile, the initialization of a simulation model has a direct effect on the simulation results. Therefore, it is likely that the initial conditions assumed during these simulation studies may have contributed towards the discrepancies seen between the measured and simulated waveforms.

The following assumptions may have affected the simulation results;

- Initial conditions of the transformer model, which was represented with a demagnetized core, instead of considering remanent flux (if any) in the core.
- Representing GIC with a constant dc current, instead of considering the actual variation of the quasi-dc current.

In addition, the initial values of the network equivalents, especially the bus voltages, have an effect on the flux in the transformers. However, the initialization of the

transformer model itself becomes more important during a GIC study, as the state of the magnetic core directly depends on its initial conditions. This is because the core of the transformer can have remanent flux as a result of the status of the magnetic core prior to this event under consideration.

In the absence of a recorded waveform of the quasi-dc current, a constant magnitude had to be assumed to represent the effects of GIC. However, a constant dc current in the neutral may not represent the actual conditions, as the history and present variation of the actual quasi-dc current has an effect on state of the core at a particular point of interest. In general, any particular change in the status of the magnetic core, which can be due to remanent flux in the core, or history of the quasi-dc current, could directly affect the harmonic content of the waveform of current and the increase in reactive power consumption in the transformer.

Therefore, the sensitivity of the simulation results to the initial conditions needs to be further investigated to identify how important these effects are. The following chapter focuses on carrying out a sensitivity analysis to consider the dependency of the simulated waveforms on the initial conditions of the transformer model, quasi-dc current, and the simulation model of the power system.

Chapter 5

GIC Studies: Sensitivity Analysis

Comparisons of a GIC event carried out in the previous chapter suggested that the initial conditions assumed may have caused the discrepancy between the simulated and recorded waveforms. However, the recorded data for this event provide waveforms of current in the transmission lines during a short time interval, and do not provide additional information about the waveform of the quasi-dc current or the status of the entire network prior to the recordings. Therefore, the effects of remanent flux in the transformer core, and the history of the quasi-dc current on the simulation results cannot be determined. Thus, it becomes an extremely difficult task to ensure that the simulation conditions closely match the conditions at the time of the recording. Hence further validations could not be carried out for this event.

Therefore, this chapter focuses on analysing the sensitivity of the waveforms of the simulated current to the history of the quasi-dc current, and the remanent flux in the transformer core. These simulation studies show that;

- An electromagnetic transient simulation carried out to model a GIC event requires not only the magnitude of the quasi-dc current, but also its history with

respect to any particular point of interest.

- If a constant neutral dc current is assumed instead of using an actual or a predicted variation of a quasi-dc current, the simulation case may not represent the worst case scenario of that point of interest.

This sensitivity study is also extended to analyse the effects of the magnetization characteristics of the transformer model, and the details of the power system model used. Therefore, this was aimed at identifying the important parameters that are required for a proper initialization of a simulation case, so that it closely matches the actual conditions that may have prevailed.

5.1 History of the Quasi-dc Current

The waveform of the quasi-dc current depends on the complex space weather cycle, its interaction with the earth, and the complex nature of a power system. Thus, the variation of this current cannot be approximated with a simple variation such as a low frequency sinusoid etc. Therefore, a recent recording of a waveform of quasi-dc neutral current obtained from the recorder at the Grand Rapids substation was considered for further analysis. However, these simulation studies do not attempt to simulate the conditions that may have prevailed on 5^{th} October 1993 since they are not known. In addition, a direct comparison cannot be carried out with the simulation results presented in this section and the recorded waveforms of current in the 500 kV line shown in Fig.4.2, due to the same reasons.

Initially a portion of the recording was considered due to the difficulties in simulating a GIC event that spans several hours. The EMTDC simulation scheme was modified to inject the recorded variation of the neutral dc current. These waveforms

were recorded on 15^{th} July 2000 at the Grand Rapids substation. Initially a demagnetized core was assumed before applying the quasi-dc current given in Fig.5.1, which has a peak value of 38 A. This waveform will be referred to as a recorded variation with a 38 A peak in this discussion. In order to analyze the effect of the history of the

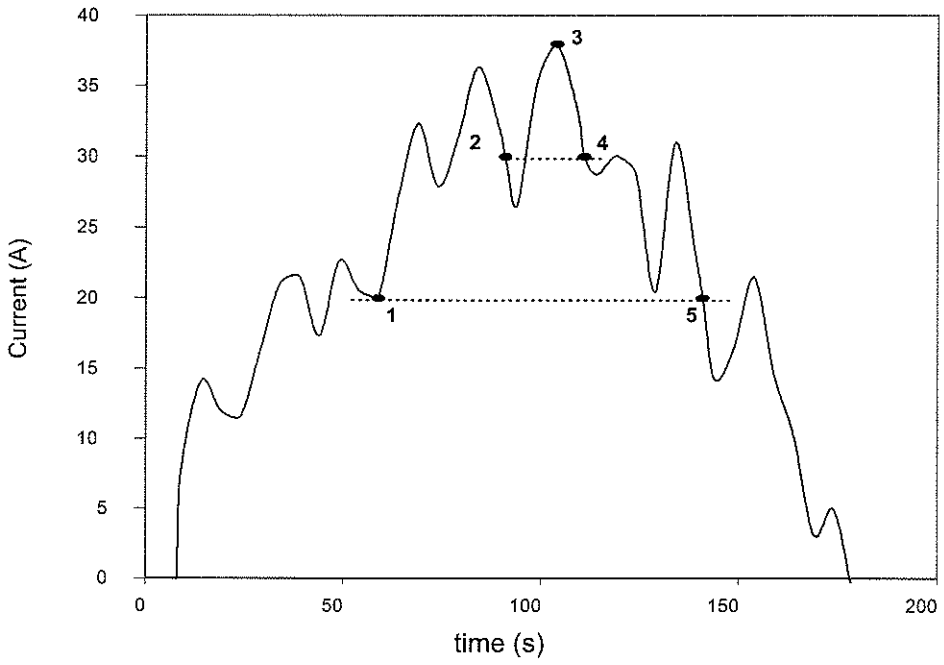

Figure 5.1: Waveform of a recorded neutral dc current considered; (38 A peak)

quasi-dc current, the simulated waveforms of current in the 500 kV line are compared when the total neutral dc current is 20 A, and 30 A respectively. The snapshots taken at points **1** and **5** in Fig.5.1 show the status of the simulated system when the neutral dc current is 20 A. Similarly, snapshots taken at points **2** and **4** in Fig.5.1 are considered when the neutral dc current is 30 A. These simulation results are presented to show the effect of the history of the quasi-dc current on the simulated waveforms.

Fig.5.2a shows the waveform of the line current when the neutral dc current is

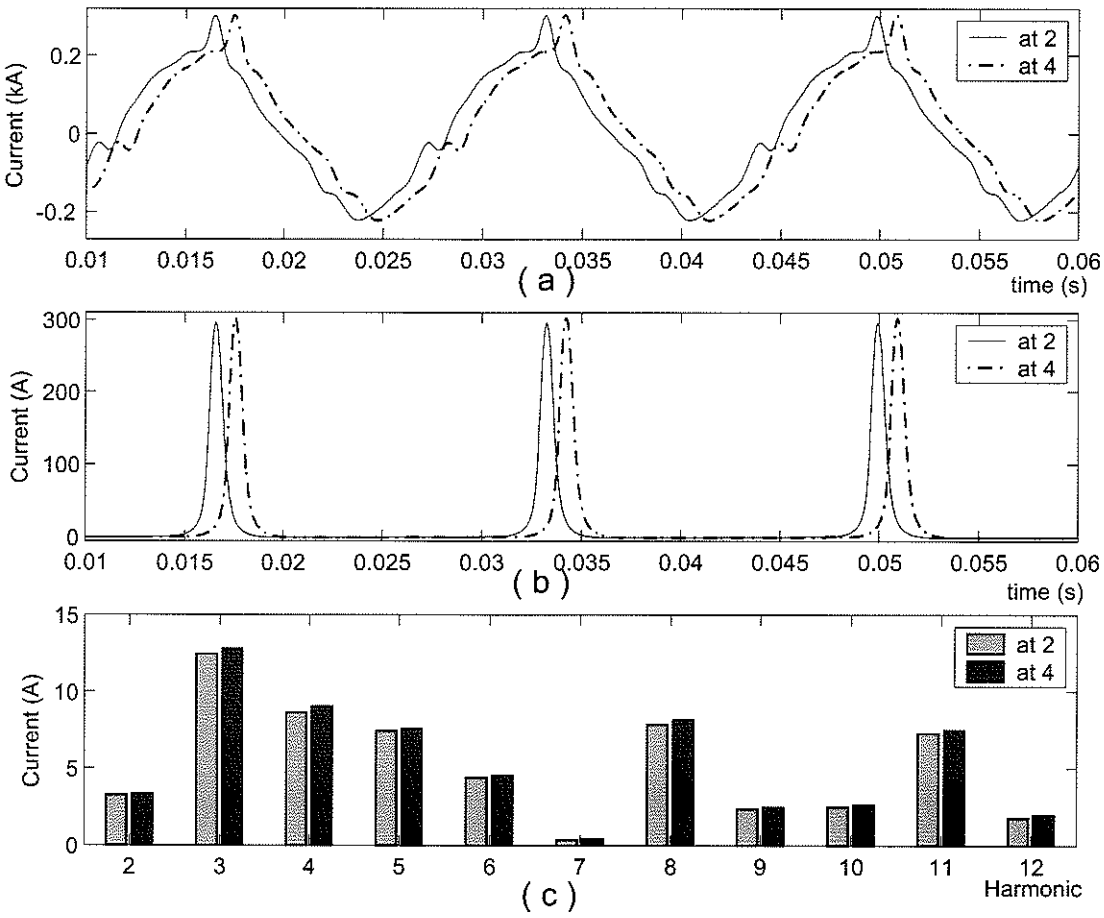

Figure 5.2: (a) Comparison of waveforms of current in the 500 kV line when the dc current was **2** and **4** in Fig.5.1; (b) Magnetizing current of the phase A transformer; (c) Harmonic contents of the waveforms shown in (a)

30A. This comparison considers two snapshots taken at points **2** and **4** in Fig.5.1, with the second snapshot being taken after 20 seconds. Fig.5.2b shows the magnetizing current of the phase A transformer at the Dorsey substation. A slight phase shift was introduced to display differences in the two waveforms. During this interval the neutral dc current has experienced the peak value of 38 A. It is seen that even if the waveforms of current in the transmission line are very similar, the peak value of the waveform of magnetizing current at point **4** is slightly higher than the peak value

at point **2** (Fig.5.2b). Fig.5.2c shows the harmonic content of the two waveforms, in which the magnitude of the fundamental component (166.5 A) was not shown to improve clarity. A slight increase in the magnitude at point **4** is due to the increase in the level of saturation in the core compared to point **2.** Since both points chosen lie closer to the peak value (point **3**), the effect of history at point **4** can be considered insignificant to the waveforms of current in this simulation. However, this effect becomes more significant as the points of interest move away from the peak value.

Figs.5.3a shows the comparison of the line currents when the neutral dc current is 20 A at points **1** and **5**. This comparison considers two snapshots taken 100 seconds apart. Fig.5.3b shows the magnetizing current of the phase A transformer at the Dorsey substation. The waveforms are not completely aligned, which makes it easier to distinguish the two. A considerable increase in the peak value of the magnetizing current at point **5** is due to a higher extent of saturation than at point **1**. The harmonic content of the two waveforms highlights the difference between the two waveforms of line current as in Fig.5.3c. Generally these effects are dependent on the nature of the waveform of quasi-dc current, that includes the peak value, and the time duration between the two snapshots considered. Therefore, this comparison shows that the history of quasi-dc current can significantly affect the extent of the saturation in the transformer core, and hence the simulated waveforms of current.

Table 5.1 shows the increase in reactive power demand (ΔQ) observed in the transformers at the Dorsey substation. The simulation results show that the increase in reactive power demand is dependent on the history of the quasi-dc current. This is consistent with the observations made previously, when the harmonic content of the waveforms of current were compared. Therefore it is clear that the history of the state of the magnetic core directly affects the harmonic content of the simulated

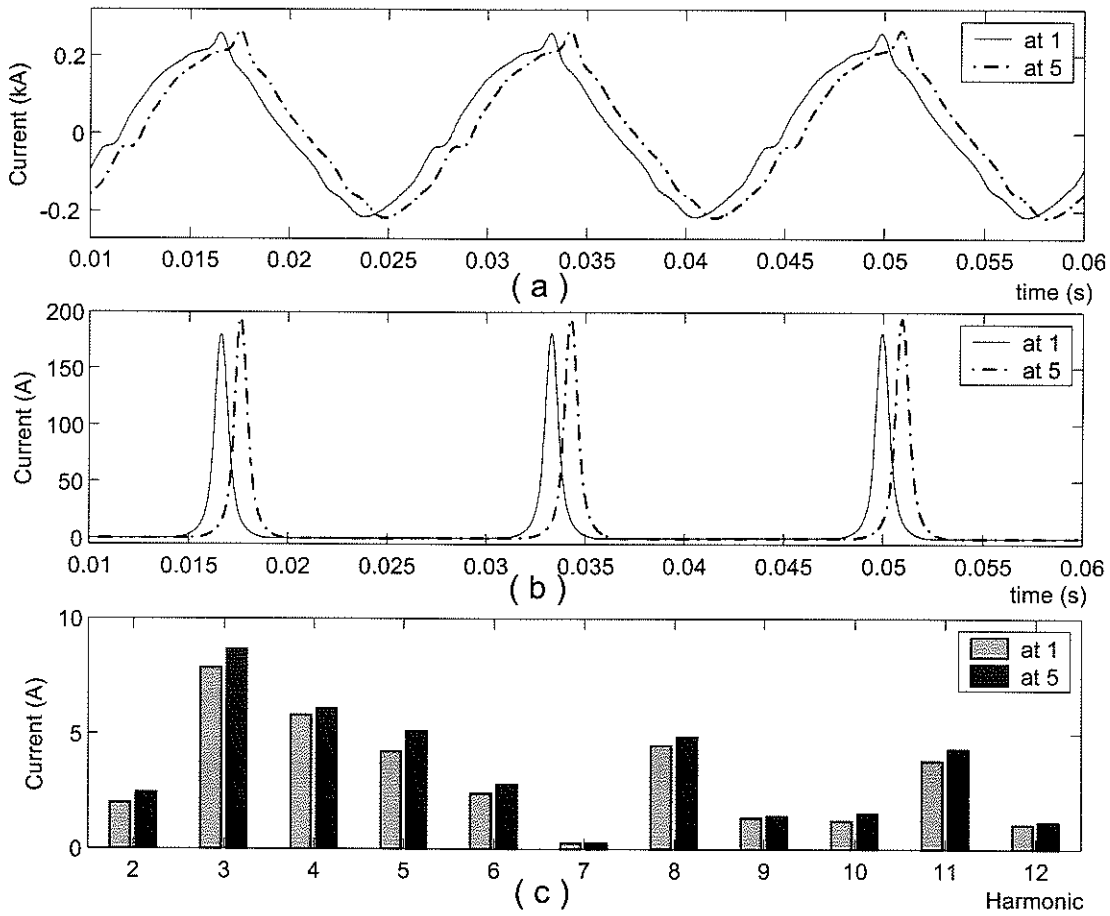

Figure 5.3: (a) Waveform of current in the 500 kV line when the dc current was at **1** and **5** in Fig.5.1; (b) Magnetizing current of the phase A transformer; (c) Harmonic content of the waveforms shown in (a).

Table 5.1: Increase in reactive power demand (ΔQ) observed with the recording of a quasi dc current that has a 38 A peak

Points in Fig.5.1	**1** (20 A$\uparrow$)	**2** (30 A$\uparrow$)	**3** (38 A peak)	**4** (30 A$\downarrow$)	**5** (20 A$\downarrow$)
ΔQ	8.0 MVar	11.8 MVar	14.4 MVar	12.0 MVar	8.4 MVar

Table 5.2: Increase in reactive power demand (ΔQ) observed with the recording of a quasi dc current that has a 65 A peak

Points in Fig.5.4	**1a** (20 A$\uparrow$)	65 A peak	**5b** (20 A$\downarrow$)
ΔQ	4.2 MVar	25.0 MVar	8.4 MVar

waveforms of current, and the increase in reactive power demand in the transformers.

In order to analyze the dependency of the nature of quasi-dc current on this analysis, a different portion of this recording given in Fig.5.4 was considered. This variation has a higher peak value (65 A), and a higher rate of change in the waveform. Similar to the previous comparisons, simulated waveforms of current in the 500 kV line are compared when the neutral dc current is 20 A, that is points **1a** and **5b** in Fig.5.4. Fig.5.5a shows waveforms of current, and Fig.5.5b shows the waveform of magnetizing current at points **1a** and **5b** respectively. A slight phase shift was introduced to display the differences. The harmonic content of the two waveforms of line current are compared in Fig.5.5c. In addition, Table 5.2 shows the magnitudes of the increased reactive power demand of the transformers at the Dorsey substation. These comparisons confirm the observations made with the previous waveform of neutral dc current.

Comparisons carried out so far have considered waveforms of neutral dc current obtained from two different segments of the recording. In the meanwhile, a direct comparison of the simulation results obtained with the two waveforms also provide some interesting observations. The waveform of neutral dc current in Fig.5.1 has a peak value of 38 A, and contains several minor peaks, whereas the waveform in Fig.5.4

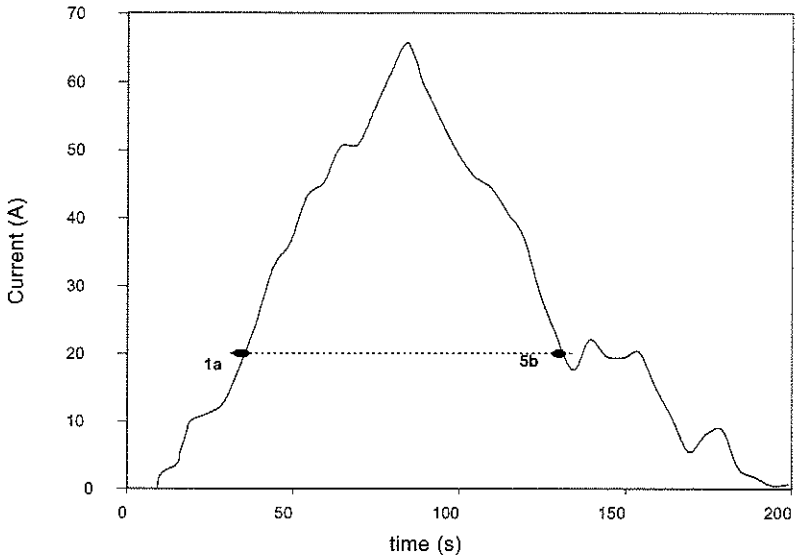

Figure 5.4: Waveform of quasi dc neutral current with a higher peak value

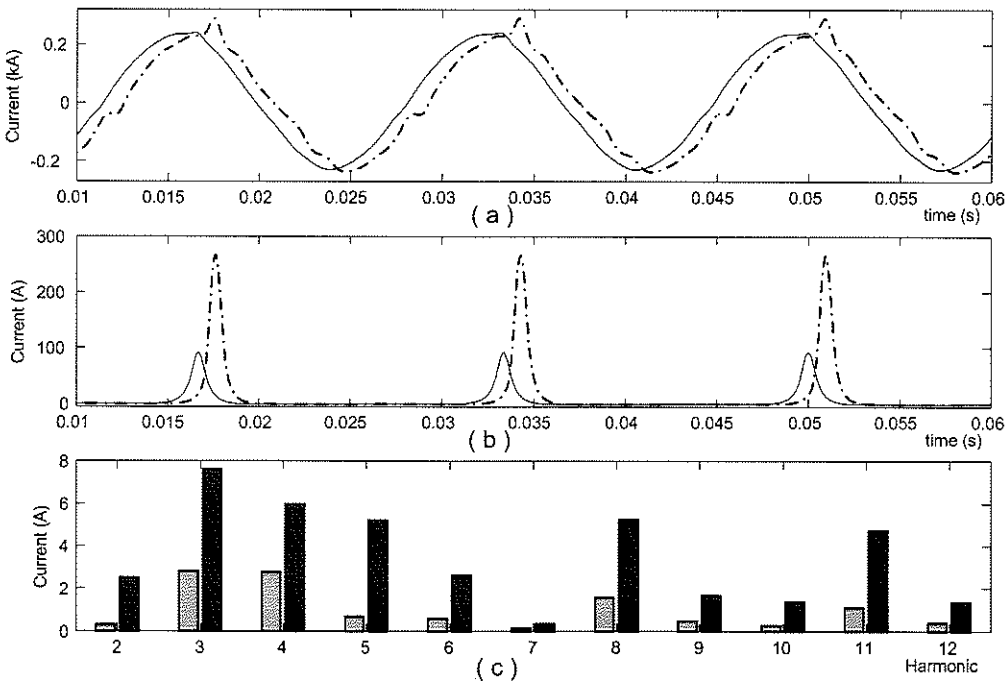

Figure 5.5: Comparison of (a) waveform of current in the 500 kV line; (b) Magnetizing current of the phase A transformer at Dorsey; (c) Harmonic content of the line current, when the neutral current was at **1a** and **5b** in Fig.5.4

has a peak value of 65 A with one major peak, and a higher rate of change. The following comparisons consider the simulated waveforms obtained with the two neutral dc current variations, when the current is either increasing at 20 A or decreasing at 20 A respectively.

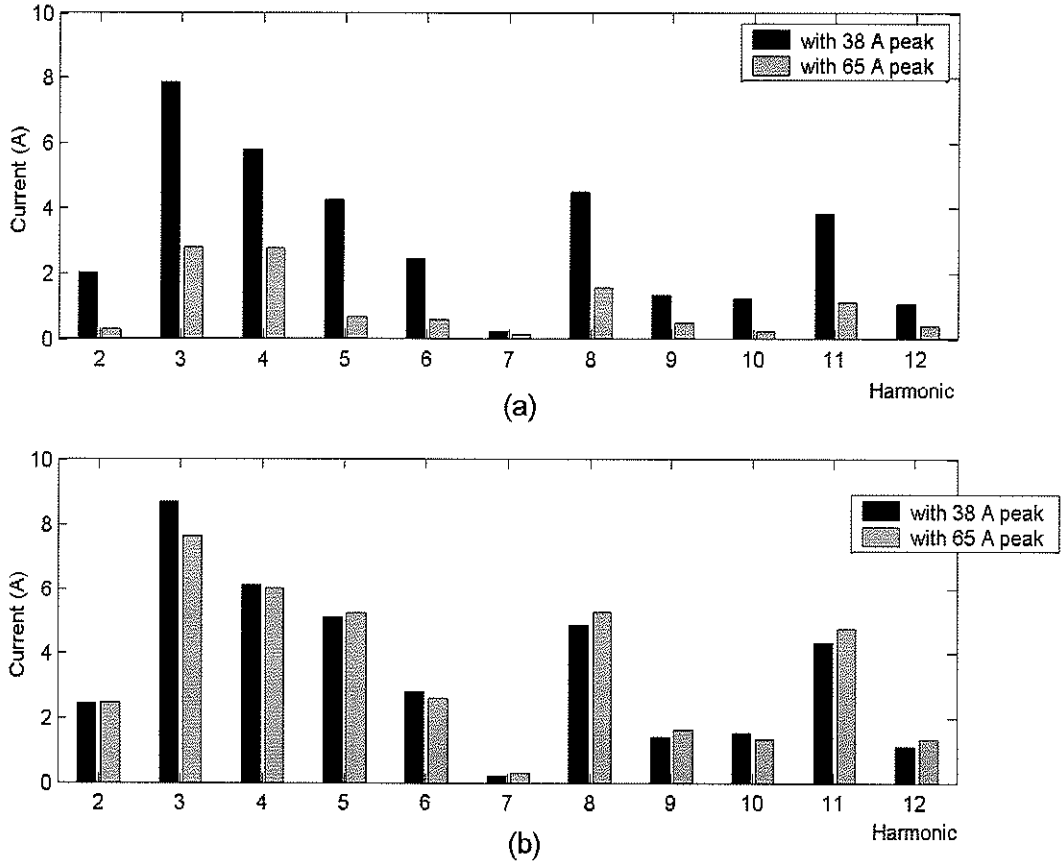

Figure 5.6: Comparison of the harmonic contents when the neutral dc current was; (a) 20 A and increasing; (b) 20 A and decreasing

Fig.5.6a shows the comparison of the harmonic contents when the neutral dc current is increasing at 20 A, that is, snapshots taken at point **1** in Fig.5.1 and point **1a** in Fig.5.4. Similarly, Fig.5.6b shows the comparison of the harmonic contents when the neutral dc current is decreasing at 20 A, that is, point **5** in Fig.5.1 and point **5b** in Fig.5.4. Comparisons in Fig.5.6a shows a significant difference in the

harmonic content of the simulated waveforms. Both simulations were initialized assuming a demagnetized core, and the harmonic contents are compared at the same magnitude of neutral dc current. Therefore, it is clear that the rate of change of dc current has affected the extent of saturation, and hence the harmonic content of the waveform of simulated current. Meanwhile, comparisons in Fig.5.6b are shown for the completeness of this analysis. That is, when the neutral dc current is decreasing at 20 A. During the two simulation cases under consideration, transformer cores have undergone different extents of saturation due to two peak currents (38 A and 65 A respectively). Since then, these have been experiencing a gradual reduction in the extent of saturation due to the nature of the dc bias. In addition, similar effects can be expected in the transformers at the Forbes substation. Comparison of the harmonic contents show that both the peak value, and the rate of change of the dc current have affected the extent of saturation, as seen in the two waveforms when the neutral dc current is decreasing at 20 A. That is, at point **5** in Fig.5.1 which has a peak value of 38 A, and at point **5b** in Fig.5.4 which has a peak value of 65 A.

The foregoing discussion has shown the dependency of the simulated waveforms of current on the history of the quasi-dc current. However, if a recorded waveform or a predicted variation of the quasi-dc current is not known, a constant dc current may be used to simulate the effects of GIC in a power system. The following comparisons analyse the sensitivity of this assumption on the simulated waveforms. These comparisons show that if a constant dc current is assumed instead of using a measured or a predicted variation of quasi-dc current, this may not represent the worst case scenario of that event.

This discussion considers a comparison previously presented in the Chapter 4. A simulation was carried out with a constant neutral dc current of 18.75 A, and its

simulation results were shown in Figs.4.6 and 4.7 respectively. During this simulation, a constant neutral dc current had to be assumed due to lack of knowledge of the past variation of the quasi-dc current.

Meanwhile, simulation results presented in this chapter have considered two segments of a recorded quasi-dc current. Therefore, a direct comparison can be carried out by considering the three simulation cases at the same level of dc current. That is; (1) a simulation carried out by assuming a constant dc current of 18.75 A (Fig.4.7), (2) simulation results obtained at the same dc current, when the recorded variation with a 38 A peak is considered, and (3) simulation results obtained at the same dc current, when the recorded variation with a 65 A peak is considered. When a constant dc current was applied, the simulation was extended for a longer duration, so that the transformer is fully saturated for the given dc bias.

Fig.5.7 shows the comparison of the harmonic content of current in phase A of the 500 kV line obtained with, (a) a constant dc current of 18.75 A, and a snapshot taken at the same current when the recorded variation with a 38 A peak is considered, (b) a constant dc current of 18.75 A, and a snapshot taken at the same current when recorded variation with a 65 A peak is considered. In both cases, simulation results obtained with the recorded variation has shown a higher extent of saturation in the core. This is due to the fact that the history of the state of the magnetic core determines its present status. Hence a higher peak current in the recorded variations have affected the status of the magnetic core at the instance when simulation results are compared.

In addition, simulations were also carried out to consider the sensitivity of representing GIC with a constant dc current, when it is used to simulate the peak dc current. Simulations carried out by applying a constant dc current of 38 A and 65

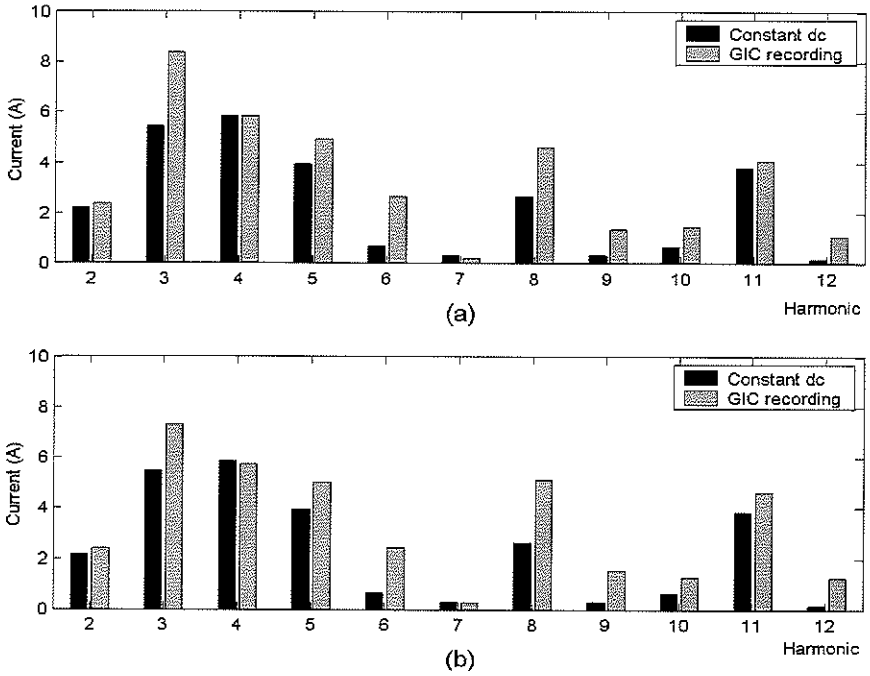

Figure 5.7: Harmonic content in the phase A current obtained with a constant neutral dc current and recorded variations; (a) recorded variation with a 38 A peak, (b) recorded variation with a 65 A peak

A are compared with the snapshots taken at the peak dc current when the recorded variations of 38 A peak and 65 A peak are considered. Fig.5.8 shows the harmonic content of the waveform of current obtained with (a) a constant dc current of 38 A, and the recorded variation with a 38 A peak, (b) a constant dc current of 65 A, and the recorded variation with a 65 A peak. This comparison shows that if the point of interest is the maximum, a simulation carried out with a constant dc current may represent the same conditions as with a recorded variation of quasi-dc current.

Meanwhile, all three simulations have assumed a demagnetized core as the initial conditions, and hence any effects of remanent flux have been ignored. Therefore, these comparisons show that a constant dc current representation of GIC may not represent the worst case scenario, unless that point of interest has the maximum dc

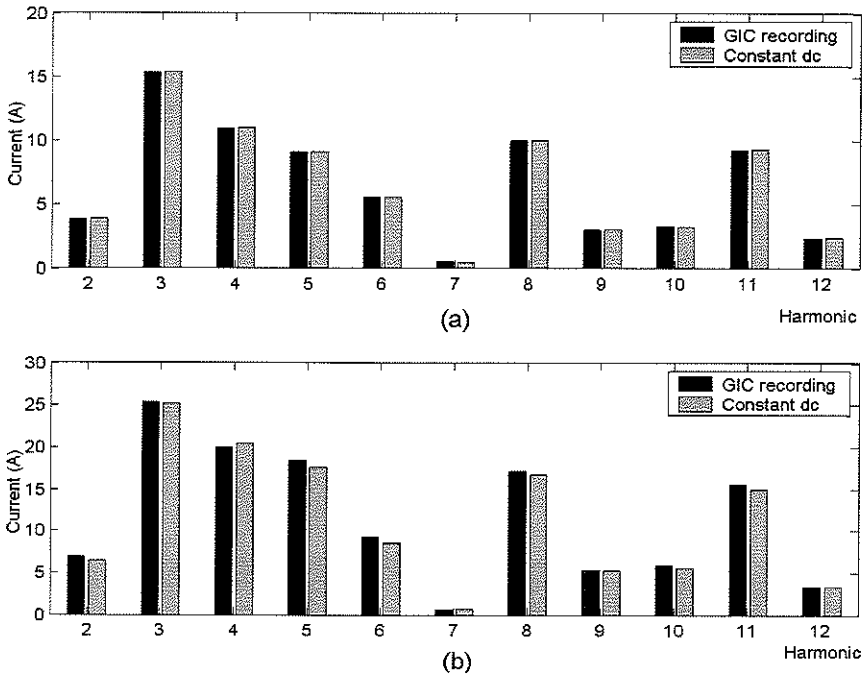

Figure 5.8: Simulation results obtained with a constant dc current, and recordings at the maximum (a) 38 A constant dc and the 38 A variation at the peak; (b) 65 A constant dc and the 65 A variation at the peak.

current, and the effects of remanence are not considered.

The presence of remanent flux in the core is expected to affect the simulations significantly. Hence, the following section focuses on establishing the effects of remanent flux on the simulated waveforms of current.

Remanent flux in the core

Comparisons presented in this chapter so far have assumed a demagnetized core as the initial condition before applying a recorded variation of neutral dc current into the simulation model. However, a GIC event could last for a few hours with a significant intensity, and sometimes the entire duration of activity could be of the order of a few days. Therefore the effect of this total quasi-dc variation could affect the remanent

flux in the core. Although it is extremely difficult to carry out a transient simulation to consider effects that span several hours, the sensitivity of the remanent flux is considered in the following comparison to show its effect on the waveforms.

Therefore, in order to analyze the effect of the history of the magnetic core (remanence effects), a seven minute segment of the recorded current prior to the variation with a 38 A peak (Fig.5.1) was considered. The entire variation considered is shown in Fig.5.9. The later portion of this waveform contains the waveform previously considered in Fig.5.1 for this analysis, indicated with a dotted line and labeled 'without history'. Therefore, direct comparisons can be carried out to analyze the effect of the history of the waveform on the simulated waveforms.

Fig.5.10 shows the comparison of the waveforms of current in the 500 kV line when the neutral dc current is point **1** in Fig.5.1 (without history) and point **1** in Fig.5.9 (with history). A slight phase shift was introduced to clearly show the difference between the two waveforms. The waveform simulated assuming a demagnetized core as the initial conditions has a higher peak value. This is due to the fact that when the history is considered, the transformer core undergoes saturation during the opposite half cycle (in the opposite direction) due to the negative peak of the neutral dc current. Meanwhile, Fig.5.11 shows the B-H loop after 420 seconds of simulation time, when the history is considered. This marks the beginning of the portion that was considered previously without the history. Therefore, this B-H loop shows the initial conditions of the magnetic core when the history of the neutral dc current is considered. Afterwards, the core undergoes half cycle saturation during the opposite half cycle due to the nature of the dc current applied. Therefore, when the effect of history is ignored, the simulation is initialized assuming a demagnetized core whereas when the history is considered, the core has some remanent flux before undergoing

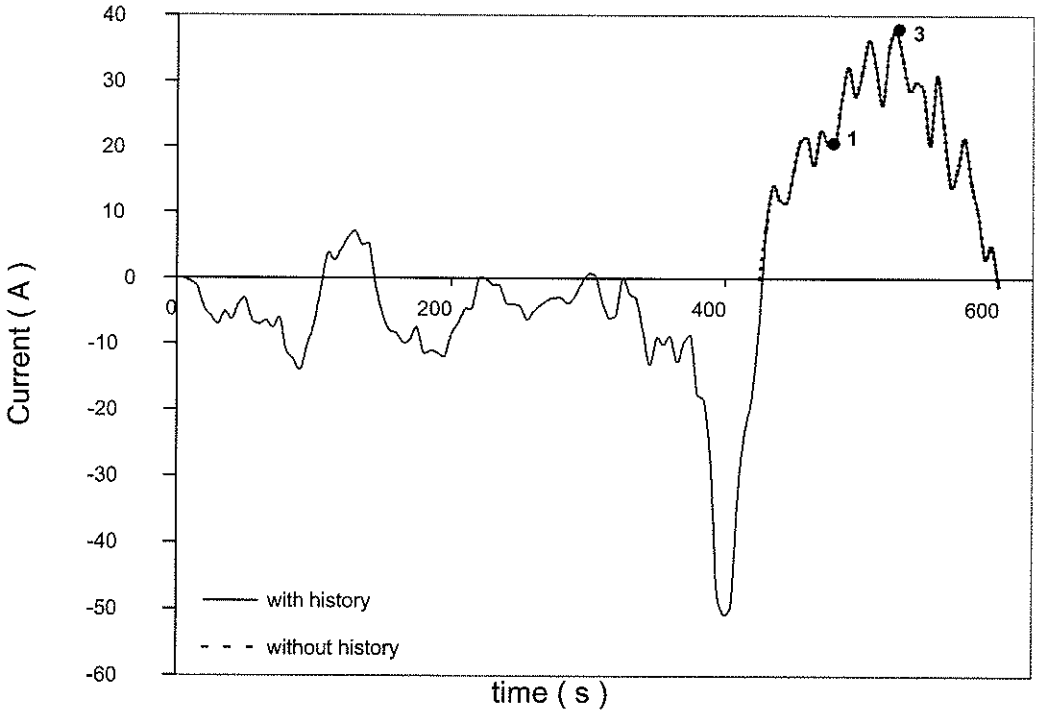

Figure 5.9: Waveform of neutral dc current considered. This includes the variation considered in Fig.5.1

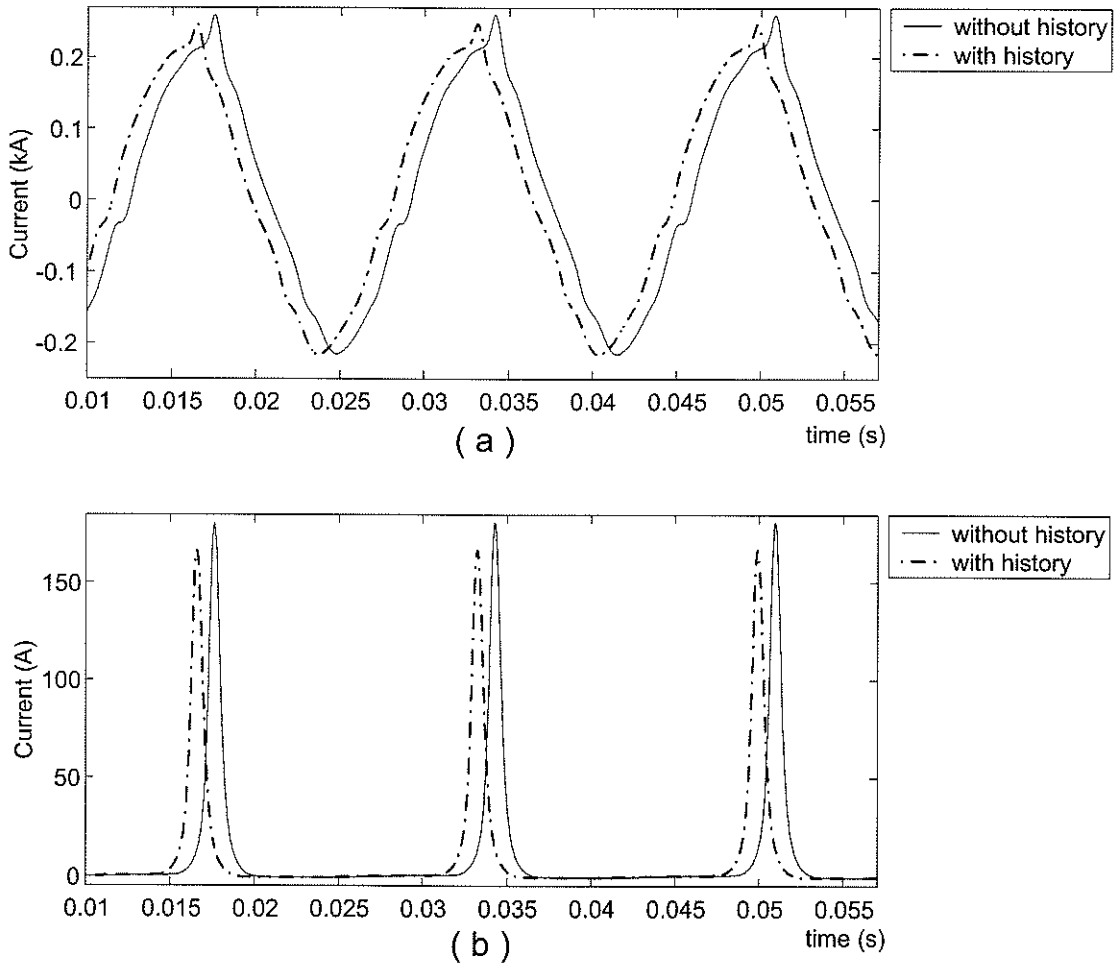

Figure 5.10: (a) Waveform of current in the 500 kV line obtained with and without the history of dc current in Fig.5.1; (b) Magnetizing current of the phase A transformer.

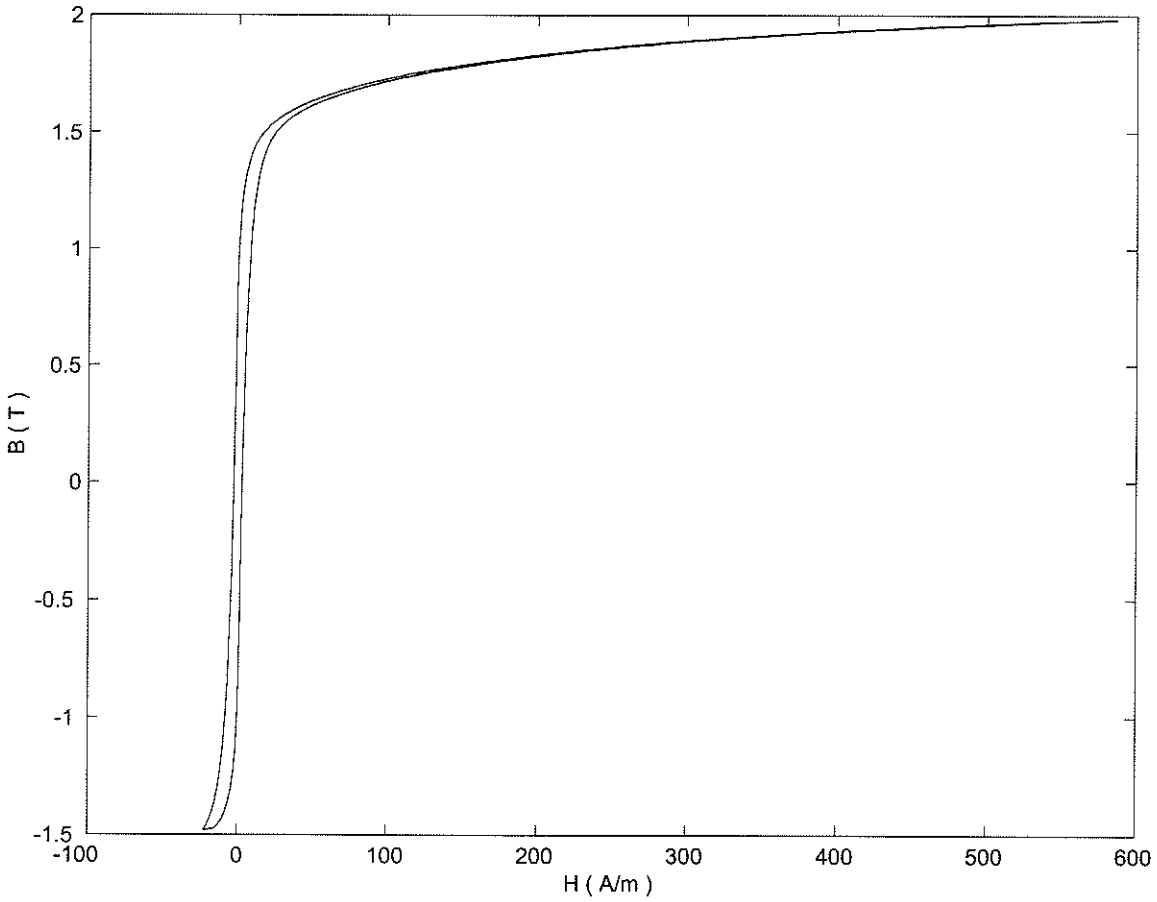

Figure 5.11: The B-H loop after 420 s of simulation using the waveform in Fig.5.9

the variation of dc current with a 38 A peak. Thus, comparisons show the effect of the remanent flux on the simulated waveform of current, in which the peak value and the harmonic content are different. Meanwhile, when the simulation reaches the peak value at point **3**, the effect of the initial condition diminishes due to the duration, and magnitude of the neutral dc current. Therefore the waveforms obtained with and without history shows a very close comparison. However, this observation does not conclude that the effect of remanent flux becomes insignificant beyond the peak value of a given neutral dc current. Because, the remanent flux could be in the opposite half cycle with respect to the dc bias considered in the present interval, however its

magnitude could be significantly higher than what was experienced in this simulation. Then the extent of half cycle saturation experienced with the same variation could be significantly lower than the values observed in this analysis. On the other hand, the remanent flux could be in the same direction as the dc bias caused by GIC. In such situations, if the remanent flux is significantly higher, the present variation could further saturate the core far beyond the extent projected by the case initialized with a demagnetized core.

Meanwhile, in addition to the effects of the history of the quasi-dc current, and remanence, the magnetizing characteristics of the transformer model, and the simulation model of the power system could also affect the simulation results. The following sections focuses on analysing the sensitivity of these models on the simulation results.

5.2 Simulation Model of a Transformer

5.2.1 Parameters for a given transformer

Power transformers are usually manufactured with different varieties of grain oriented silicon steel, and have a typical peak operating flux density of 1.60 $\sim$ 1.70 T. In a simulation model, these conditions can be accurately represented if dimensions of the core and number of turns in each winding are available. In addition, further verifications can be carried out by comparing the simulated and recorded waveforms. However, if the core dimensions, number of turns, and recorded waveforms are not available, a typical peak operating flux density can be assumed, and the transformer can be represented with an equivalent inductance matrix (Appendix A). The sensitivity of this assumption for the simulated waveforms of current in the 500 kV line is considered in this section.

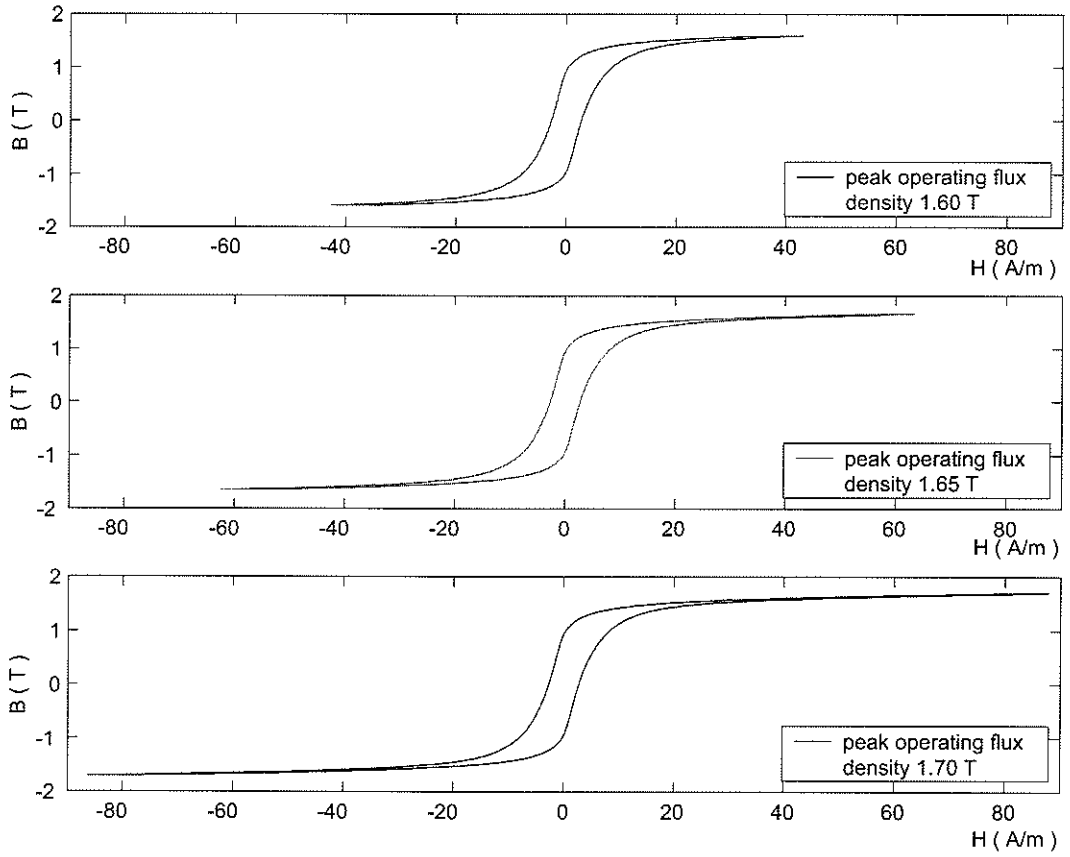

Figure 5.12: Simulated B - H loops obtained, assuming different peak operating flux densities

Fig.5.12 shows the simulated B-H loops considered, which have peak operating flux densities of 1.60 T, 1.65 T, and 1.70 T respectively. The harmonic content of the simulated waveforms of current in the 500 kV line are analysed considering these characteristics. Fig.5.13 shows that an increase in the peak operating flux density results in an increase in the harmonic content of the simulated waveform. Since all three comparisons were carried out with the same magnitude of GIC, these transformers have experienced the same bias. However, the different peak operating flux densities assumed have caused the state of the magnetic core to be different when the waveforms are compared. This is reflected in the magnitudes of each harmonic

shown in Fig.5.13.

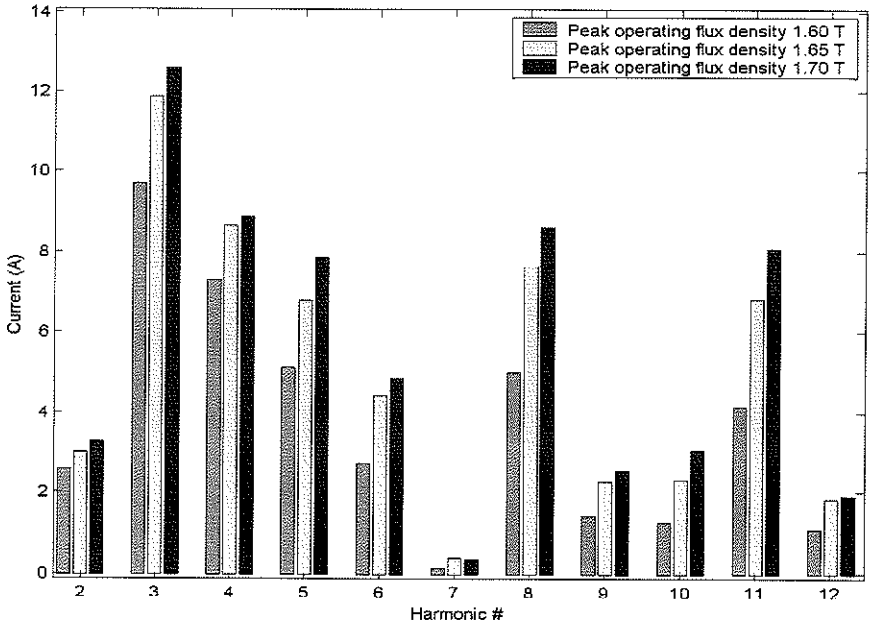

Figure 5.13: Harmonic content of the waveform of 500 kV line current obtained with B-H loops shown in Fig.5.12

5.2.2 Parameters of the B-H model

A three phase transformer bank that consists of three single phase units may not show identical characteristics. This could be due to slight deviations in the manufacturing process or due to ageing. Therefore power transformers with the same name plate rating could have slightly different magnetizing characteristics. The measured normal magnetizing characteristics (V_{rms} vs I_{rms}) of three autotransformers at Dorsey show similar deviations in the shoulder region. Therefore simulations were carried out considering two characteristic curves to analyse how sensitive this variation would be. Parameters that represent the hysteresis and eddy current effects were recalculated to represent the second characteristic (Table 5.3). Fig.5.14a shows the simulated normal

Table 5.3: Parameters of the new model that represent the magnetizing Curve 1 and Curve 2

Description	α	k	a_1	a_2	a_3	A_w	L_w
Curve 1	1.0e-6	4.96e-6	173	236	437	2.27	3.93
Curve 2	1.0e-6	4.94e-6	227	303	621	2.27	4.01

magnetizing curves, and Fig.5.14b shows the waveforms of current in the 500 kV line obtained with the two characteristics. The waveforms of line current are slightly phase shifted for display purposes. This comparison shows that even if the measured curves are not identical, a slight deviation in the measured V - I characteristic does not affect the waveform of simulated line current during half cycle saturation. This is due to the fact that a slight deviation in the shoulder region does not affect the extent of saturation that a core experiences. However, some negligible differences can be seen in the two waveforms, which are generally insignificant to the results of any GIC analysis. Therefore, this observation confirms that even if the three single phase transformers are not identical, if the normal magnetizing curves are close enough, these can be simulated with a single characteristic curve.

However, if the normal magnetizing curves are significantly different as in Fig.5.15, this considerably affects the waveform of the simulated line current. Comparison of the simulated waveforms of current in the 500 kV line obtained with two significantly different characteristics is shown in Fig.5.16. This comparison also shows the sensitivity of the waveform of current to the shape of the hysteresis loop, particularly in the saturation region. A significant difference can be seen in the magnitudes of the 8^{th} $\sim 12^{th}$ harmonics. These two characteristics are represented in simulation models by properly tuning the parameters of the JA model, mainly the slope of the anhysteretic function in the saturation region.

The anhysteretic curve determines the general shape of the hysteresis loop, and

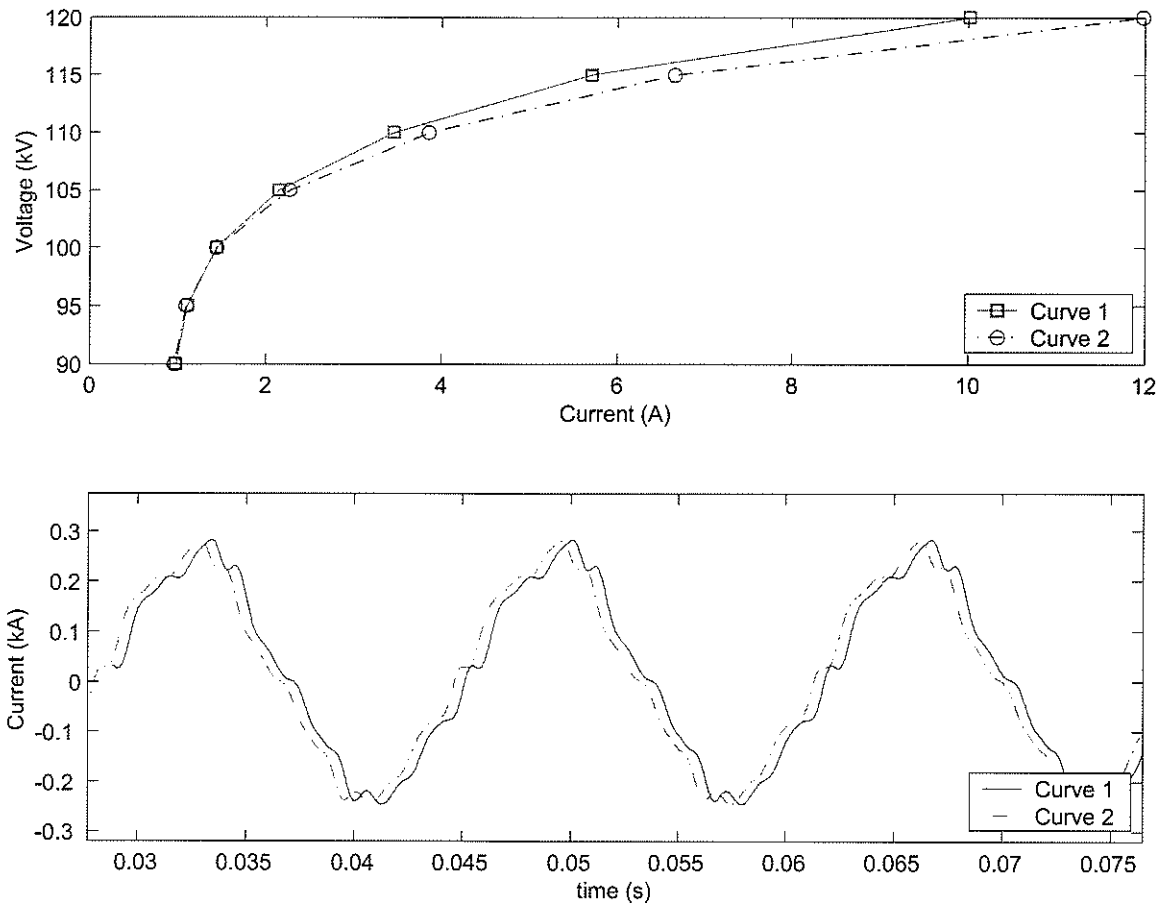

Figure 5.14: (a) Simulated normal magnetizing curves; (b) waveform of current in the 500 kV line obtained with two magnetizing characteristics

Table 5.4: Parameters of the new model that represent the magnetizing Curve 1 and Curve 3

Description	α	k	a_1	a_2	a_3	A_w	L_w
Curve 1	1.0e-6	4.96e-6	173	236	437	2.27	3.93
Curve 3	3.0e-6	7.27e-6	2123	2643	9214	2.27	3.77

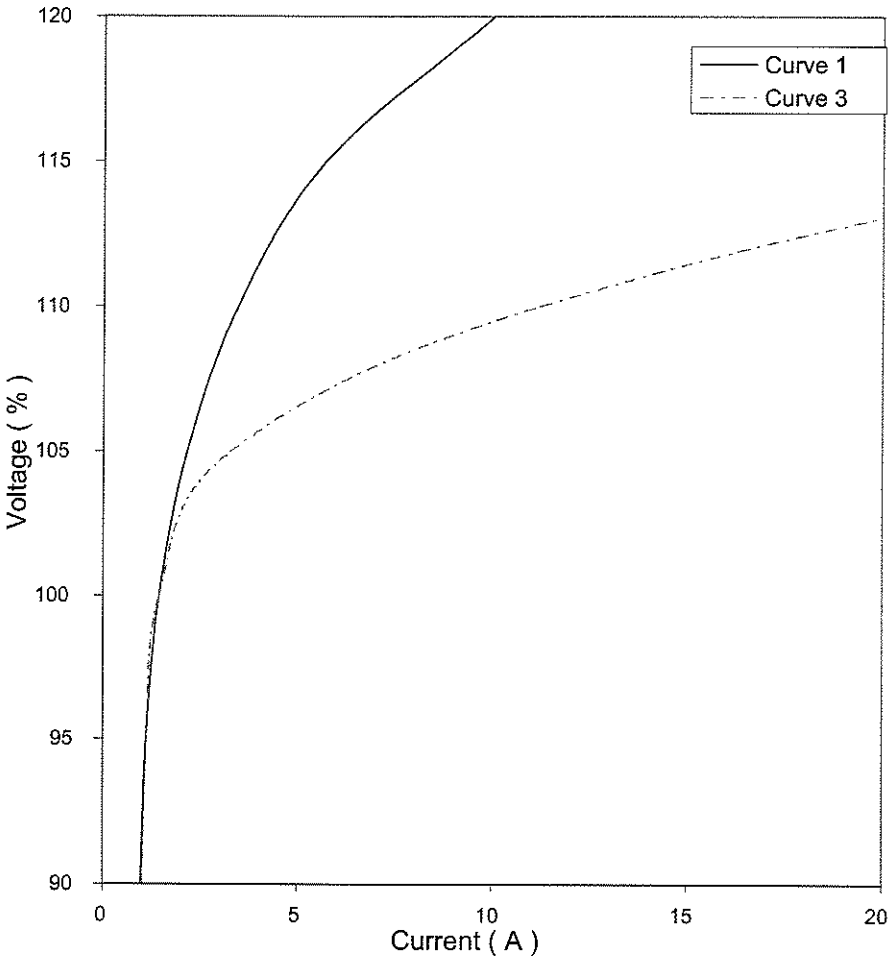

Figure 5.15: Simulated normal magnetizing curves

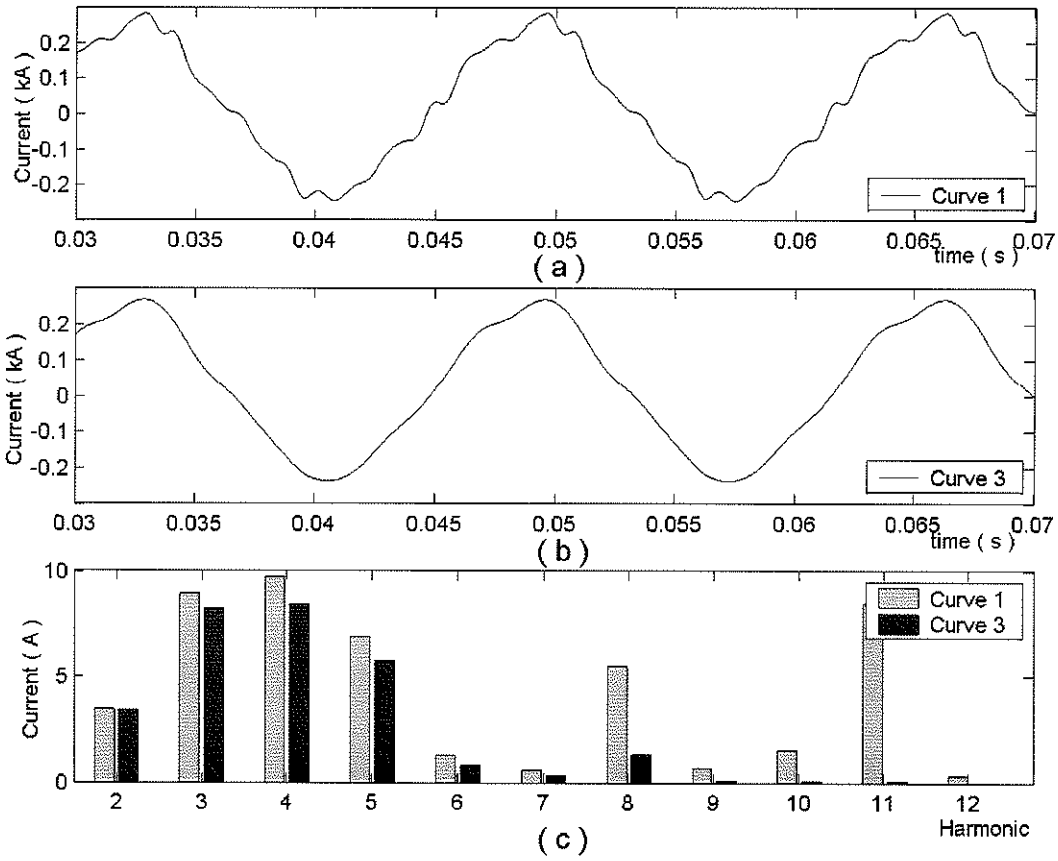

Figure 5.16: Simulation results obtained with the magnetizing curves given in Fig.5.15

hence the permeability of the core and the extent of saturation for a given flux density. Therefore the comparisons given in Figs. 5.14 and 5.16 show the sensitivity of the simulated waveform of current to the parameters of the anhysteretic curve.

In this simulation model, the total magnetization losses are determined by the width of the B-H loop. If the width of the B-H loop is increased, the total simulated power loss is increased. However, analysis of the harmonic content of the open circuit magnetizing current shows that a change in the width of the B-H loop affects the fundamental component only. Similar observations were made with simulations carried out in the presence of GIC.

5.2.3 Comparisons with the existing model

This section focuses on comparing the simulation results obtained using the existing model, which was described in section 2.2.2, and the new model developed. The existing model uses a piece-wise linear curve to represent saturation. Therefore, these comparisons allow us to analyse the sensitivity of the simulation results to a B-H model and a piece-wise linear saturation model.

The recorded variation of quasi dc current, that has a 65 A peak (Fig.5.4), was considered for this analysis. Simulation results are compared when the total dc neutral current is either increasing at 20 A, or decreasing at 20 A. Simulation results obtained with the new model under the influence of this recorded quasi dc current are already presented in section 5.1: Fig.5.5. Meanwhile, Fig.5.17 shows the comparison of the harmonic content obtained with the new model, and the existing model, (a) when the current is increasing at 20 A, and (b) when the current is decreasing at 20 A respectively. These comparisons show that the harmonic contents produced by the two models can be significantly different, and these changes can be attributed to the

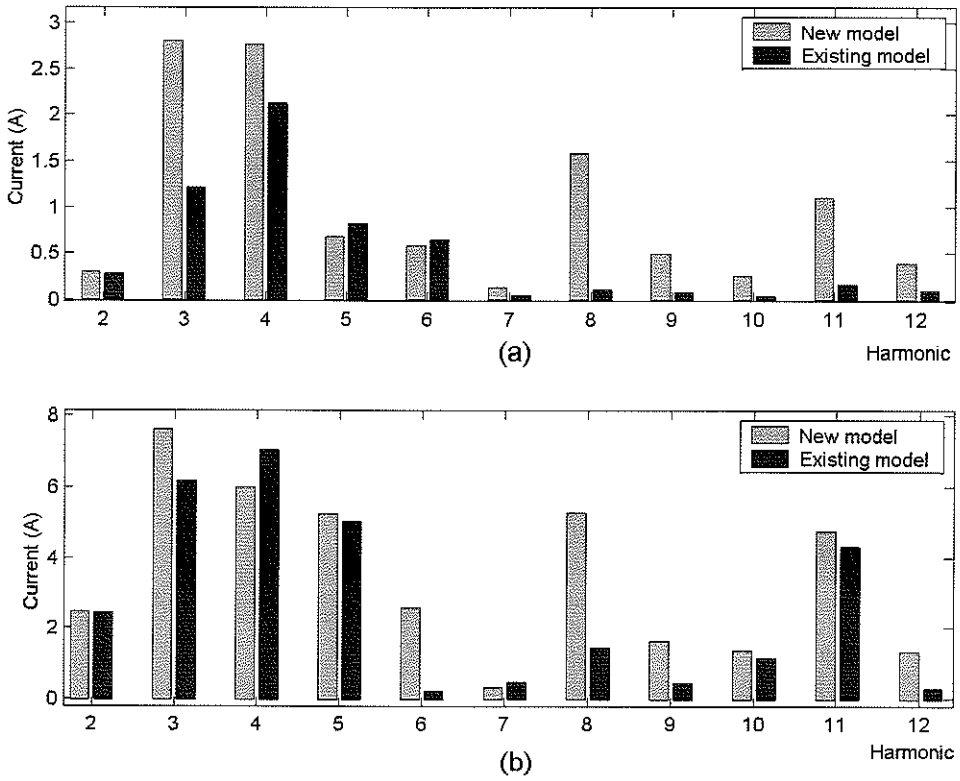

Figure 5.17: Comparison of the harmonic content obtained using the new model and the existing model; (a) when the neutral current is increasing at 20 A; (b) when the neutral current is decreasing at 20 A.

nature of their representation of magnetizing characteristics. In addition, Table 5.5 shows the comparison of the increased reactive power demand observed. It is seen that the existing model shows a higher reactive power demand over the new model.

This leaves us with two interesting observations.

1. The new model has shown a higher harmonic content in Fig.5.17.

2. The existing model, however, has shown a higher increase in reactive power demand under the same conditions.

It is clear that if an iron core experiences a higher state of saturation, it causes a higher content of harmonics in the simulated waveforms. Therefore, simulation results

Table 5.5: Increase in reactive power demand (ΔQ) observed with the new model, and the existing model

Points in Fig.5.4	**1a** (20 A$\uparrow$)	**5b** (20 A$\downarrow$)
New model	4.2 MVar	8.4 MVar
Existing model	5.2 MVar	10.8 MVar

in Fig.5.17 indicates that the new model has experienced a higher extent of saturation than does the existing model. This can be due to two reasons. The permeability of the core changes significantly in the saturation region. In the new model, the permeability is governed by the shape of the anhysteretic magnetization curve and the magnitude of the saturation magnetization (M_{sat}), whereas in the existing model this is entirely dependent on the slope of the piece-wise linear curve. Therefore, the input data (that is, the V_{rms} *vs* I_{rms} curve in the existing model) can affect the simulation results significantly. In addition, the effects of remanent flux could also cause the new model to indicate a different state of the magnetic core than does the existing model.

Meanwhile, the increase in reactive power demand is closely tied to the magnitude, and the phase angle of the fundamental component of the magnetizing current. If the correct shape of the hysteresis loop is represented in the model, it closely reproduces the phase angle of the magnetizing current, whereas a piece-wise linear representation always shows a current that lags the voltage by 90°. Therefore, this discrepancy in modelling the phase angle will have contributed to the difference seen in the reactive power demand shown by the two models. Hence, it is seen that a piece-wise linear representation models a higher reactive power demand and a lower extent of saturation due to the inherent nature of this representation.

5.3 Simulation Model of the Power System

The simulation model of a power system consists of several components such as electrical substations and transmission lines that are as important as the model of a power transformer in simulating a GIC event. Therefore, the sensitivity to some of the key parameters in these models is considered in this section.

5.3.1 Transmission Lines

A transmission line model may be represented using a travelling wave model such as the frequency dependent phase model [42]. In order to define the transmission line, parameters such as tower dimensions, conductor data, and earth resistivity are required. Simulations carried out in [32] had considered details of the transmission lines from Dorsey - Forbes and Forbes - Chisago to represent them in the simulation model. The two sections of transmission line had used earth resistivities of 65 Ωm and 125 Ωm respectively. In order to analyse the sensitivity to the earth resistivity, the entire line was simulated with 10 Ωm or 100 Ωm respectively. Both simulations showed negligible differences in the harmonic content. Similar observations were made in [75] where zero sequence currents in ac lines caused by transients in an adjacent dc line was analysed. Results of this study have shown that it is important to include the earth resistivity in a simulation model, however the variation of magnitudes from 10 Ωm to 1000 Ωm does not affect the waveforms significantly. These observations are consistent with the sensitivity studies carried out in our study. In both situations, the phenomena studied are of low frequency which has a higher depth of penetration, and hence the effect of earth resistivity becomes minimal. The simulation study has also confirmed that the transmission lines can be adequately represented with the data made available by utilities.

5.3.2 Substations

The neutral grounding resistance is an important feature that is required to be represented in an electrical substation. If the measured data are not available, typical values may be used. Simulations carried out with low neutral grounding resistances such as 0.3 Ω, 0.5 Ω at each substation showed that the change in the neutral grounding resistance does not affect the simulated waveforms, as long as the magnitude of the source voltage is adjusted to drive the same current. However, if the magnitude of the neutral grounding resistance is high enough, the magnitude of the peak flux density in the core could be affected. This is due to the effect of an increased potential at the transformer neutral as a result of a higher resistance. As a result of the higher potential at the neutral, the time taken for the transformer to reach the fully saturated state under the influence of a constant neutral dc current is also decreased. These effects were observed during simulations, when the neutral grounding resistance was increased from 0.5 Ω to 1.0 Ω and 3.0 Ω respectively.

In addition, a simulation model may contain several equivalent source models to represent the rest of the network. These network equivalents are also useful in initializing the load flow. The sensitivity to the initial conditions of the network equivalents were analysed considering the parameters of the local substation (Dorsey) and remote substation (Forbes) respectively. The simulation model of the Dorsey substation takes a more complicated form due to the presence of ac side filters at the converter station. It was observed that the extent of saturation and the increased reactive power consumption are closely tied to the bus voltage, and hence any significant difference in the bus voltage could affect the simulated waveforms. Therefore, this confirmed the importance of proper initialization of a simulation model to closely represent the power flow and bus voltages.

5.4 Summary

The sensitivity analysis presented in this chapter showed that the history of the quasi-dc current, and the remanent flux in the transformer core could affect the simulated waveforms significantly. The simulation results confirmed that an electromagnetic transient simulation carried out to model a GIC event requires not only the magnitude of the quasi-dc current, but also its history with respect to any particular point of interest. In addition, if a constant neutral dc current is assumed instead of using an actual or a predicted variation of a quasi-dc current, the simulation case may not represent the worst case scenario of that point of interest, unless that point of interest has the maximum dc current, and the effect of remanence is ignored. Meanwhile, simulations carried out to analyse the effects of remanence showed that the presence of remanent flux in the core could significantly affect the simulated waveforms. The remanent flux considered in this analysis was not large enough to affect the simulated waveforms at the peak value of the quasi-dc current. However, depending on the level of remanent flux in the core, and the nature of the quasi-dc current, it is likely that a higher level of remanence could affect the simulation results even beyond the peak value.

Simulations were also carried out to analyse the sensitivity of the parameters in the transformer model and the simulation model of the power system. It was shown that the magnetizing characteristics of the transformer model could have some effect on the simulation results, depending on the parameters chosen to represent them in the model. The sensitivity of the simulation results to a B-H model and a piece-wise linear saturation model was analysed by comparing the simulation results obtained using the new model and the existing model. This study has also analysed the adequate representation, and the initialization, of the simulation model of the power system.

Chapter 6

Conclusions

6.1 General Conclusions

Development of an improved transformer model for use in electromagnetic transient simulations has been investigated in this dissertation. Further, the effects of Geomagnetically Induced Currents (GIC) on a power system has been investigated using the new model. The following description summarizes the major goals accomplished in this dissertation.

In Chapter 2, an overview of an existing transformer model was presented to show how the Jiles Atherton theory of ferromagnetic hysteresis is incorporated to represent the hysteresis characteristics of the iron core. The new model accurately represents hysteresis characteristics that include recoil loops and long term remanence. The simulation model was also extended to include the effects of eddy currents. An expression for excess and anomalous losses was incorporated. Therefore when the simulation algorithm determines the magnitude of current injected across each winding, the eddy current effects are taken into account. This approach is useful in the simulation of multi-winding transformers, such as three phase three limb or three phase five limb

etc., whereas the commonly used approach would represent losses at the terminals with three resistors. PSCAD/EMTDC was considered as an example to show how this model could be implemented in an electromagnetic transient simulation software package. This allowed us to use the new model along with existing models such as the frequency dependent transmission line models to carry out system studies.

In Chapter 3, simulation results of open circuit tests, and waveforms of inrush current for a single phase two winding transformer model were compared with test results. Simulation results are in good agreement with recorded waveforms. Comparisons carried out at different frequencies of excitation have highlighted the importance of modeling the frequency dependency of the B-H loop. Simulations were also carried out to compare the simulated waveforms obtained with the new model against an existing transformer model that has a piece-wise linear representation of saturation. Simulation results show that the new model properly represents long term remanence in the core, whereas a piece-wise linear model fails to maintain the remanent flux beyond several hundred milliseconds.

In Chapter 4, a simulation model of a power system was considered to analyse the effects of GIC in a power system. Simulation results were compared with recorded waveforms to validate the simulation model. Although these simulation results showed general characteristics of the recorded waveforms, it did not closely match some of the harmonics seen in the recordings. Therefore, at this stage it was reasonable to examine whether the information provided for this recording was adequate to simulate the actual conditions.

A sensitivity study carried out in Chapter 5 showed that the history of the quasi-dc current, and remanent flux in the core could affect the simulated waveforms significantly. The simulation studies showed that an electromagnetic transient simulation

carried out to model a GIC event requires not only the magnitude of the quasi-dc current, but also its history with respect to any particular point of interest. In addition, if a constant neutral dc current is assumed instead of using an actual or a predicted variation of a quasi-dc current, the simulation case may not represent the worst case scenario of that point of interest. This analysis has further highlighted the need for proper initialization of the simulation model of the power system, to represent the actual conditions that may have prevailed at the time of the recording.

Therefore, based on the simulation studies carried out in Chapters 4 and 5, and considering previous work in this area, the following may be described as the major steps in carrying out a GIC study of a power system using an electromagnetic transient simulation programme.

- Modelling the power system. This involves an assessment of the vulnerability of a power system considering the geophysical data and the configuration of the network, to identify an area that needs to be modelled.

- Collection of data for a GIC event. This include the recordings or predicted variations of quasi-dc current, and adequate information on the state of the power system to represent that in a simulation model.

- Initialization of the simulation model. Simulation studies have shown that the initial conditions could significantly affect the outcome of a simulation case. Thus, initial conditions must closely represent the actual conditions that may have prevailed.

Modelling a power system

A section of a large transmission network that is vulnerable to GIC may be represented in detail to analyse the effects of GIC on that power system. Historical data indicates that high geomagnetic latitude areas in Canada, parts of USA, and some Nordic countries are more vulnerable. Because of that, many studies have been carried out to analyse the effects of GIC in these areas. Most studies have concentrated on looking at the vulnerability of the bulk power transmission network, which in turn determines the security, and the stability of the power system under the influence of GIC.

For example, simulation studies carried out in [32], which was the basis of analysis in Chapter 4, had considered the 500 kV transmission line in the Manitoba Hydro network. A similar study has been carried out in [64], where the effects of GIC in the BC Hydro 500 kV system were analysed. Meanwhile, even if the focus of a study is to analyse the effects on the 500 kV transmission network, effects of the power transformers, and transmission lines in the lower voltage networks, such as the 230 kV network, may have to be considered. The simulation studies carried out have shown that the waveforms of current and voltage in the 230 kV bus could be distorted due to the half cycle saturation of the power transformers.

Therefore, the presence of long transmission lines, their orientation, and geophysical conditions at different sites etc., at different voltage levels have to be considered in identifying the section of a power system that requires detailed modelling. In addition, the core configuration of the power transformer (single phase banks, three phase three limb etc.), and their winding configurations also have to be considered. Once the network has been identified, a detailed model of this power system can be represented as described in section 4.3.

Collection of data

Simulation results presented in the previous chapters have shown that the simulated waveform of current is dependent on the history of the quasi-dc neutral current. Field measurements carried out during GIC events have shown that there could be large scale differences in the magnetic and electric fields measured at different recording sites spread over a large area [71][72]. These differences can be attributed to the distance between the sites and the electrojet, and differences in the local geology. In addition, if the simultaneity of measured samples are considered, it is likely that the maximum recorded GIC may not have occurred simultaneously across all the sites [76]. Therefore, a simulation carried out to validate a GIC event requires the actual variation of quasi-dc current to be considered to properly represent conditions that may have prevailed at the time of the recording. This becomes more important as the simulated waveforms of current are dependent on the variation of the quasi-dc current in the neutral.

In addition, the core of the transformer can have remanent flux as a result of the status of the magnetic core prior to this event under consideration. If the core of the transformer has remanent flux, it also affects the extent of saturation experienced. In general, any particular change in the status of the magnetic core, which can be due to remanent flux in the core, or history of the quasi-dc current, could directly affect the harmonic content of the waveform of current and the increase in reactive power consumption in the transformer.

Therefore, collection of data during a GIC event must address the above requirements. If a SUNBURST recorder is used for monitoring GIC, it provides the details of current in the transmission lines and at the neutral of the power transformer. Meanwhile, if a detailed model of electrojet is used to predict the electric field at

the surface of the earth, this paves the way for the calculation of GIC driven by this electric field in a network.

In addition, the power flow in the transmission lines and voltage at the system buses are also needed to closely represent the conditions in the actual system. Further, the simulated power system intends to represent a snapshot of the system at a particular point of interest, hence the status of each substation has to be accounted for. For example, if a substation has capacitor banks or filter banks, as in Dorsey, the status of each component needs to be taken into account.

Initial conditions

Simulation studies carried out to analyze the effects of GIC on a power system may involve validation of a GIC event using measured data as well the prediction of the worst case scenario using the estimated values of electric fields and GIC. Meanwhile, initialization of a simulation model could significantly affect the outcome of a simulation case. The initial values of the network equivalents, especially the bus voltages, have an effect on the flux in the transformers. However, the initialization of the transformer model itself becomes more important during a GIC study, as the state of the magnetic core directly depends on its initial conditions. It is usually possible to initialize remanence in a typical transformer model, however it requires outside intervention whereas the new transformer model will do it automatically. Therefore, the availability of a recorded variation or the estimated values of the quasi-dc neutral current becomes useful in this endeavour.

Usually GIC events can last for several hours. A simulation study, however, may focus on the maximum reported dc current in the neutral or focus on a specific event that may have happened. If an analysis considers the instant where the maximum dc

current was reported, it is likely that the initialization of the transformer assuming a demagnetized core would have negligible effects on the simulation results, provided that the duration of the dc current is long enough to reach the fully saturated state, and the level of remanent flux (if any) is fairly small so that it does not affect the overall extent of the saturation. Similarly, if the network under consideration experiences the maximum dc current simultaneously across the network, a constant dc current may be used in the simulation for the same reasons.

However, if different points in a network do not experience the peak dc current simultaneously, it requires proper consideration of the recorded variation or the predicted values of quasi-dc current. Similar consideration is required if a simulation study is carried out to analyze a specific recorded event. In such situations, the remanent flux in the transformer core can be initialized by considering a portion of the variation of dc current prior to the point of interest.

6.2 Contributions

The main contributions of the work presented in this dissertation are as follows.

- It has developed a new simulation model of a power transformer for use in electromagnetic transient simulation studies by;
    1. Incorporating the Jiles Atherton theory of ferromagnetic hysteresis to represent the hysteresis characteristics of the iron core of the transformer,
    2. Incorporating the eddy current effects in the same model, so that the simulated B-H loop is frequency dependent.
- It has developed an algorithm to incorporate this new model into an existing transformer model of an electromagnetic transient simulation programme.

- It has developed a methodology to determine parameters for the model to represent the magnetization characteristics of a given transformer.

- It has validated the new model by comparing simulation results with recorded waveforms to confirm the suitability of the new model for electromagnetic transient simulations.

- It has analysed the effects of GIC using a simulation model of a power system in an electromagnetic transient simulation programme. Simulation results were compared with recorded waveforms for validations.

- A sensitivity study was carried out to show the effects of the history of the quasi-dc current and remanent flux in the core on simulation results.

These contributions have led to the following publications;

- W. Chandrasena, P. G. McLaren, U. D. Annakkage, and R. P. Jayasinghe, "An Improved Low Frequency Transformer Model for Use in GIC Studies", *accepted for publication in the IEEE Transactions on Power Delivery*, paper TPWRD-00354-2002. This paper was also presented at the IEEE Power Engineering Society General Meeting, Toronto, July 2003.

- W. Chandrasena, P. G. McLaren, U. D. Annakkage, and R. P. Jayasinghe, "Modeling the Effects of Geomagnetically Induced Currents (GIC) in a Power System", *the IEEE Transactions on Power Delivery*, in preparation.

- W. Chandrasena, P. G. McLaren, U. D. Annakkage, and R. P. Jayasinghe, "Modeling GIC Effects on Power Systems: The Need to Model Magnetic Status of Transformers", *in proceedings of the IEEE Bologna Power Tech 2003*, Bologna, Italy, June 23-26, 2003.

- W. Chandrasena, P. G. McLaren, U. D. Annakkage, R. P. Jayasinghe, D. Muthumuni, and E. Dirks, "Simulation of Hysteresis and Eddy Current Effects in a Power Transformer", *in proceedings of International Conference on Power Systems Transients - IPST 2003,* New Orleans, USA, 2003.

- W. Chandrasena, P. G. McLaren, U. D. Annakkage, R. P. Jayasinghe, and E. Dirks "Simulation of Eddy Current Effects in Transformers", in *proceedings of the IEEE Canadian Conference on Electrical and Computer Engineering (CCECE), Winnipeg, Canada*, vol. 1, pp. 122 - 126, 2002.

6.3 Suggestions for future research

The work presented in this dissertation has focused on developing an improved power transformer model for use in electromagnetic transient simulations. The mathematical model developed in Chapter 2 was incorporated into an existing transformer model in PSCAD/EMTDC. Although the validations were carried out with a single-phase two-winding model, this algorithm is capable of simulating multi-limb, multi-winding transformers. Therefore this algorithm can be extended to three-phase three-limb, and three-phase five-limb models. Further, simulation results can be compared with recorded waveforms to validate such models.

The effects of GIC on a power system was analysed in Chapters 4 and 5. The simulation studies have identified a number of important recordings, and measurements, which include long term recordings with snapshots of current at regular intervals. These are required to ensure that a simulation model closely represents the actual conditions. The same information is required if predicted values are considered. These suggestion will be useful in validating a simulation model in future studies. With the availability of accurate models of current transformers [36][77]-[80], and the power

transformer model developed, the future studies could also focus on investigating the problems associated with power system protection. In general, once the vulnerability of a power system is determined, simulation studies can focus on mitigating the effects of GIC in a power system.

Although the new model developed was used in studying the effects of GIC in a power system, this model could also be used in electromagnetic transient simulation studies that require an accurate representation of magnetization characteristics of the iron core such as in ferroresonance studies and switching studies where the new model could significantly improve the accuracy. In addition, comparative studies can be carried out to quantify advantages and provide recommendations for future studies using the new model, and to compare the simulation time with the existing models.

Reference

[1] W.H. Barlow, "On the Spontaneous Electric Currents Observed in the Wires of the Electric Telegraph", *Philosophical Transactions of Royal Society, London*, vol. 139, pp. 61 – 72, 1849.

[2] W.H. Preece, "Earth Currents", *Nature*, vol. 49, pp. 554, April 12 1894.

[3] W.J.S. Lockyer, "Magnetic Storms, Aurorae and Solar Phenomena", *Nature*, vol. 69, pp. 9–10, 1903.

[4] W.F. Davidson, "The Magnetic Storm of March 24, 1940 - Effects in the Power System", The Edison Electric Bulletin, July 1940, pp. 365 –366.

[5] V.D. Albertson et al., "Geomagnetic Disturbance Effects on Power Systems", *IEEE Transactions on Power Delivery*, vol. 8, pp. 1206–1216, July 1993.

[6] B. Bozoki et al., "The Effects of GIC on Protective Relaying", *IEEE Transactions on Power Delivery*, vol. 11, pp. 725–739, April 1996.

[7] G. Blais and P. Metsa, "Operating the Hydro-Quebec Grid under Magnetic Storm Conditions Since the Storm of 13 March 1989", in *Proceedings of Solar-Terrestrial Predictions Workshop*, Ottawa, 1993, vol. 1, pp. 108 – 130.

[8] R. Pirjola, "Geomagnetically Induced Currents During Magnetic Storms", *IEEE Transactions on Plasma Science*, vol. 28, pp. 1867–1873, December 2000.

[9] E.N. Parker, "The Solar Wind", *Scientific American*, p. 66, April 1964.

[10] S.I. Akasofu, "The Aurora", *Scientific American*, pp. 55–62, December 1965.

[11] S.I. Akasofu, "The Dynamic Aurora", *Scientific American*, pp. 90–97, May 1989.

[12] S. Chapman and V.C.A. Ferraro, "A New Theory of Magnetic Storms", *Nature*, vol. 126, pp. 129–130, July 1930.

[13] J.W. Dungey, "Interplanetary Magnetic Field and the Auroral Zones", *Physical Review Letters*, vol. 6, no. 2, pp. 47–48, January 1961.

[14] C.T. Russell, "The Solar Wind Interaction with the Earth's Magnetosphere : A Tutorial", *IEEE Transactions on Plasma Science*, vol. 28, no. 6, pp. 1818–1830, December 2000.

[15] V.D. Albertson, "Electric and Magnetic Fields at the Earth's Surface to Auroral Currents", *IEEE Transactions on Power Apparatus and Systems*, vol. PAS-89, no. 4, pp. 578–584, April 1970.

[16] R.J. Ringlee and J.R. Stewart, "Geomagnetic Effects on Power Systems", *IEEE Power Engineering Review*, pp. 6–9, July 1989.

[17] R.P. Jayasinghe, P.G. McLaren, and T. Gouldsborough, "Effect of GIC on Overcurrent Protection for Filter Banks", in *Proc. WESCANEX'93*, 1993, pp. 36–42.

[18] M. Lahtinen and J. Elovaara, "GIC Occurrences and GIC Test for 400kV System Transformer", *IEEE Transactions on Power Delivery*, vol. 17, pp. 556–56, April 2002.

[19] D. L. Dickmander, S. Y. Lee, G. L. Desilets, and M. Granger, "AC/DC Harmonic Interaction in the Presence of GIC for the Quebec - New England Phase II HVDC Transmission", *IEEE Transactions on Power Delivery*, vol. 9, no. 1, pp. 68 – 78, January 1994.

[20] W. B. Gish, W. E. Feero, and G. D. Rockefeller, "Rotor Heating Effects from Geomagnetically Induced Currents", *IEEE Transactions on Power Delivery*, vol. 9, no. 2, pp. 712 – 719, April 1994.

[21] N. Takasi, T. Oshi, F. Miyawaki, S. Saito, and Y. Fujiwara, "An Experimental Analysis of DC Excitation of Transformers by Geomagnetically Induced Currents", *IEEE Transactions on Power Delivery*, vol. 9, no. 2, pp. 1173–1182, April 1994.

[22] D. Dooling, "Stormy Weather in Space", *IEEE Spectrum*, pp. 64 – 72, June 1995.

[23] J. G. Kappenman, R. Radasky, J. L. Gilbert, and I. A. Erinmez, "Advanced Geomagnetic Storm Forecasting: A Risk Management Tool for Electric Power System Operations", *IEEE Transactions on Plasma Science*, vol. 28, no. 6, pp. 2114 – 2121, December 2000.

[24] R. Pirjola, "On Currents Induced in Power Transmission Systems During Geomagnetic Variations", *IEEE Transactions on Power Apparatus and Systems*, vol. PAS-104, no. 10, pp. 2825–2829, October 1985.

[25] D.H. Boteler and R.J. Prijola, "Modelling Geomagnetically Induced Currents Produced by Realistic and Uniform Electric Fields", *IEEE Transactions on Power Delivery*, vol. 13, no. 4, pp. 1303–1308, October 1998.

[26] F.de Leon and A. Semlyen, "Complete Transformer Model for Electromagnetic Transients", *IEEE Transactions on Power Delivery*, vol. 9, pp. 231–239, 1994.

[27] T. Fujiwara and R. Tahara, "Eddy Current Modeling of Silicon Steel for Use on SPICE", *IEEE Transactions on Magnetics*, vol. 31, pp. 4059–4061, November 1995.

[28] B.A. Mork, "Five Legged Wound Core Transformer Model: Derivation, Parameters, Implementation, and Evaluation", *IEEE Transactions on Power Delivery*, vol. 14, pp. 1519–1526, October 1999.

[29] X. Chen, "A Three Phase Multi-Legged Transformer Model in ATP Using the Directly Formed Inverse Inductance Matrix", *IEEE Transactions on Power Delivery*, vol. 11, pp. 1554–1562, July 1996.

[30] J. Arrillaga, W. Enright, N.R. Watson, and A.R. Woods, "Improved Simulation of HVDC Converter Transformers in Electromagnetic Transient Programs", *IEE Proc.-Gener. Transm. Distrib.*, vol. 144, pp. 100–106, March 1997.

[31] J. D. Aspnes, R. P. Merritt, and S. I. Akasofu, "Effects of Geomagnetically Induced Current on Electric Power Systems", *The Northern Engineer*, vol. 13, no. 3, pp. 34 – 38, 1981.

[32] R. P. Jayasinghe, *Investigation of Protection Problems Due to Geomagnetically Induced Currents*, PhD thesis, University of Manitoba, 1997.

[33] F.de Leon and A.Semlyen, "A Simple Representation of Dynamic Hysteresis Losses in Power Transformers", *IEEE Transactions on Power Delivery*, vol. 10, pp. 315–321, January 1995.

[34] F. Liorzou, B. Phelps, and D. L. Atherton, "Macroscopic Models of Magnetization", *IEEE Transactions on Magnetics*, vol. 36, pp. 418–428, March 2000.

[35] D.C. Jiles and D.L. Atherton, "Theory of Ferromagnetic Hysteresis", *Journal of Magnetism and Magnetic Materials*, vol. 61, pp. 48–60, 1986.

[36] U.D. Annakkage, P.G. McLaren, E. Dirks, R.P. Jayasinghe, and A.D. Parker, "A Current Transformer Model Based on the Jiles-Atherton Theory of Ferromagnetic Hysteresis", *IEEE Transactions on Power Delivery*, vol. 15, pp. 57–61, January 2000.

[37] F.de Leon and A. Semlyen, "Detailed Modeling of Eddy Current Efects for Transformer Transients", *IEEE Transactions on Power Delivery*, vol. 9, pp. 1143–1150, April 1994.

[38] C.D. Graham Jr., "Physical Origin of Losses in Conducting Ferromagnetic Materials", *J. Appl. Phys.*, vol. 53, no. 11, pp. 8276–8280, November 1982.

[39] G. Bertotti, "General Properties of Power Losses in Soft Ferromagnetic Materials", *IEEE Transactions on Magnetics*, vol. 24, no. 1, pp. 621–630, January 1988.

[40] D.C. Jiles, "Modelling the Effects of Eddy Current Losses on Frequency Dependent Hysteresis in Electrically Conducting Media", *IEEE Transactions on Magnetics*, vol. 30, pp. 4326–4328, 1994.

[41] W. Enright, O.B. Nayak, G.D. Irwin, and J. Arrillaga, "An Electromagnetic Transient Model of Multi-Limb Transformers Using Normalized Core Concept", in *Proc. International conference on Power Systems Transients (IPST)*, June 1997, pp. 93–98.

[42] Manitoba HVDC Research Centre, *EMTDC Users' Manual*, 2001.

[43] J. A. Ewing, "On the Production of Transient Electric Currents in Iron and Steel Conductors by Twisting Them When Magnetized or by Magnetized Them When Twisted", *Proceedings of Royal Society*, vol. 33, pp. 21 – 22, 1881.

[44] J. A. Ewing, "Theory of Induced Magnetism", *The London, Edinburgh and Dublin Philosophical Magazine and Journal of Science*, , no. 5, pp. 205 – 222, September 1890.

[45] J. A. Ewing, *Magnetic Induction in Iron and Other Metals*, "The Electrician" printing and publishing Co. Ltd., London, third edition, revised edition, 1900.

[46] P. Weiss, "Hypothesis of the Molecular Field and Ferromagnetic Properties", *Journal of Physics*, vol. 6, pp. 661 – 690, 1907.

[47] C. Kittel, "Physical Theory of Ferromagnetic Domains", *Reviews of Modern Physics*, vol. 21, no. 4, pp. 541 – 583, October 1949.

[48] R. M. Bozorth, *Ferromagnetism*, D. Van Nostrand Co. Inc, New York, USA, first edition, March 1951.

[49] D. C. Jiles, *Introduction to Magnetism and Magnetic Materials*, Chapman and Hall, London UK, 1991.

[50] D.C. Jiles, J.B. Thoelke, and M.K. Devine, "Numerical Determination of Hysteresis Parameters for the Modeling of Magneic Properties Using the Theory of Ferromagnetic Hysteresis", *IEEE Transactions on Magnetics*, vol. 28, pp. 27–35, 1992.

[51] G. W. Swift, "Power Transformer Core Behaviour under Transient Conditions", *IEEE Transactions on Power Delivery*, vol. PAS90, no. 5, pp. 2206 – 2210, September 1971.

[52] H.J. Williams, R.M. Bozorth, and W. Shockley, "Magnetic Domain Patterns on Single Crystal of Silicon Iron", *Physical Review*, vol. 75, pp. 155–177, 1949.

[53] H.J. Williams and W. Shockley, "A Sample Domain Structure in an Iron Crystal Showing a Direct Correlation with the Magnetization", *Physical Review*, vol. 75, pp. 178–183, 1949.

[54] H.J. Williams, W. Shockley, and C. Kittel, "Studies of the Propagation Velocity of a Ferromagnetic Domain Boundary", *Physical Review*, vol. 80, pp. 1090–1094, 1950.

[55] R.H. Pry and C.P. Bean, "Calculation of the Energy Loss in Magnetic Sheet Materials Using a Domain Model", *Journal of Applied Physics*, vol. 29, pp. 532–533, March 1958.

[56] J.W. Shilling and G.L. Houze Jr., "Magnetic Properties and Domain Structure in Grain-Oriented 3 percent Si-Fe", *IEEE Transactions on Magnetics*, vol. MAG-10, pp. 195–222, 1974.

[57] F. Brailsford, *Physical Principles of Magnetism*, D. Van Nostrand Co., London, 1966.

[58] G. Bertotti, "Physical Interpretation of Eddy Current Losses in Ferromagnetic Materials I. Theoretical Considerations", *Journal of Applied Physics*, vol. 57, pp. 2110–2117, March 1985.

[59] G. Bertotti, "Physical Interpretation of Eddy Current Losses in Ferromagnetic Materials II . Theoretical Considerations", *Journal of Applied Physics*, vol. 57, pp. 2118–2126, March 1985.

[60] S. Chikazumi, *Physics of Magnetism*, John Wiley, NY, 1964.

[61] F. Fiorillo and A. Novikov, "An Improved Approach to Power Losses in Magnetic Laminations under Nonsinusoidal Induction Waveform", *IEEE Transactions on Magnetics*, vol. 26, no. 5, pp. 2904 – 2910, September 1990.

[62] R. Hasegawa, "Metallic Glasses in Devices for Energy Conversion and Conservation", *Journal of Non-Crystalline Solids*, vol. 61 and 62, pp. 725–736, 1984.

[63] R. L. Lesher, J. W. Porter, and R. T. Byerly, "SUNBURST - A Network of GIC Monitoring Systems", *IEEE Transactions on Power Delivery*, vol. 9, no. 1, pp. 128 – 137, January 1994.

[64] D. H. Boteler, R. M. Shier, T. Watanabe, and R. E. Horita, "Effects of Geomagnetically Induced Currents in the BC hydro 500 kV System", *IEEE Transactions on Power Delivery*, vol. 4, no. 1, pp. 818 – 823, January 1989.

[65] R. A. Walling and A. H. Khan, "Characteristics of Transformer Exciting Current During Geomagnetic Disturbances", *IEEE Transactions on Power Delivery*, vol. 6, no. 4, pp. 1707 – 1714, October 1991.

[66] X. Dong, Y. Liu, and J. G. Kappenman, "Comparative Analysis of Exciting Current Harmonics and Reactive Power Consumption from GIC Saturated Transformers", in *Power Engineering Society Winter Meeting, 2001*, Jan - Feb 2001, pp. 318 – 322.

[67] F. S. Prabhakara, J. Z. Ponder, and J. N. Towle, "Computing GIC in Large Power Systems", *IEEE Computer Applications in Power*, pp. 46 – 50, January 1992.

[68] F. S. Prabhakara, L. N. Hannett, R. J. Ringlee, and J. Z. Ponder, "Geomagnetic Effects Modelling Part II - Geomagnetically Induced Current Study Results", *IEEE Transactions on Power Systems*, vol. 7, no. 2, pp. 565– 571, May 1992.

[69] V. D. Albertson, Jr. J. M. Thorson, R. E. Clayton, and S. C. Tripathy, "Solar-Induced- Currents in Power Systems : Cause and Effects", *IEEE Transactions on Power Apparatus and Systems*, vol. V PAS-92, no. 2, pp. 471 – 477, March - April 1973.

[70] D. H. Boteler, Q. Bui-Van, and J. Lemay, "Directional Sensitivity of Geomagnetically Induced Currents of the Hydro-Quebec 735kV Power System", *IEEE Transactions on Power Delivery*, vol. 9, no. 4, pp. 1963 –1971, October 1994.

[71] L. Bolduc, P. Langlois, D. Boteler, and R. Pirjola, "A Study of Geomagnetic Disturbances in Quebec, 1. General Results", *IEEE Transactions on Power Delivery*, vol. 13, no. 4, pp. 1251 – 1256, October 1998.

[72] L. Bolduc, P. Lanlois, D. Boteler, and R. Pirjola, "A Study of Geomagnetic Disturbances in Quebec, 2. Detailed Analysis of a Large Event", *IEEE Transactions on Power Delivery*, vol. 15, no. 1, pp. 272 – 278, January 2000.

[73] A. Morched, B. Gustavsen, and M. Tartibi, "A Universal Model for Accurate Calculation of Electromagnetic Transients on Overhead Lines and Underground Cables", *IEEE Transactions on Power Delivery*, vol. 14, no. 3, pp. 1032 –1038, July 1999.

[74] B. Gustavsen, G. Irwin, R. Mangelord, D. Bandt, and K. Kent, "Transmission Line Models for the Simulation of Interaction Phenomena Between Parallel AC

and DC Overhead Lines", Budapest - Hungary, jun 1999, International Conference on Power System Transients, pp. 61 – 67, IPST'99.

[75] N. Chopra, A. M. Gole, J. Chand, and R. W. Haywood, "Zero Sequence in AC Lines Caused by Transients in Adjacent DC Lines", *IEEE Transactions on Power Delivery*, vol. 3, no. 4, pp. 1873 – 1879, October 1988.

[76] A. Viljanen and R. Pirjola, "Geomagnetically Induced Currents in the Finnish High-Voltage Power System - A Geophysical Review", *Surveys in Geophysics*, vol. 15, pp. 383 – 408, 1994.

[77] U. D. Annakkage, Ming Yu, P. G. McLaren, E. Dirks, and A. D. Parker, "Simulation of a Differential Current Protection Scheme Involving Multiple Current Transformers", *IEEE Transactions on Power Delivery*, vol. 15, no. 2, pp. 515–519, April 2000.

[78] D. Muthumuni, P. G. McLaren, W. Chandrasena, A. Parker, and Ming Yu, "Simulation of Delta Connected Current Transformers in a Differential Protection Scheme", in *Developments in Power System Protection, 2001, Seventh International Conference on (IEE)*, 2001, pp. 222 –225.

[79] D. Muthumuni, P. G. McLaren, W. Chandrasena, and A. Parker, "Simulation Model of an Air Gapped Current Transformer", in *IEEE Power Engineering Society Winter Meeting*, 2001, pp. 705 –709.

[80] W. Chandrasena, P. G. McLaren, R. P. Jayasinghe, D. Muthumuni, E. Dirks, and A. Parker, "Simulation of Differential Current Protection Schemes Involving Multiple Current Transformers and a Varistor", in *IEEE Power Engineering Society Summer Meeting*, 2001, pp. 1169 –1174.

[81] *A712-97(2002) Standard Test Method for Electrical Resistivity of Soft Magnetic Alloys*, vol. 03.04 of *Sec.3*, American Society for Testing and Materials., 2000.

[82] *A876/A876M-98 Standard Specification for Flat-Rolled, Grain-Oriented, Silicon-Iron, Electrical Steel, Fully Processed Types*, vol. 03.04 of *Sec.3*, American Society for Testing and Materials., 2000.

Appendix A

Determination of Parameters

This appendix focuses on describing how the parameters are determined to represent a given magnetizing characteristic using the new model. Validations carried out in Chapter 3 were based on laboratory tests carried out using a 115 V / 2300 V, 60 Hz, 3 kVA single phase distribution transformer. During laboratory tests, the waveform of magnetizing current at different voltages, and at different frequencies were recorded. In addition, the open circuit normal magnetizing curve, and the core loss were also measured.

The calculation of parameters for the hysteresis model was already discussed in section 3.1.1. However, a brief review of this process is presented here for the completeness of this discussion. Further, it also describes how the new model is interfaced with EMTDC by calculating the parameters for a given transformer.

Hysteresis model

The anhysteretic magnetization (M_{an}) at a given field (H_e) represents the global minimum energy state. The function given in (2.40) is used to represent the anhys-

teretic magnetization curve, and its slope is given in (2.41). These two expressions are reproduced below in (A.1), and (A.2) respectively.

$$M_{an} = M_{sat} \frac{a_1 H_e + H_e^2}{a_3 + a_2 H_e + H_e^2} \tag{A.1}$$

$$\frac{dM_{an}}{dH_e} = M_{sat} \frac{a_1 a_3 + 2a_3 H_e + (a_2 - a_1) H_e^2}{(a_3 + a_2 H_e + H_e^2)^2} \tag{A.2}$$

- M_{sat}, the saturation magnetization is a constant for a given material. A typical value of M_{sat} for iron is used in this calculation. That is 1.71e6 A/m (Table 4.1 of [49]).

- The anhysteretic function has three constants a_1, a_2, and a_3 in (A.1). In addition, since the slope of the anhysteretic curve is greater than or equal to zero for all H_e ($\frac{dM_{an}}{dH_e} \geqslant 0$), the three constants, a_1, a_2, and a_3 should be greater than zero and $a_2 \geqslant a_1$.

- α represents interdomain coupling, and it is used in determining effective field H_e in (2.35). That is, $H_e = H + \alpha M$.

If the values of the α and M_{sat} are known, then the determination of a_1, a_2 and a_3 is a constrained optimization problem of minimizing the error between the reference anhysteretic characteristic and the model. The initial value of α can be assumed by comparing the magnetization curve of the core material M4 with a known curve such as the anhysteretic magnetization curve of the core material of current transformers used in [36] (as in Fig.3.1). Generally, when α is increased, it increases the slope of the B-H loop at the H axis. Therefore, based on the comparison of the two characteristics, an initial value of 1.0e-6 is assumed for α.

A measured B-H loop of a core material, is used to obtain $B_{anhys} vs\ H_{anhys}$ data for the anhysteretic curve. It is assumed that the curve that symmetrically intersects the measured B-H loop represents the values of $B_{anhys} vs\ H_{anhys}$ curve. A measured B-H loop of the core material M4 is used in determining the values of this curve, which are given in Table 3.1. During the calculation, these values are converted to represent a normalized anhysteretic curve as in (A.3) - (A.6). Then, the initial guess of α was used in a numerical iterative routine of least squares estimation to determine the three constants a_1, a_2 and a_3.

$$\text{from } B = \mu_0(M + H) \tag{A.3}$$

$$M = \frac{B}{\mu_0} - H \tag{A.4}$$

$$M_{normalized} = \frac{M}{M_{sat}} \tag{A.5}$$

$$H_e = H + \alpha M \tag{A.6}$$

Once the parameters of the anhysteretic curve are found, the magnitudes of c and k are calculated. The value of c can be calculated from the ratio of the initial normal susceptibility $\chi'_{in} = \left(\frac{dM}{dH}\right)_{M=0,\ H=0}$ to the initial anhysteretic susceptibility $\chi'_{an} = \left(\frac{dM_{an}}{dH}\right)_{M=0,\ H=0}$[50]. However this method could not be used due to lack of data. Typical values of c for some iron core materials are given in [50]. Thus value of c is set to 0.1. The same value has been used in the current transformer models in [35], and has shown that small changes in c have negligible effect on the simulated B-H loop.

The value of k can be calculated using (3.1), which is reproduced below as (A.7). The general relationship between k and H_c can be expressed if the differential sus-

ceptibility at the coercive point χ'_{H_c} is known. In general $\chi'_{H_c} = \chi'_{\max}$ denote the differential susceptibility around the coercive point, which in the model is always the maximum value observed around the hysteresis loop [50]. The values of H_c and $\chi'_{\max}$ obtained from the reference $B - H$ loop of the core material M4 [62], and are given in Table 3.3.

$$k = \frac{M_{an}(H_c)}{1-c}\left[\alpha + \frac{1}{\frac{\chi'_{\max}}{1-c} - \frac{c}{1-c}\frac{dM_{an}(H_c)}{dH}}\right] \tag{A.7}$$

Eddy Current effects and the interface with EMTDC

Once the parameters of the hysteresis model are determined, the model can be interfaced with the existing model. This can be achieved by one of the following methods;

1. If the core dimensions such as the length (l) and the cross-sectional area (A) of each limb, and the actual number of turns (N) in each winding are known, then the model can be readily interfaced with EMTDC.

   or,

2. If the actual values of core dimensions (l and A) of each limb and number of turns (N) in each winding are not known, the existing model uses an equivalent inductance matrix representation to model the transformer in EMTDC. Therefore this method can be adopted if the actual values are not known.

In addition, there are two constants in (2.53), that represent the effects of excess and anomalous loss. Therefore, irrespective of the method in which the inductance matrix is determined, the values of these two constants k_1 and k_2 need to determined such that the total power loss measured at rated conditions are simulated in the model.

The actual number of turns in the windings, and core dimensions are usually not available. Therefore, this discussion focuses on determining the parameters using the second method. In the existing model, the number of turns N_1 and N_2 are set equal to the rated voltage of the windings (2.26). In addition, the existing model uses a unity cross sectional area by scaling the entire piece-wise linear curve. However, since the JA theory is based on the physics of ferromagnetic hysteresis, the range of values used in the new model must correspond to the actual values. Therefore, a peak operating flux density (B_{max}) was assumed, which is typically 1.6 $\sim$ 1.7 T at the rated conditions.

In order to represent the test transformer, a peak flux density of 1.65 T is assumed. Then, the cross sectional area A is determined such that the actual value of the product of NA is matched by the product of NA used in the simulation model as in (A.9) - (A.10).

$$\text{from } v = N\frac{d\phi}{dt} \Longrightarrow \sqrt{2}|V| = N\omega\phi_{peak} \tag{A.8}$$

$$\therefore \quad A = \frac{\sqrt{2}|V|}{N\omega B_{peak}} \tag{A.9}$$

$$\text{since } N = |V| \text{ (units kV)}$$

$$\text{substituting values; } A = \frac{\sqrt{2} * 1000}{2 * \pi * 60 * 1.65} = 2.273 \tag{A.10}$$

The eddy current effects are represented using the expression given in (2.53), reproduced below as (A.11).

$$H_{tot} = H_{hyst} + k_1\frac{dB}{dt} + k_2\left(\frac{dB}{dt}\right)^{\frac{1}{2}} \tag{A.11}$$

The initial values of the two constants in this expression are calculated using (2.50), and (2.52) respectively.

$$\begin{aligned} \text{from (2.50) } k_{1_{initial}} &= \frac{D^2}{2\rho\beta} \qquad (A.12) \\ \text{where } D &= \text{thickness of laminations} \\ \rho &= \text{resistivity} \\ \beta &= \text{a constant } (\beta = 6 \text{ for laminations}) \end{aligned}$$

Typical commercially available electrical steels are low carbon, silicon-iron, or silicon-aluminum-iron alloys containing up to 3.5% silicon, and only a small amount of aluminum. In addition, the electrical resistivity in $\Omega.m$ at 25^0C can be represented as in (A.13). This equation is based on the average line drawn through many test points obtained on commercial grades of electrical steels of various compositions, published by the American Society for Testing and Materials [81]. Therefore, based on this information, a typical value of 0.48×10^{-6} $\Omega.m$ is considered in this calculation, which approximately represents a 3% silicon content.

$$\rho = 0.1325 \times 10^{-6} + 0.113 \times (\text{percent silicon} + \text{percent aluminum}) \times 10^{-6}\ \Omega.m \qquad (A.13)$$

Meanwhile, the thickness of laminations (D) typically varies between 0.18 mm to 0.35 mm [82]. A 0.30 mm thickness was assumed in this calculation, as manufacturers data sheets suggest a range between 0.27 mm and 0.35 mm for the core materials M3 $\sim$ M5.

Therefore, substituting these values in (A.12) gives;

$$k_{1_{initial}} = \frac{(0.3e\text{-}3)^2}{2 \times 0.48e\text{-}6 \times 6} = 15.6e\text{-}3$$

Similarly, from (2.52);

$$k_{2_{initial}} = \left(\frac{GSH_o}{\rho}\right)^{\frac{1}{2}} \tag{A.14}$$

where G = a constant; 0.1356 [39]

S = cross sectional area of laminations

H_o = represents the internal potential experienced by domain walls

ρ = resistivity

H_o is 0.15 A/m for grain oriented silicon steel (3% SiFe) [39]. S is the cross sectional area of laminations. This requires the width, and the thickness of laminations in meters. The thickness has already been used in the calculation of $k_{1_{initial}}$. However, the width of laminations depends on the design of the transformer and its capacity etc. Therefore, the initial value of k_2 ($k_{2_{initial}}$) is calculated without taking the width of laminations into consideration. However, this does not cause any significant errors, as both the $k_{1_{initial}}$ and $k_{2_{initial}}$ are tuned along with the length of the winding limb (l) to ensure that the simulation results closely match the recorded data.

In addition, the existing model has a current source that injects the 'linear component' of the saturation current. The magnitude of this source is based on the initial slope of the piece-wise linear curve used. Even if the JA model represents

the hysteresis characteristics in the new model, this linear current component cannot be removed completely, as it is an integral part of the existing model. However, the magnitude of this source can be reduced to a very small value. In addition, the tuning of parameters also compensates for any discrepancies that may have been caused by this additional current component.

$$\begin{aligned} k_{2_{initial}} &= \left(\frac{GDH_o}{\rho}\right)^{\frac{1}{2}} = \left(\frac{0.1356 \times 0.3e\text{-}3 \times 0.15}{0.48e\text{-}6}\right)^{\frac{1}{2}} \\ &= 3.565 \end{aligned}$$

Therefore, once the initial values of k_1 and k_2 are found, these values, and the length of the winding limb l, are tuned so that the correct magnitude of the magnetizing current and power loss are simulated at the rated conditions. In addition, if the open circuit normal magnetizing curve is available, these measured values can be compared with the simulation results. If the simulation results do not closely match the measured data, the parameters that represent the anhysteretic curve need to be modified. This can be achieved by extrapolating the values and by changing the permeability represented by these extrapolated values in the saturation region. Meanwhile, if the parameters of the anhysteretic curve are re-calculated, the procedure described above needs to be followed to ensure that the rest of the parameters are appropriately determined.

The iteration histories corresponding to the tuning of parameters are given in Table A.1. Initially the length of the winding limb, $l = 1.0$ is assumed. In addition, the initial values of k_1 and k_2 calculated above are considered. A simulation of an open circuit test is carried out using these initial values. This is followed by the determination of the error function (f_{error}), which contains the percentage errors of

Table A.1: Iteration histories corresponding to the tuning of parameters

#	l	k_1	k_2	f_{error}	$\frac{\partial f_{error}}{\partial l}$	$\frac{\partial f_{error}}{\partial k_1}$	$\frac{\partial f_{error}}{\partial k_2}$
1	1.0	$15.6e^{-3}$	3.565	603.86	803.9	63.8	638
2	0.839	$10.6e^{-3}$	2.428	283.07	575.8	52.6	527
3	0.810	$6.5e^{-3}$	1.488	116.9	388.9	47.0	537
4	0.791	$3.6e^{-3}$	0.721	2.634			

the simulated core loss and the rms value of the magnetizing current;

$$f_{error} = \left[\frac{|P_{measured} - P_{simulation}|}{P_{measured}}\right] \times 100 + \left[\frac{|I_{measured} - I_{simulation}|}{I_{measured}}\right] \times 100 \quad \text{(A.15)}$$

This is followed by the determination of the sensitivity of the error function with l, k_1, and k_2 respectively, and tuning of these parameters until the error is minimized. After three iterations, the simulated rms value of the magnetizing current showed an error less than 1% , and the simulated core loss produced an error less than 2%. Therefore, iterations were terminated at this point, and the tuned parameters were considered as the basis for further simulations carried out to represent different test conditions.

The laboratory tests carried out with the test transformer provided waveforms of magnetizing current, measured data at (a) different excitation voltages at 60 Hz, and (b) different frequencies, while maintaining a constant $\frac{V}{f}$ ratio. Therefore, when the parameters for the laboratory test transformer are determined, this process did not limit itself to the rated conditions. The tuned values obtained at the rated conditions were used in simulation studies to compare the waveforms and analyse any discrepancies, at different frequencies, and excitation voltages. This is followed by further tuning of l, k_1, and k_2. The parameters given in Table A.2 shows parameters obtained (a) by tuning the parameters considering the measured data at the rated

Table A.2: Parameters determined using different measured data for tuning

Description	l	k_1	k_2
(a) Considering the measurements at rated conditions	0.791	3.6e-3	0.72
(b) Considering the measurements at different V and f	0.717	3.5e-3	0.79

condition as the basis, (b) by tuning the parameters considering the measured data at different voltages and frequencies as the basis. The simulated waveforms obtained with these parameters are given in Fig.A.1

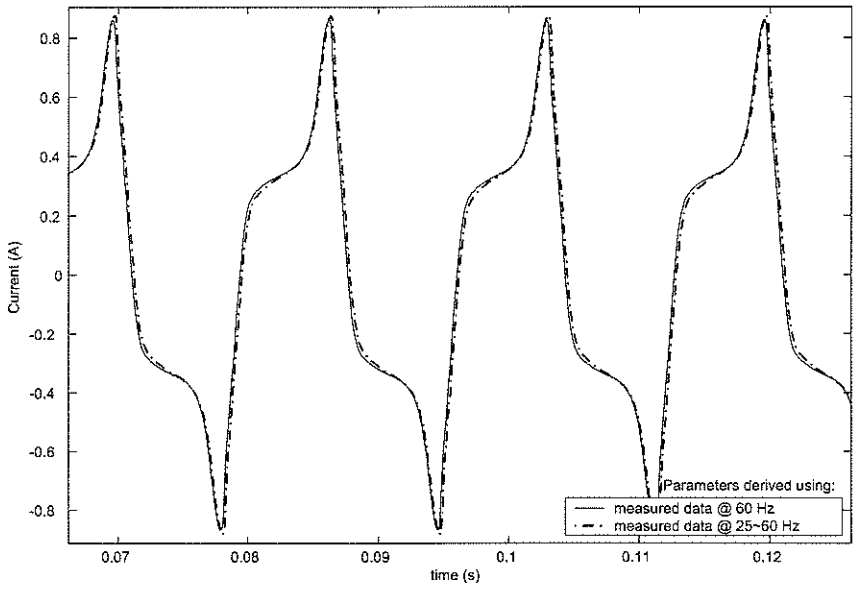

Figure A.1: Simulated waveforms obtained using the parameters given in Table A.2

Summary

The foregoing discussion was focused on describing how the parameters were calculated to represent a given transformer using the new model in EMTDC. The laboratory test transformer was considered as an example to describe the procedure followed. A similar process was followed to determine the parameters that represent the 230 kV/ 500 kV/ 46 kV auto transformers considered in Chapters 4 and 5. During this

process, open circuit test results, and the measured normal magnetizing curve were used as the basis of tuning l, k_1, and k_2.

It is expected that the measured data such as the open circuit test results and normal magnetizing curve are available, so that the core loss and the permeability in the shoulder region are adequately represented in the simulation model. Meanwhile, the function that was considered to represent the anhysteretic curve is more appropriate for the magnetizing characteristics of grain oriented electrical steel. A different function may have to be used for different core materials, such as High-Permeability Grain Oriented Electrical Steel, Laser-Scribed High-Permeability Electrical Steel, amorphous metal (METGLAS®) etc.

Appendix B

Comparisons with recorded waveforms

Details of the laboratory test system, and the comparisons carried out with recorded waveforms are presented in this appendix.

Laboratory test system

A separately excited dc motor was used to drive a three phase synchronous generator to obtain a variable voltage, variable frequency ac supply (Fig.B.1). The field current of the synchronous generator was varied to control the magnitude of voltage ($|v|$), and the field of the dc motor was varied to control the frequency (f). Whenever the frequency was changed, a constant $\frac{v}{f}$ ratio was maintained, so that a constant flux is maintained in the core.

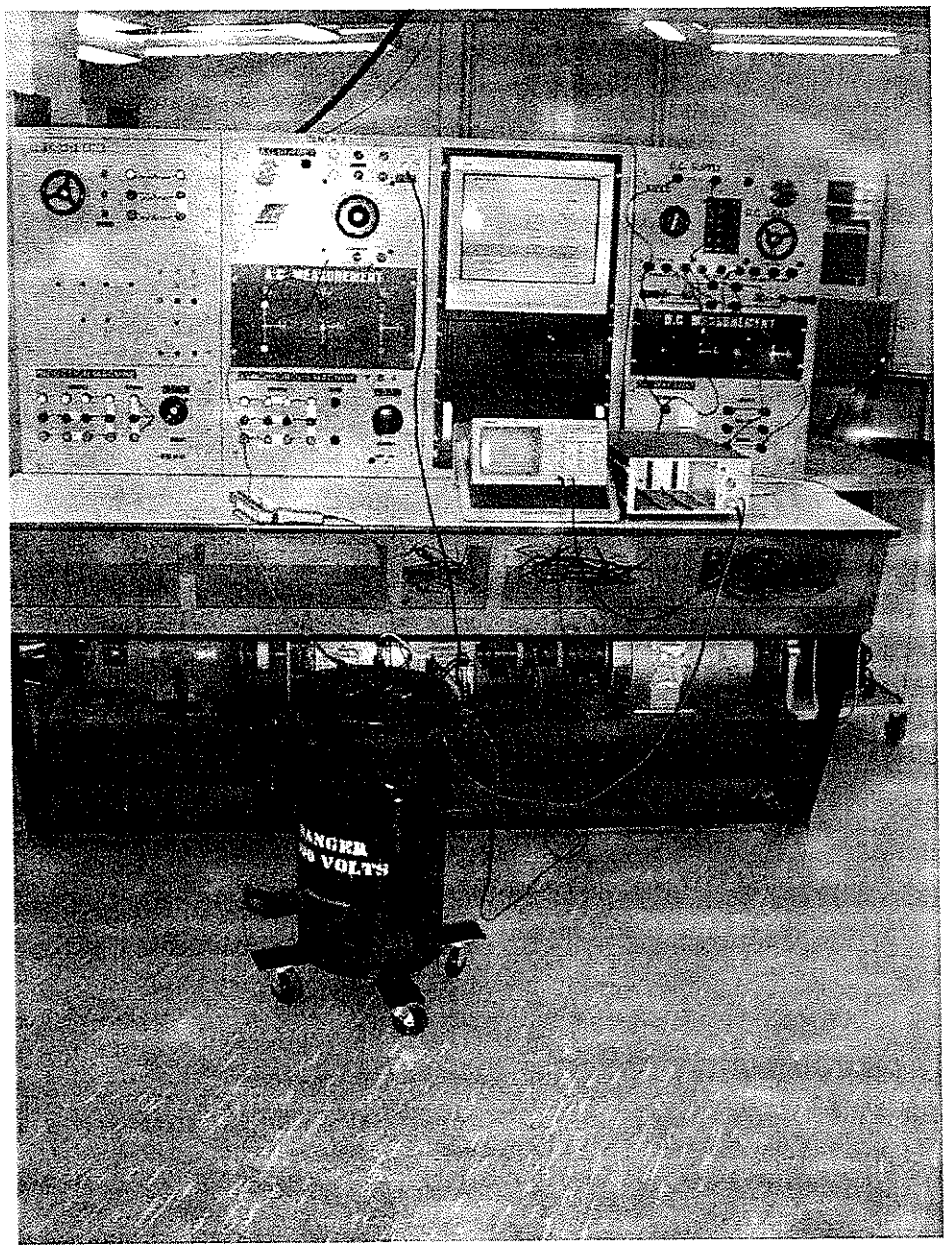

Figure B.1: Laboratory Test System

Details of the laboratory test system are;

1. Transformer

   - 3 kVA, 115 V / 2300 V, 60 Hz single phase distribution transformer.
   - Measured data at the rated conditions are: Core loss[1] = 33.8 W; rms value of the magnetizing current = 0.48 A.

2. Synchronous generator

   - Three phase, 3 kVA, 208 V,1800 rpm.
   - Field circuit 120 V dc, 1.25 A.

3. DC motor

   - 2.5 kW, 110 V, 20 A, 1750 rpm.
   - Field circuit 110 V, 1.5 A.

Comparisons with recorded data

A series of tests carried out in the laboratory covered a range of voltages and frequencies. Each recorded waveform was compared with a simulated waveform. Some of the comparisons carried out with recorded data are already presented in section 3.2.1. This include the waveforms at 0.9 pu, 1.0 pu, and 1.1 pu voltages at 60 Hz. In addition, in section 3.2.2, a comparison carried out at 25 Hz was presented. The following consists of the comparisons which are not presented in Chapter 3.

[1]When the eddy current effects are represented with an external resistor in the simulation model (called the 'resistor model') as in section 3.2, an external resistance of $R_{eddy} = 548\ \Omega$ referred to 115V winding was used.

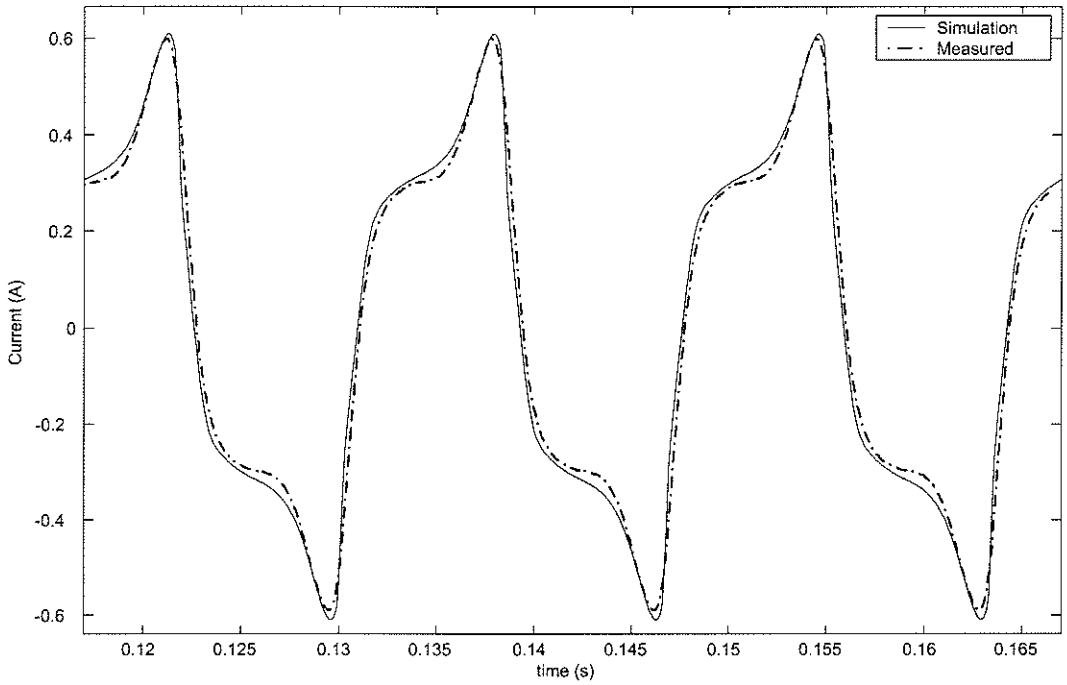

Figure B.2: Magnetizing current compared at 0.92 pu voltage, 60 Hz

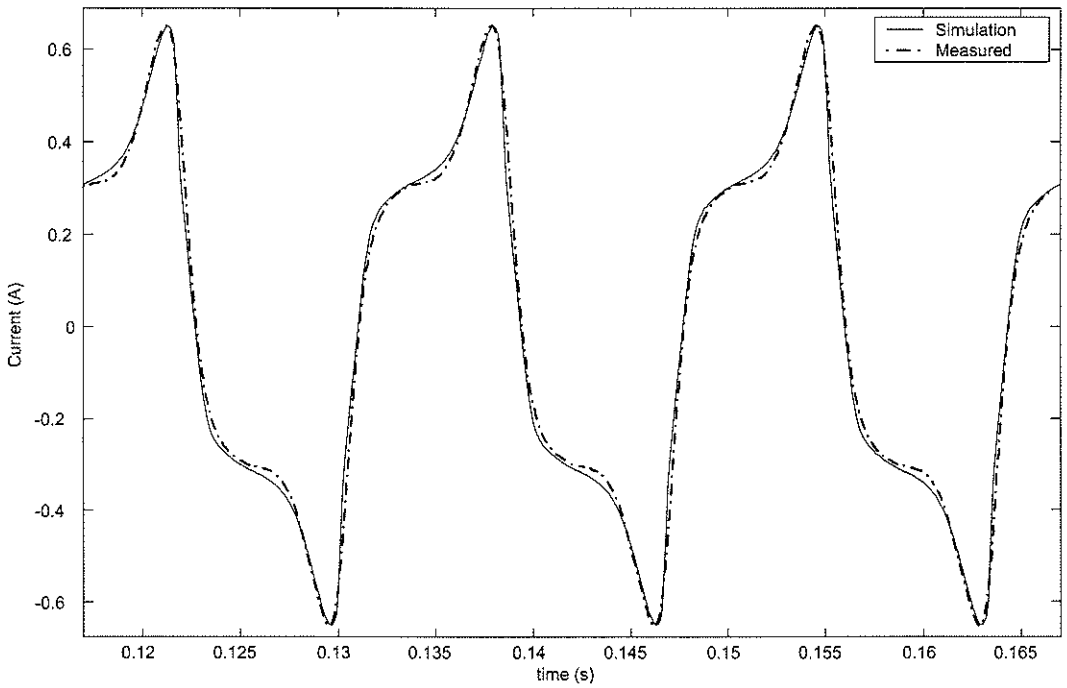

Figure B.3: Magnetizing current compared at 0.94 pu voltage, 60 Hz

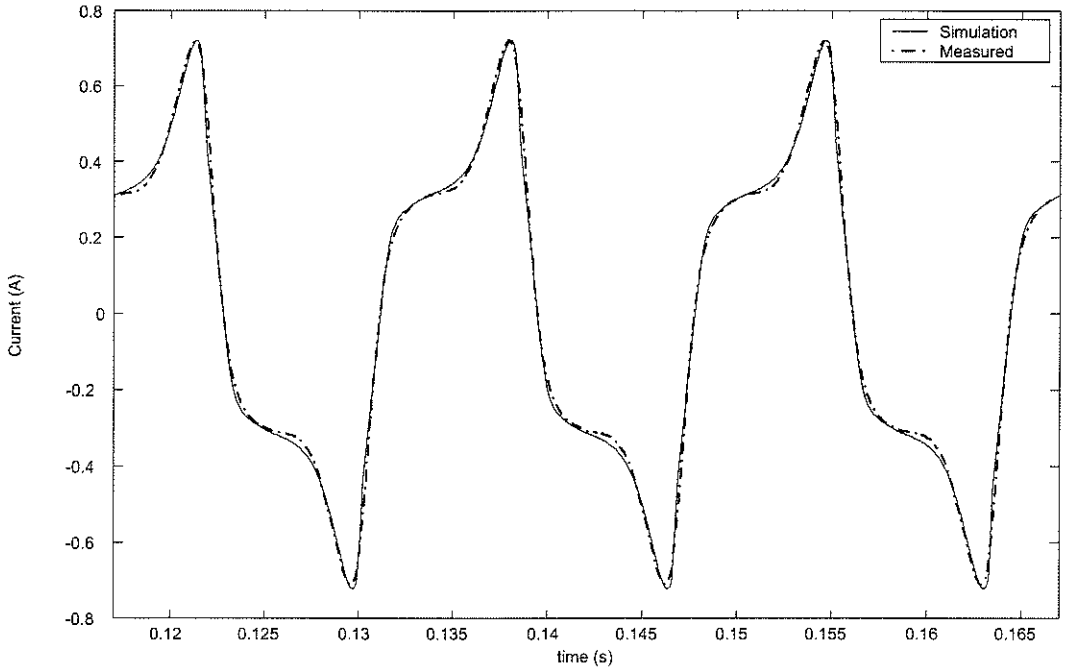

Figure B.4: Magnetizing current compared at 0.96 pu voltage, 60 Hz

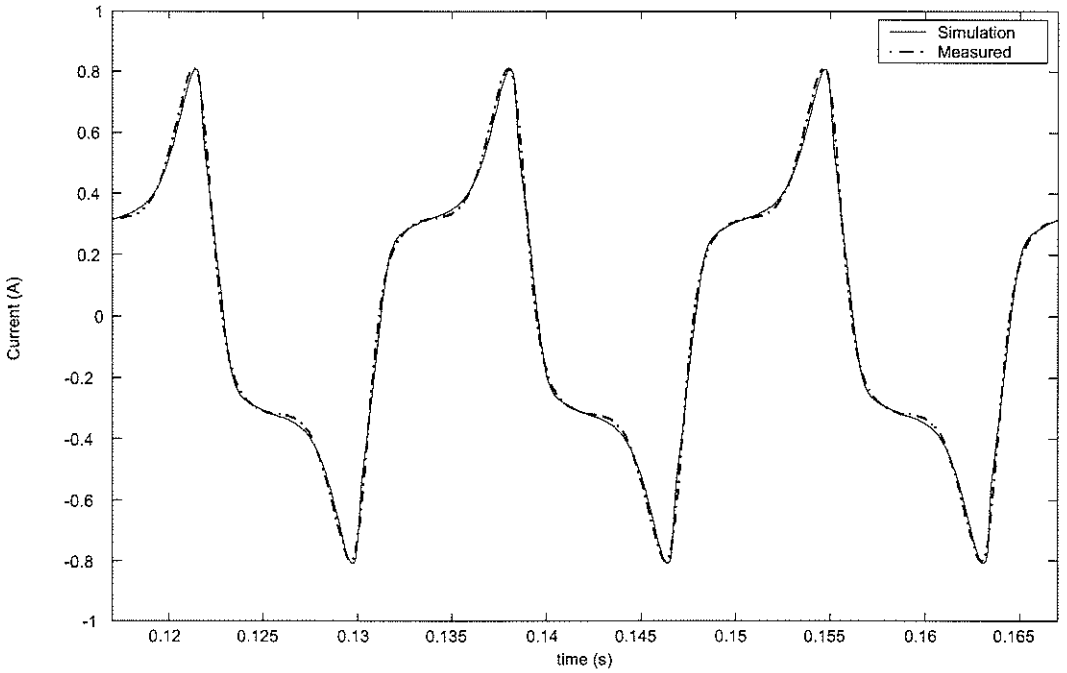

Figure B.5: Magnetizing current compared at 0.98 pu voltage, 60 Hz

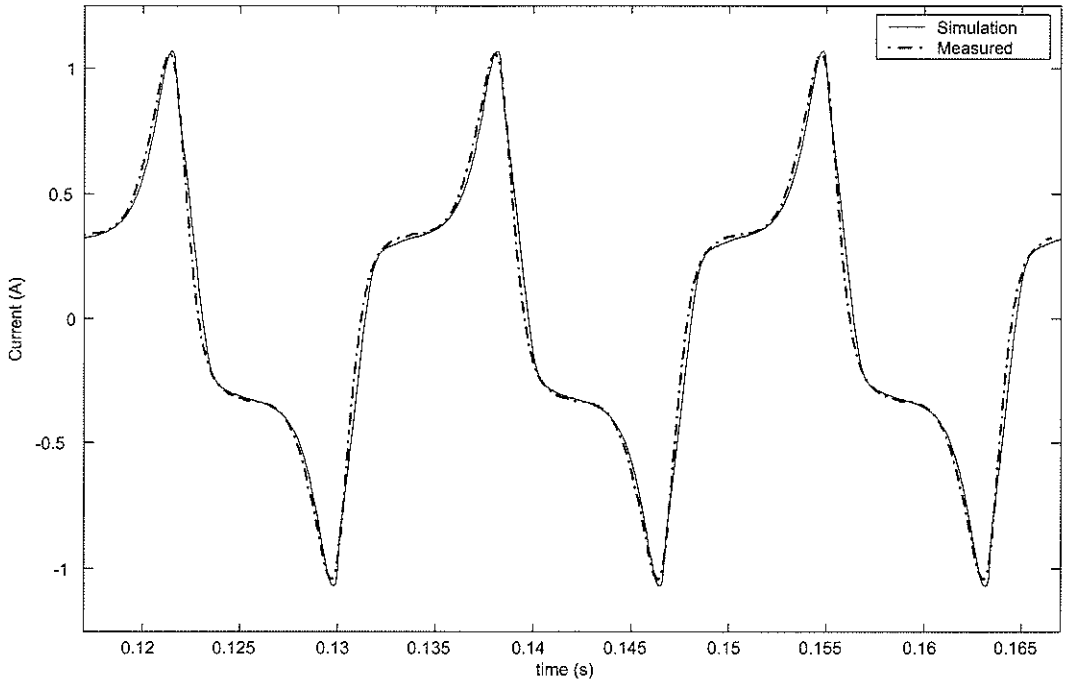

Figure B.6: Magnetizing current compared at 1.02 pu voltage, 60 Hz

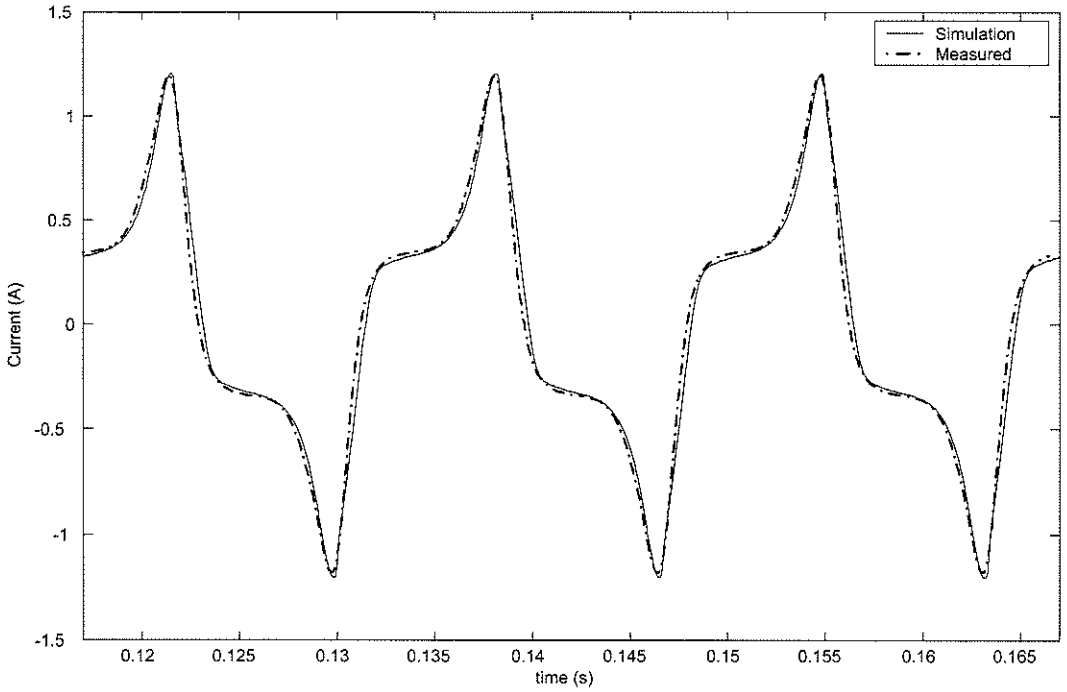

Figure B.7: Magnetizing current compared at 1.04 pu voltage, 60 Hz

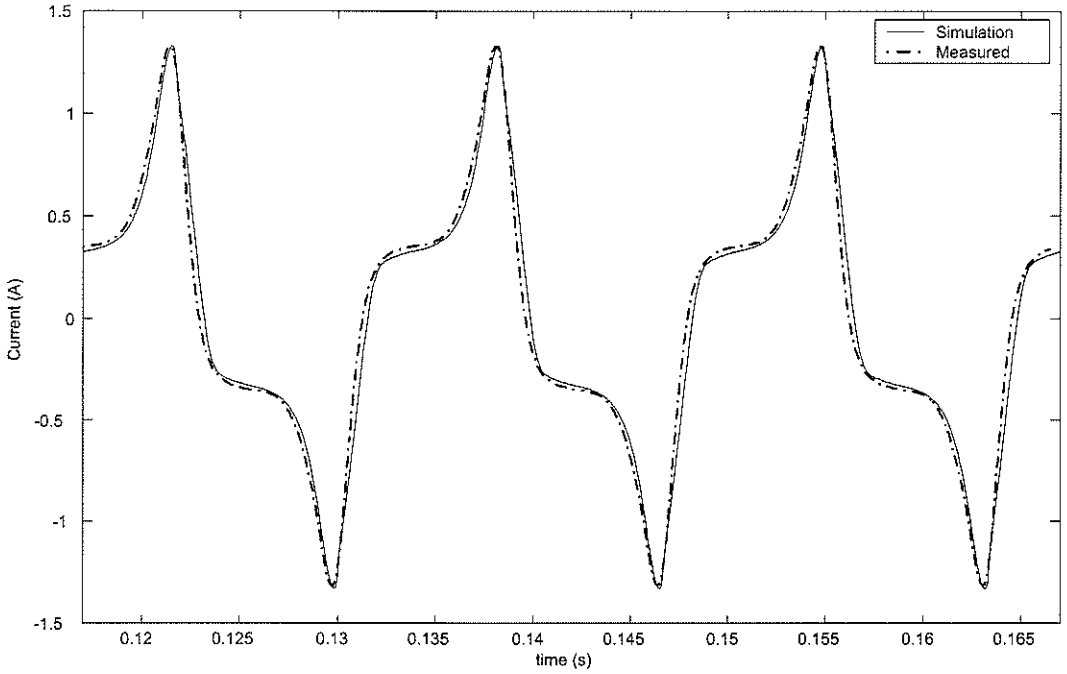

Figure B.8: Magnetizing current compared at 1.06 pu voltage, 60 Hz

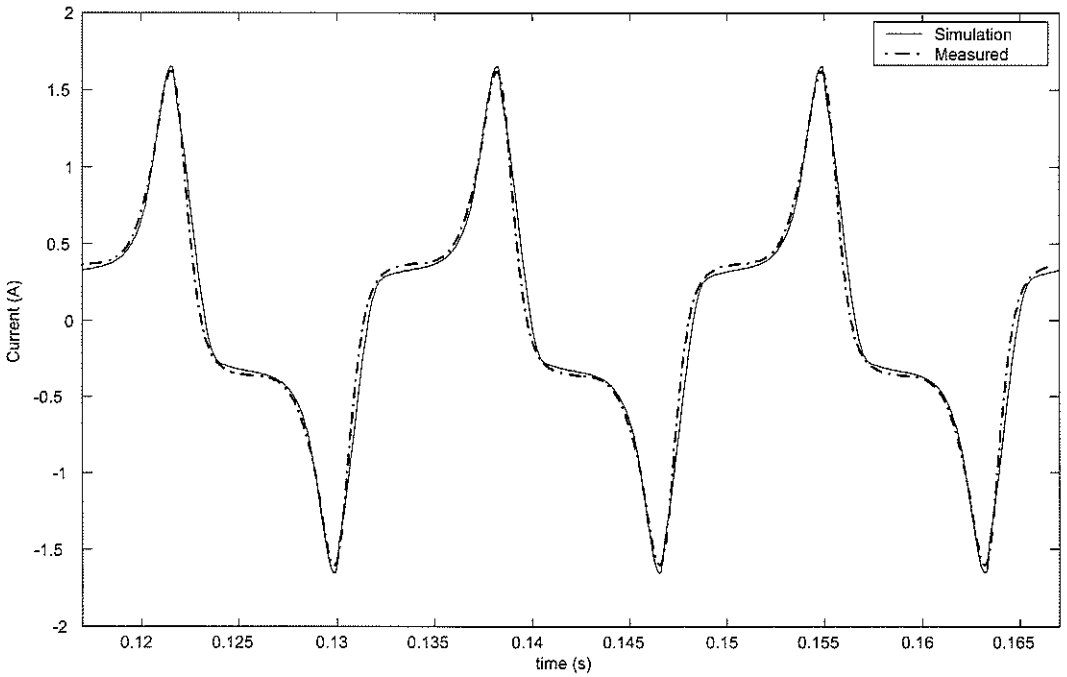

Figure B.9: Magnetizing current compared at 1.08 pu voltage, 60 Hz

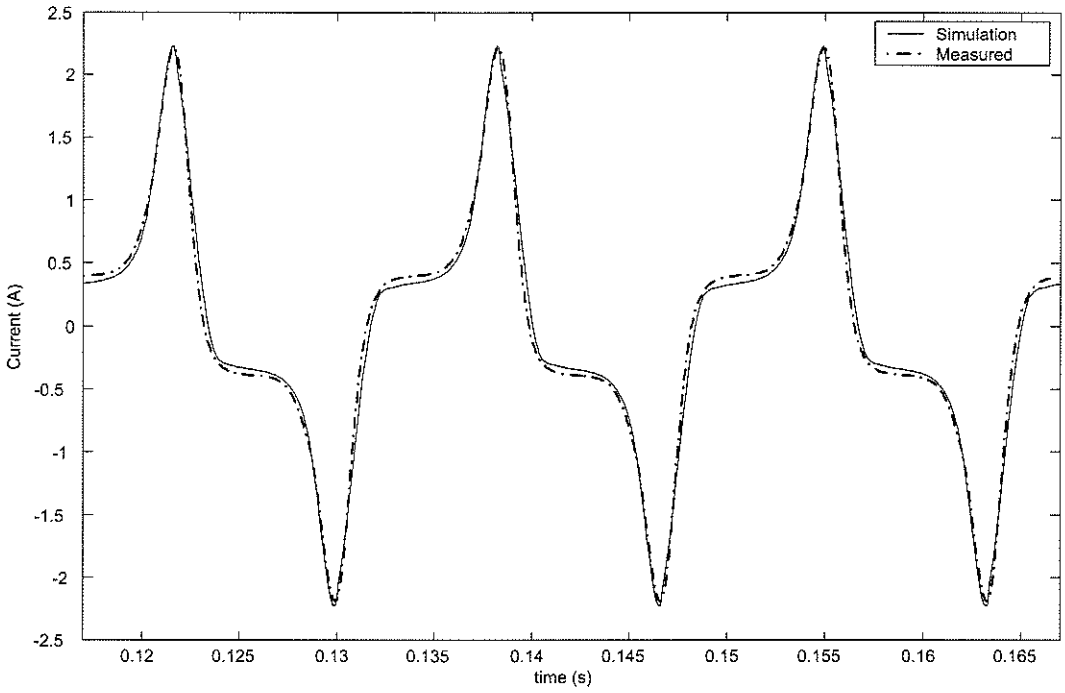

Figure B.10: Magnetizing current compared at 1.12 pu voltage, 60 Hz

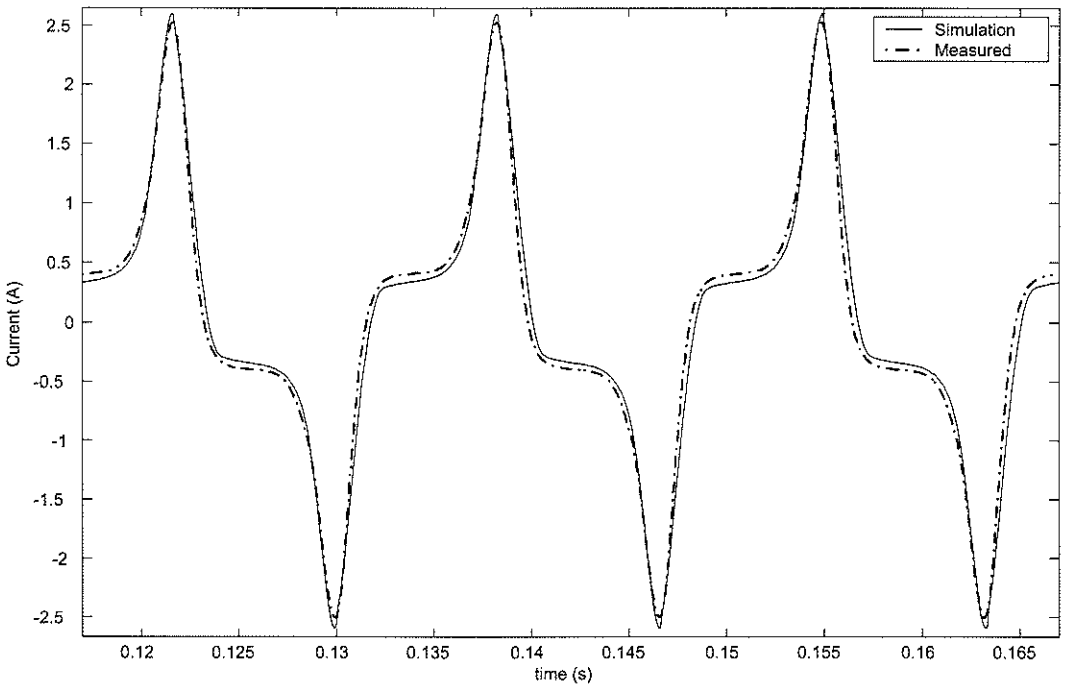

Figure B.11: Magnetizing current compared at 1.14 pu voltage, 60 Hz

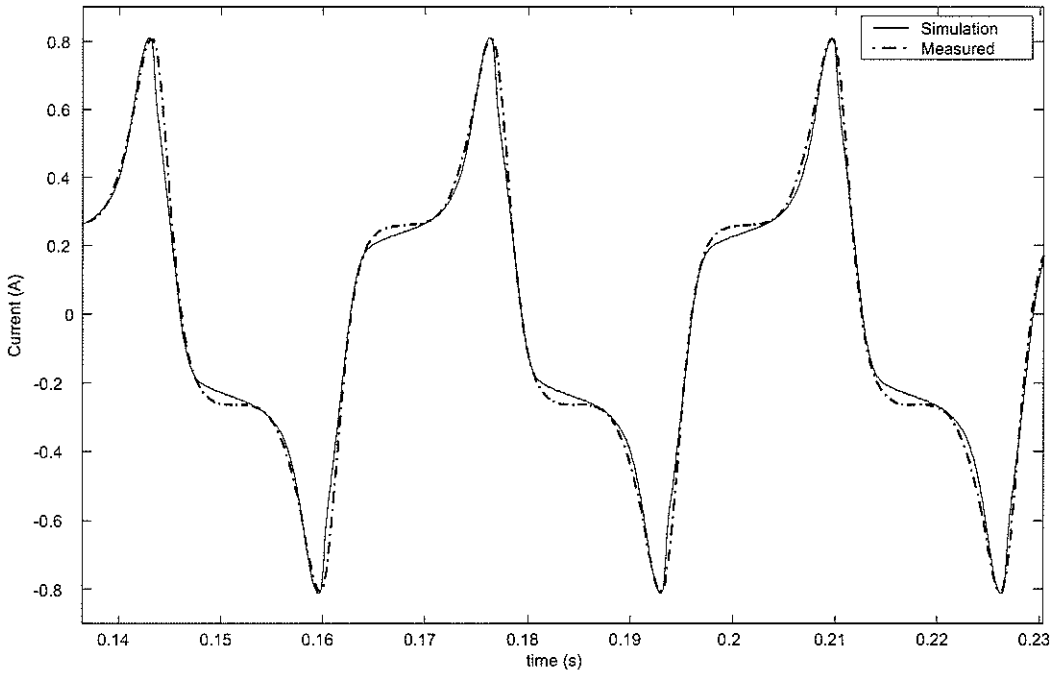

Figure B.12: Magnetizing current compared at 30 Hz.

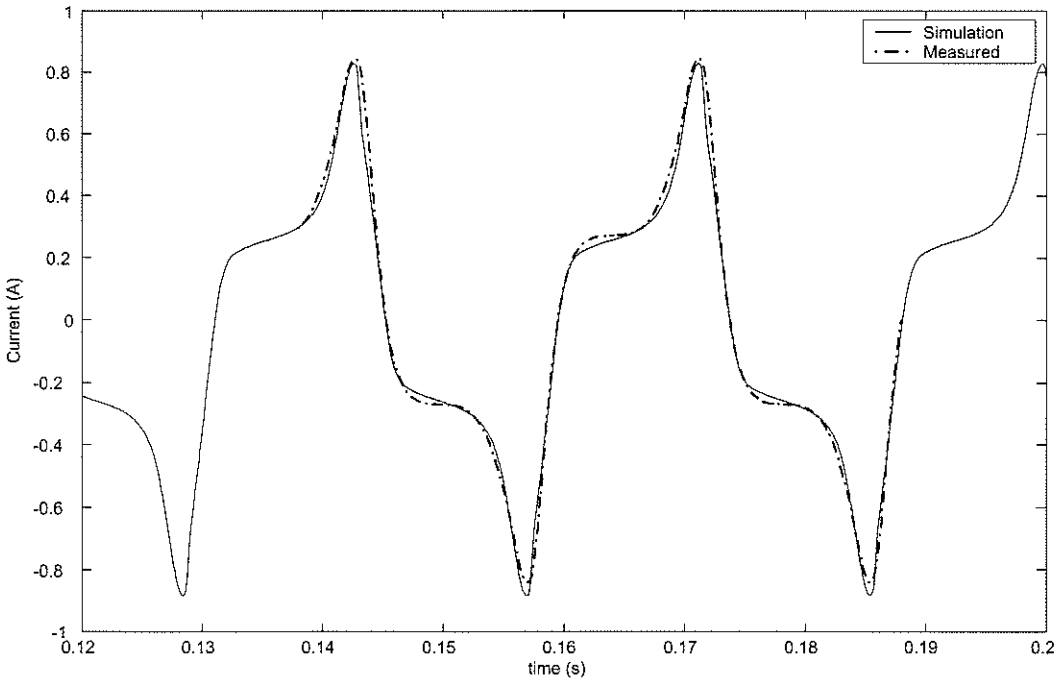

Figure B.13: Magnetizing current compared at 35 Hz.

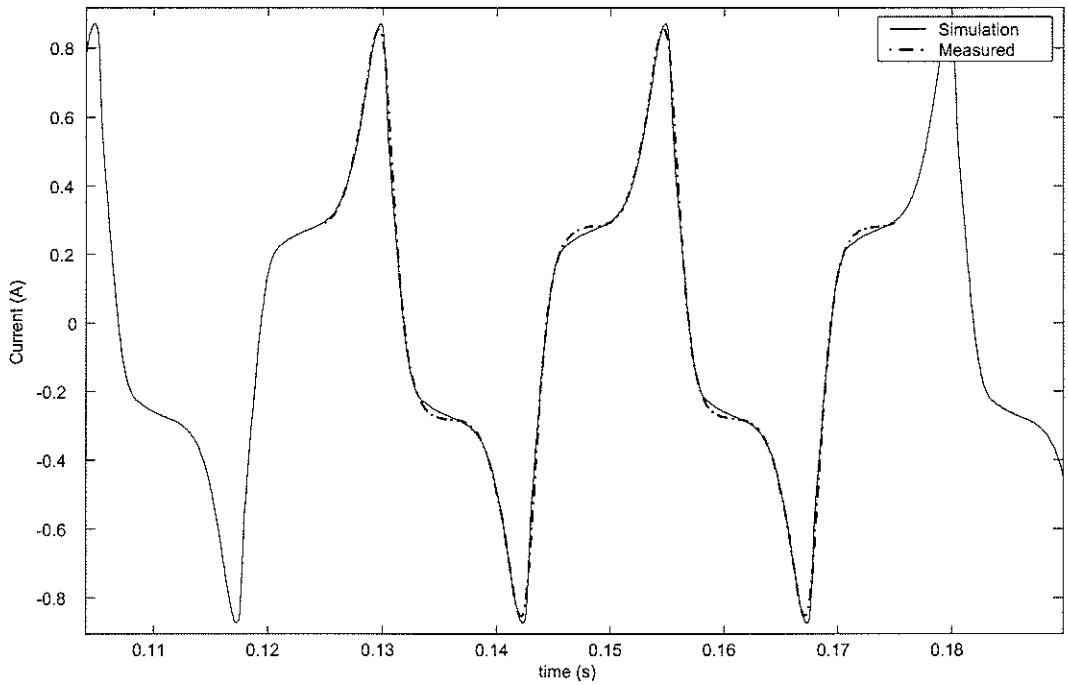

Figure B.14: Magnetizing current compared at 40 Hz.

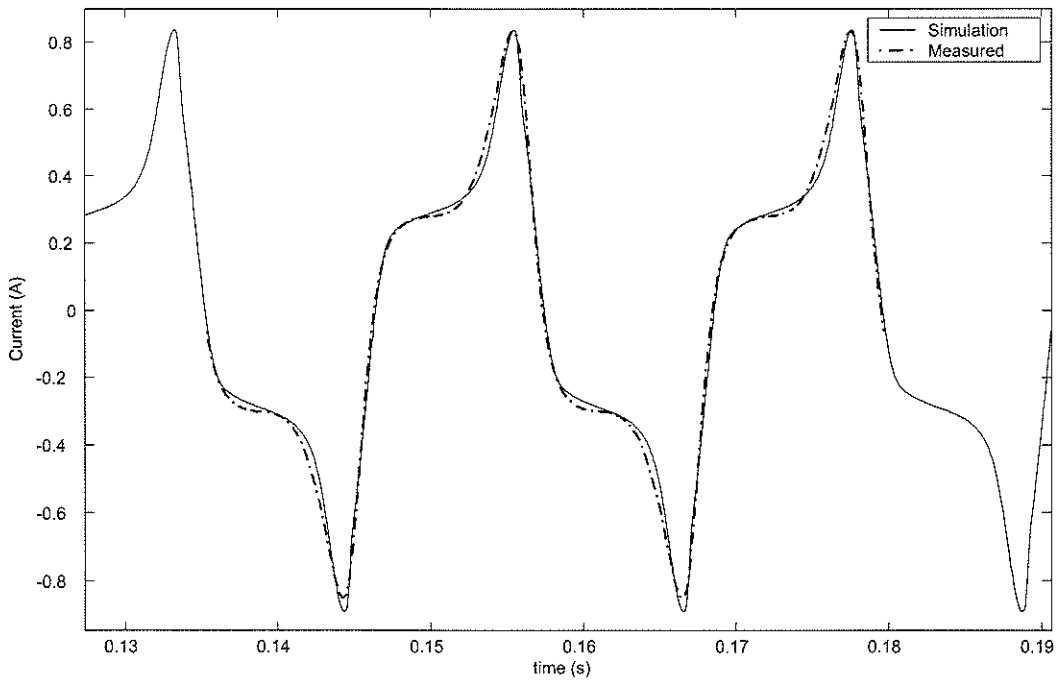

Figure B.15: Magnetizing current compared at 45 Hz.

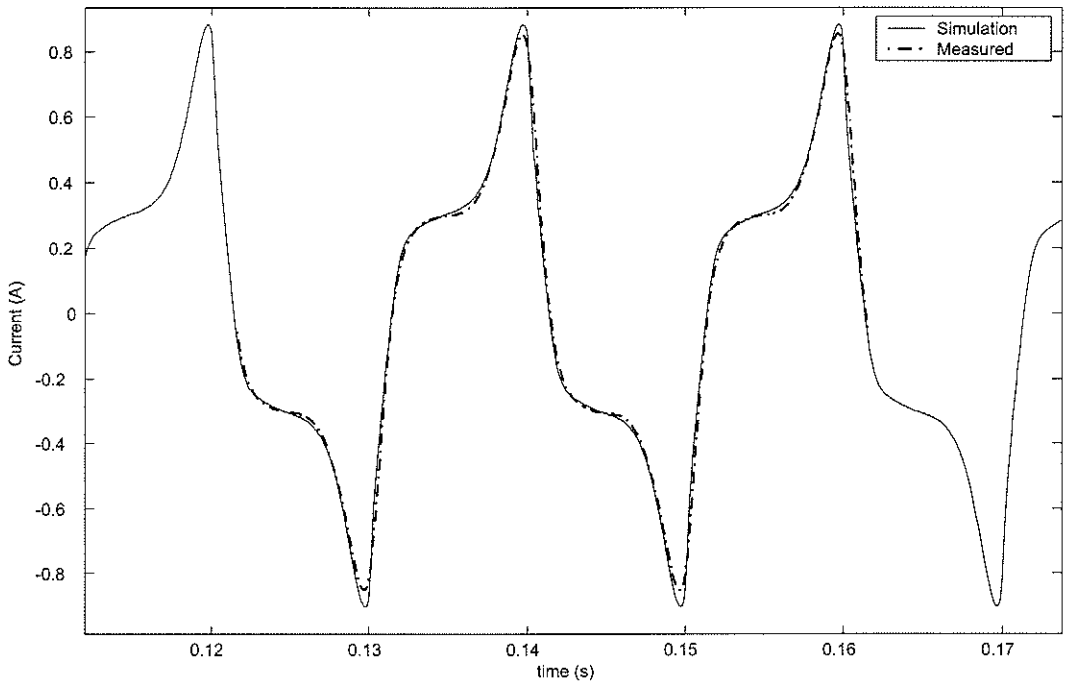

Figure B.16: Magnetizing current compared at 50 Hz.

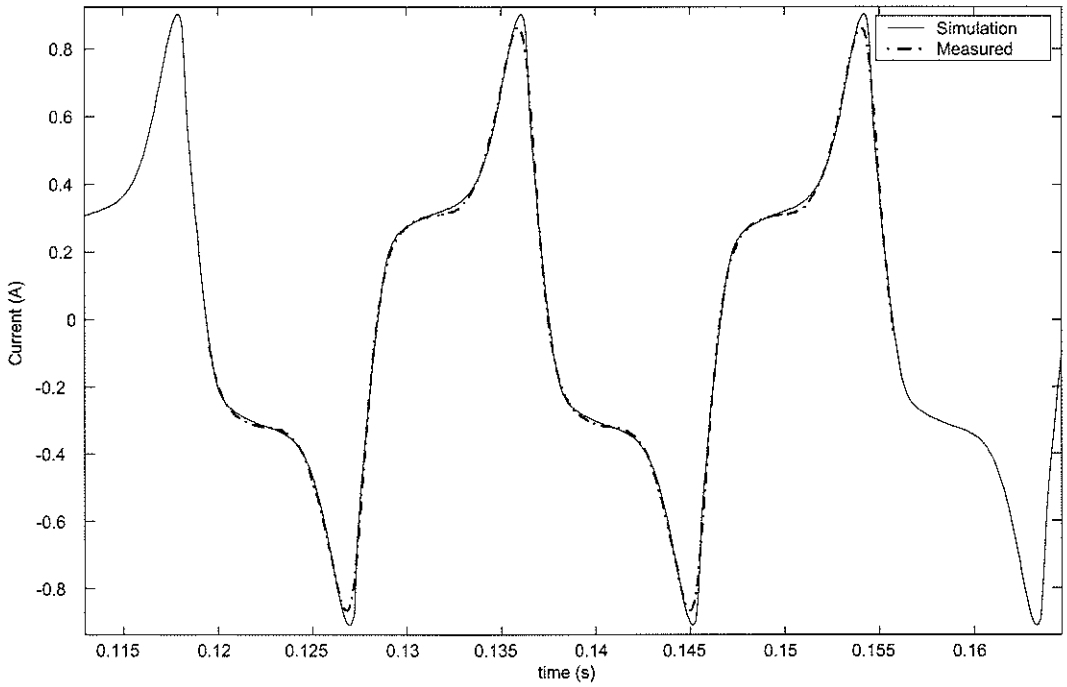

Figure B.17: Magnetizing current compared at 55 Hz.

Appendix C

Simulation model of the power system: Parameters

Parameters of the simulation model of the power system considered in Chapters 4 and 5 are presented in this appendix. This consists of a number of individual models such as the simulation model of a power transformer, a transmission line, and a three phase source etc. In order to represent a power system using these models, a large number of parameters and data are required. The following presents how each individual model is represented in PSCAD/EMTDC. A single line diagram of the Dorsey-Forbes-Chisago system is shown in Fig.C.1. The simulation model considered is based on the work carried out in [32].

Power transformer model

The 230/500/46 kV, 240 MVA auto transformers at Dorsey and Forbes substations are represented with the new model. The new model is based on the existing single phase three winding UMEC model in EMTDC [42].

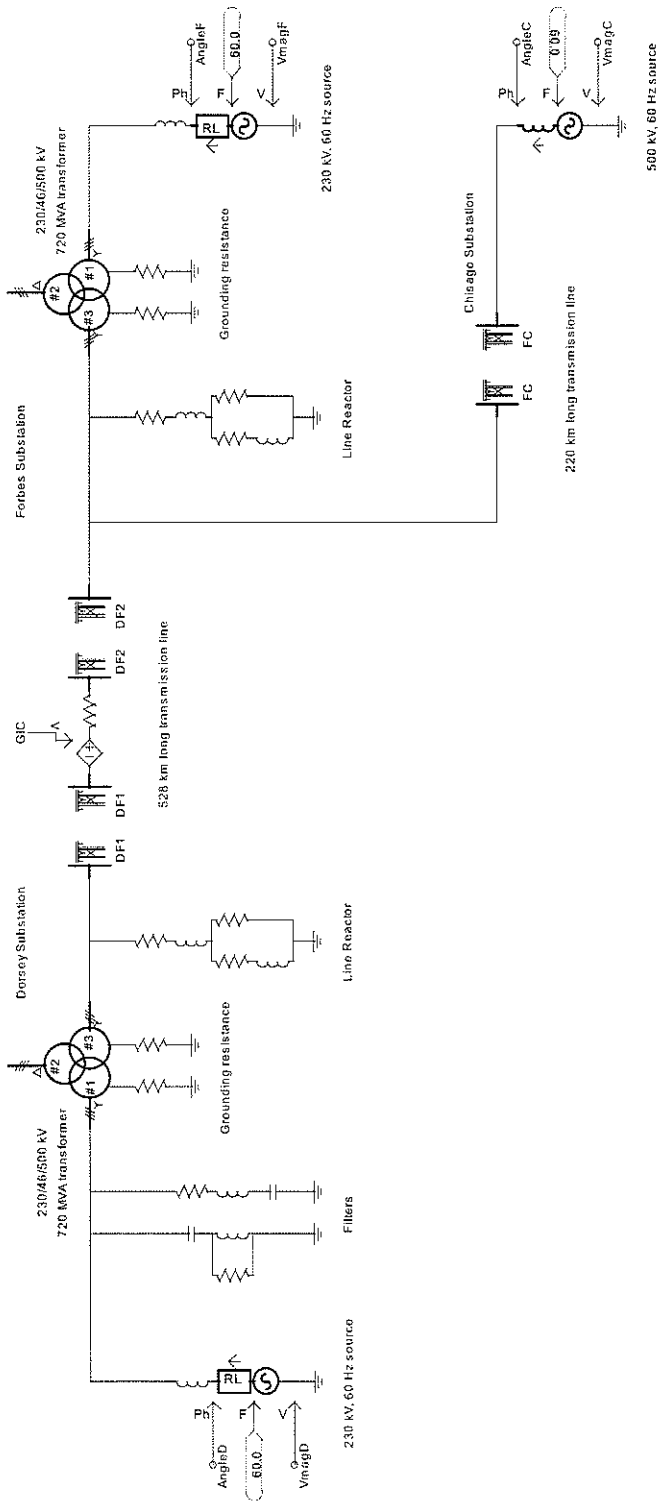

Figure C.1: Single line diagram of Dorsey - Forbes - Chisago system

The following data are required as input parameters;

1. Configuration

Description of the transformer	Dorsey	Forbes
Rated MVA $[MVA]$	240	240
Voltage rating of the winding # 1$[kV]$	132.8	132.8
Voltage rating of the winding # 2$[kV]$	46	13.8
Voltage rating of the winding # 3$[kV]$	288.67	288.67
Resistance of winding # 1 $[\Omega]$	0.015	0.015
Resistance of winding # 3 $[\Omega]$	0.219	0.219
Base frequency (Hz)	60	60
Model saturation?	'Yes'	'Yes'
Tap changer winding	'None'	'None'

2. Saturation Curve

The existing model uses a piece-wise linearly interpolated curve to represent saturation. The following information is required under this menu;

- Magnetizing Current at Rated Voltage: This is used only if core saturation is disabled. Therefore it is not required for our simulations.

- Enable Saturation $(Enab)$ must be set to 1, to enable core saturation. Even if 'Yes' has been selected in the section 'Configuration', this parameter needs to be enabled to represent saturation.

- Data points in the V *vs* I curve are entered, with current (I) as a % of Rated Current, and voltage (V) in pu. The existing model has provided provisions for 10 data points. However, in our implementation the first data point is

used, as these values are considered in determining the magnitude of the 'linear component' of the current source. The data points are chosen such that the injected 'linear component' of current has a negligible effect on the simulated waveforms. Point (X_2,Y_2) is made (0,0), because if 0.0 value is entered, PSCAD will ignore all points following the 0.0.

Description of the saturation curve	
Magnetizing current at the rated voltage	n/a
Enable saturation	1.0
Point X_1: Current as a % of the rated current	4.0e-5
Point Y_1: Voltage in pu	0.5
Point X_2: Current as a % of the rated current	0.0
Point Y_2: Voltage in pu	0.0

3. Core aspect ratios

The core aspect ratios are useful if the equivalent inductance matrix representation is used.

- Ratio of the length of yoke (l_y) to the length of winding limb (l_w)

$$r_L = \frac{l_y}{l_w} = 0.5$$

- Ratio of the area of yoke (A_y) to the area of winding limb (A_w)

$$r_A = \frac{A_y}{A_w} = 1.0$$

Modifications to the existing model

In addition to the default parameters described above, the following parameters are required in the new model.

- In order to enter the value of the cross sectional area (A_w) and the length of the winding limb (l_w), a new section was added to the component definition of the existing model. If the actual values are not known, the tuned parameters can be entered using this menu. In the absence of actual values, the values of A_w and l_w are tuned as described in Appendix A.

- A new section was added to enter the leakage reactances of the three windings.

Parameters for the new B-H model

Determination of parameters for the new B-H model was described in Appendix A. In this discussion, a 3 kVA, 115 V/2300 V, 60 Hz single phase distribution transformer was considered as an example. The same procedure was followed to determine the parameters that represent the magnetizing characteristics of the 230/500/46 kV, 240 MVA auto transformers at Dorsey and Forbes substations. The open circuit test results and measured normal magnetizing curves are considered to tune some of the parameters, as explained in the Appendix A. There are three normal magnetizing curves considered in Chapters 4 and 5. The Curves 1 and 2 are shown in Fig.5.14a, and Curves 1 and 3 are shown in Fig.5.15. The parameters determined to represent the three magnetizing characteristics are given in Table C.1.

Table C.1: Parameters for the new model that represent the magnetizing curves 1, 2, and 3

Description	α	k	a_1	a_2	a_3	k_1	k_2	A_w	L_w
Curve 1	1.0e-6	4.96e-6	173	236	437	10.3e-3	0.528	2.27	3.93
Curve 2	1.0e-6	4.94e-6	227	303	621	9.80e-3	0.498	2.27	4.01
Curve 3	3.0e-6	7.27e-6	2123	2643	9214	10.2e-3	0.518	2.27	3.77

Transmission line model

The 500 kV transmission network connects three utility companies. The first section is 528 km long, and it connects Dorsey converter station to Forbes substation. The second section is 220 km long, and it connects Forbes substation to Chisago substation. Each section was represented using the frequency dependent (phase) model in EMTDC [42][74].

Details of the tower configurations, types of conductors etc., can be obtained from data sheets. Fig.C.2 shows the graphical overview of the transmission line model, that represents the 528 km long line from Dorsey to Forbes (called Line 1), and Fig.C.3 shows the graphical overview of the transmission line model, that represents the 220 km long line from Forbes to Chisago (called Line 2)

1. Geometric data

Description	Line 1	Line 2
Height of lowest conductors (Measured at Tower) [m]	28.956	30.48
Vertical distance of centre conductor above outer conductor [m]	9.692	n/a
Horizontal spacing between phases [m]	6.706	9.756
Relative X position of tower centre on right of way [m]	0	0
Shunt conductance [mhos/m]	1.0e-10	1.0e-10
Is this circuit ideally transposed	'Yes'	'Yes'
How many ground wires	2	2

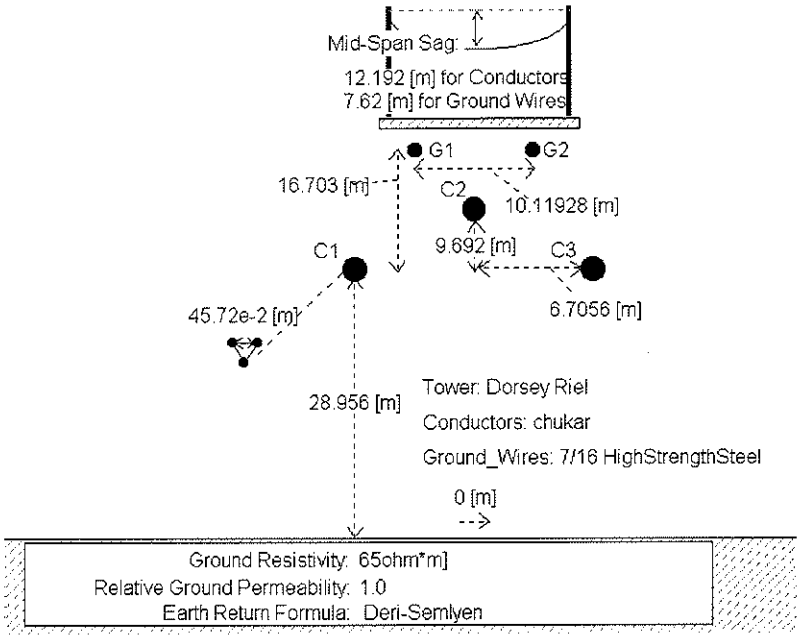

Figure C.2: Tower data for the 528 km long line: Line 1

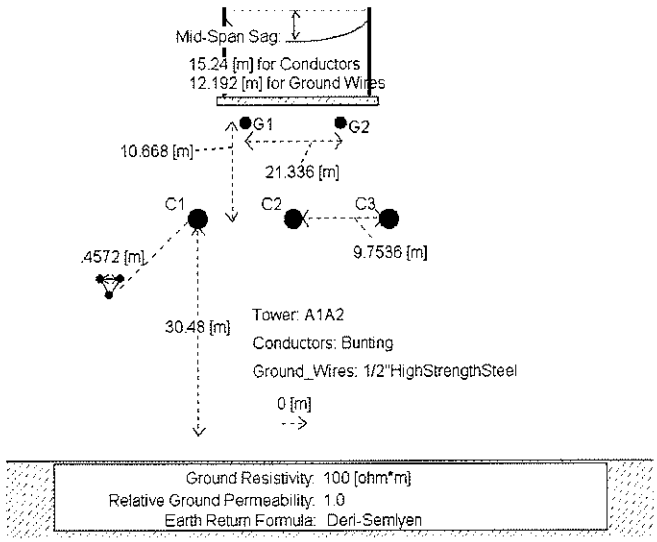

Figure C.3: Tower data for the 220 km long line: Line 2

2. Conductor data

Description	Line 1	Line 2
Conductor name	'Chukar'	'Bunting'
Conductor radius $[m]$	1.755e-2	1.6535e-2
Conductor dc resistance $[\Omega/km]$	0.04486	0.0489
Conductor sag $[m]$	12.2	15.24
Number of sub-conductors in a bundle	3	3
Bundle configuration	symmetrical	symmetrical
Bundle spacing $[m]$	0.457	0.457

3. Ground wire data

Description	Line 1	Line 2
Ground wire name (HSS: High Strength Steel)	7/16" HSS	1/2" HSS
Ground wire radius $[m]$	0.5486e-2	0.5486e-2
Ground wire dc resistance $[\Omega/km]$	2.81	2.865
Sag for all ground wires	7.6	12.192
Height of ground wires above lowest conductor $[m]$	16.7	10.668
Spacing between ground wires $[m]$	10.2	21.336

4. Ground resistivity

Description	Line 1	Line 2
Ground resistivity $[\Omega.m]$	65	100

Substations

The following describes the parameters used in modelling the Dorsey, Forbes, and Chisago substations respectively.

1. Source equivalents

Description	Dorsey	Forbes	Chisago
Base MVA (3 phase) $[MVA]$	720	720	645
Base Voltage (L-L, rms) $[kV]$	230	230	500
Base frequency $[Hz]$	60	60	60
Source impedance type	(R//L)+L	(R//L)+L	L
Positive sequence R (parallel)$[\Omega]$	5.79	9.85	n/a
Positive sequence L (parallel)$[H]$	1.13e-2	1.85e-2	n/a
Positive sequence L (series)$[H]$	1.81e-2	3.7e-2	0.127
Source Values for external control			
Voltage $[kV]$	206	235	477.7
Phase $[deg]$	-0.525	0	7.3
Frequency $[Hz]$	60	60	60

2. Filter banks at Dorsey

Description	R $[\Omega]$	L [H]	C $[\mu F]$
Filter bank 1 [(R//L)+C]	65.8	9.49e-4	14.0
Bi-pole 2 - 11 [R+L+C]	1.08	1.43e-2	4.10
Bi-pole 2 - 13 [R+L+C]	1.27	1.43e-2	2.90

3. Line reactors

Description	Dorsey	Forbes
Shunt reactor		
R (series) [Ω]	65.8	8.05
L (series) [H]	1.08	2.21
Neutral reactor		
R (series) [Ω]	5.22	4.56
L (series) [H]	1.13	0.862
R (parallel) [Ω]	8000	5000